GENETIC DISSECTION OF FACTORS THAT PROMOTE GENOME STABILITY IN THE *CAENORHABDITIS ELEGANS* GERM LINE

by

Tiffany Brooke McClendon

B.S. Biology, Palm Beach Atlantic University, 2004

Submitted to the Graduate Faculty of

School of Medicine in partial fulfillment

of the requirements for the degree of

PhD in Molecular Genetics and Developmental Biology

University of Pittsburgh

2016

UNIVERSITY OF PITTSBURGH

SCHOOL OF MEDICINE

This dissertation was presented

by

Tiffany Brooke McClendon

It was defended on

March 14, 2016

and approved by

Karen Arndt, PhD, Professor

Chris Bakkenist, PhD, Associate Professor

Kara Bernstein, PhD, Assistant Professor

Andrew VanDemark, PhD, Assistant Professor

Thesis Director/Dissertation Advisor: Judith L. Yanowitz, PhD, Assistant Professor

GENETIC DISSECTION OF FACTORS THAT PROMOTE GENOME STABILITY IN THE *CAENORHABDITIS ELEGANS* GERM LINE

Tiffany Brooke McClendon, PhD

University of Pittsburgh, 2016

Genome stability encompasses the mechanisms that ensure the integrity of DNA is kept intact amidst constant insults, the most toxic of which are DNA double-strand breaks. Deficiencies in factors that detect, respond to, and repair DNA are associated with cancer predisposition and, in some cases, accelerated aging. Maintenance of genome stability is paramount in germ cells, which undergo meiosis to give rise to haploid gametes for reproduction. A key step during meiosis I is the formation of crossovers between homologous chromosomes, which are created by the induction of a DNA double-strand break followed by homologous recombination repair. Crossovers allow homologous chromosomes to segregate such that daughter cells have equal DNA content. Errors stemming from DNA repair or chromosome segregation defects during meiosis are often fatal. Consequently, the process of crossover formation is tightly regulated, though not completely understood. *Caenorhabditis elegans* offers an advantageous model for studying factors that promote meiotic genome stability, with a well-organized germ line and clear read-outs of defects in DNA repair and chromosome segregation. Here, we explore two factors that promote genome stability in the *C. elegans* germ line through distinct mechanisms, *sws-1* and *xnd-1*. *sws-1* was identified as a potential member of the conserved Shu complex, which promotes homologous recombination by regulating RAD51 filament dynamics. Using a novel allele of *sws-1*, we found that *sws-1* indeed promotes homologous recombination in the germ line, especially at replication forks. Moreover, SWS-1 functions with the RAD-51 paralogs,

thus forming a *C. elegans* Shu complex. Our work provides a new translational model in which to expand our understanding of the Shu complex in a metazoan. *xnd-1* was identified as a regulator of meiotic recombination with phenotypes suggestive of a broader role in maintaining genome stability, including sensitivity to ionizing radiation. We found that the high lethality of *xnd-1* mutants is not due to chromosome missegregation during meiosis. Rather, our data suggests that the histone acetyltransferase *mys-1* may induce genome instability through increased acetylation of histone H2A lysine 5. Our work provides *xnd-1* as a model in which to study the link between chromatin factors, gene expression, and genome stability.

TABLE OF CONTENTS

LIST OF TABLES

LIST OF FIGURES

PREFACE

To all who have been there along the way:

To Drs. Gary Goss and Carol Wise, who introduced me to Genetics and Research;

To the Yanowitz lab crew, especially Mainpal and Nico, who taught me Photoshop;

To Judy, who catalyzed my transition from student to colleague;

To the members of my thesis committee, who kept me focused;

To my co-authors and collaborators, especially Meghan, who supported this work;

To the Volunteer Office, Demonstration Theaters staff, and Visitors of the Carnegie Science Center, who reminded me that Science is full of wonder;

To Abbie Lade, my partner in Science and Baking;

To my family, who reminded me that there's life to be lived outside the lab;

To the Newmans, who became my Pittsburgh family;

and To Ellie, who is my anchor and made this, all of this, possible;

My most sincere thanks. Here's to more good times.

And finally, to the story that starts before the beginning…

LIST OF ABBREVIATIONS

DNA deoxyribonucleic acid

DSB double-strand break

HR homologous recombination

IR ionizing radiation

CO crossover

HAT histone acetyltransferase

H2AK5ac acetylation of lysine 5 on histone H2A

1.0 INTRODUCTION

1.1 DEFINING GENOME STABILITY

1.1.1 DNA is dynamic and subject to modification

Deoxyribonucleic acid (DNA) serves as the blueprint dictating the structure and function of cells. Moreover, DNA is the primary unit of hereditary for organisms. As such, the integrity of DNA must be maintained.

The structure of DNA – a double helix – gave the impression that it was a highly stable molecule; and yet, the stability of DNA is constantly under threat (FRIEDBERG 2003). DNA replication creates the opportunity for mutations to be introduced into the newly-synthesized strands. The natural physiology of the nucleus is an environment conducive for loss or chemical alteration of nucleotides. Environmental factors – such as UV light, X rays, and chemical agents – can alter DNA bases or damage the DNA backbone. Left unchecked, a cell could accumulate tens of thousands of DNA lesions per day (LINDAHL AND BARNES 2000; VILENCHIK AND KNUDSON 2003; CLANCY 2008), leading to problems in cell growth and function.

In a retrospective, Francis Crick wrote that he and James Watson "totally missed the possible role of…[DNA] repair although…[he] later came to realise that DNA is so precious that probably many distinct repair mechanisms would exist" (CRICK 1974). Indeed, prokaryotic and eukaryotic cells have evolved a myriad of mechanisms to detect, respond to, and repair DNA damage; such factors are involved in maintaining genome stability. This section describes some

of these mechanisms, with a particular focus on the *Caenorhabditis elegans* germ line, which has been the context of the research discussed in Chapters 2 and 3.

1.1.2 Sensing DNA damage

DNA damage checkpoint factors maintain genome stability by monitoring the condition of the genome and triggering events that lead to either induction of cell cycle arrest to allow time for DNA repair, or apoptosis if the cell is too compromised. Genes that govern both responses in the *C. elegans* germ line include *mrt-2*, *clk-2*, *hus-1*, and *atl-1* (GARTNER *et al.* 2000; AHMED *et al.* 2001; HOFMANN *et al.* 2002; GARCIA-MUSE AND BOULTON 2005). *atl-1* and *clk-2* are also required for the S-phase checkpoint in mitotic cells, whereas *mrt-2* and *hus-1* are not (AHMED *et al.* 2001; GARCIA-MUSE AND BOULTON 2005). Although *atm-1* also appears to be required for cell cycle arrest and apoptosis in response to irradiation (IR), its requirement appears to be dose-dependent (GARCIA-MUSE AND BOULTON 2005; STERGIOU *et al.* 2007). Interestingly, *atm-1* progeny survival following IR is only affected at higher doses ((JONES *et al.* 2012) and Chapter 3), suggesting that *atm-1* is either non-essential in the DNA damage response or redundant with other factors up to a certain threshold.

1.1.3 DNA repair mechanisms

Different repair mechanisms have evolved to handle the various types of DNA lesions. They can be broadly grouped into three categories: excision repair, encompassing base excision repair (BER), nucleotide excision repair (NER), and mismatch repair (MMR); strand break repair, encompassing homologous recombination (HR) and non-homologous end-joining (NHEJ); and

damage tolerance, encompassing translesion synthesis (TLS). A simplified overview of each pathway is shown in Figure 1, and introduced below. Although meiotic HR is the subject of this dissertation, the other DNA repair pathways are mentioned to further emphasize the importance of maintaining genome stability. HR as pertains to *C. elegans* meiosis I is discussed in more detail in Section 1.3.

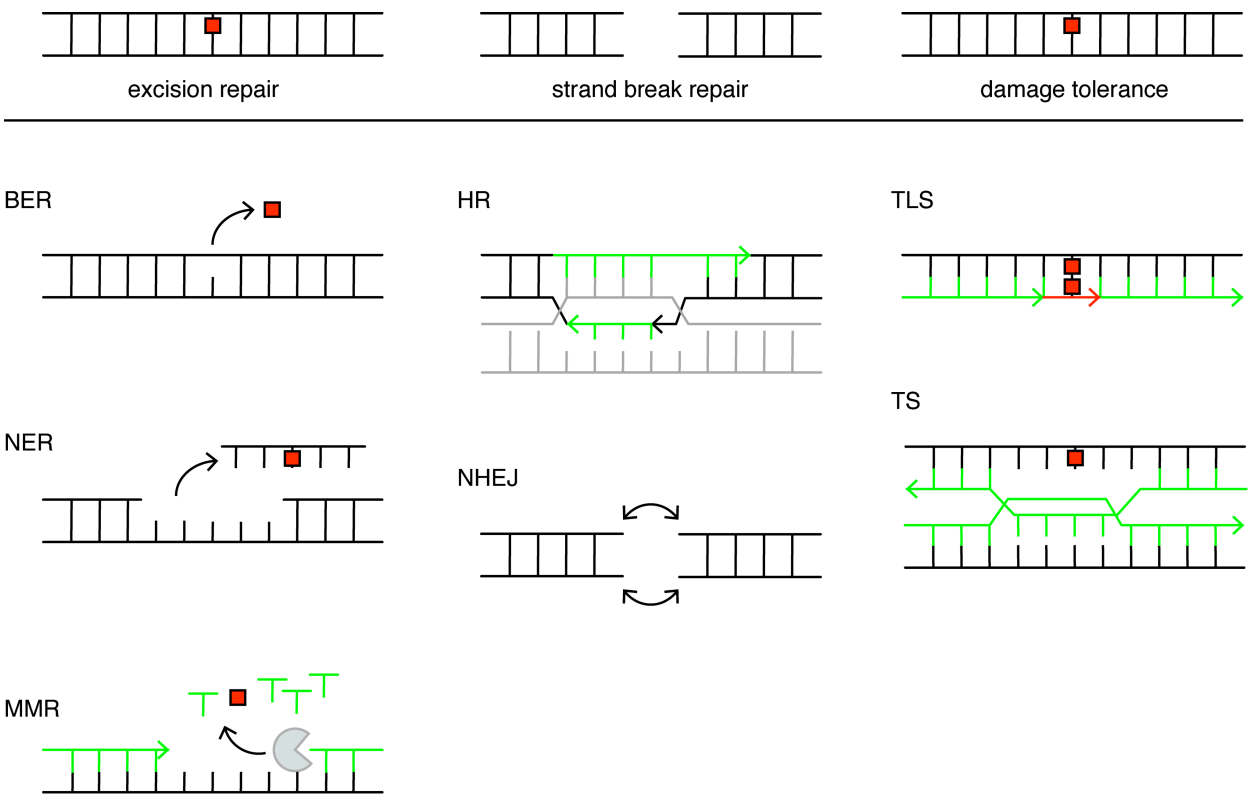

Figure 1. Overview of DNA repair mechanisms: Cartoons illustrate the defining characteristic of excision repair pathways (BER, NER, MMR), strand break repair pathways (HR, NHEJ), and damage tolerance (TLS, TS). Red square, DNA damage; green arrows and lines, DNA synthesis; Gray sector, Exo1. Gray DNA in HR represents homologous DNA.

1.1.3.1 Base excision repair Base excision repair (BER) is the primary repair mechanism for alkylation damage and spontaneous alterations in DNA base chemistry. Repair involves removal of the damaged base, followed by cleavage of the sugar-phosphate backbone. DNA synthesis replaces the missing nucleotide, and DNA ligase seals the nick (reviewed in (KROKAN AND BJORAS 2013)).

1.1.3.2 Nucleotide excision repair Nucleotide excision repair (NER) is the primary repair mechanism for bulky single-stranded DNA adducts, such as cyclopyrimidine dimers (CPDs) and 6-4 photoproducts. Repair involves removal of 21-22 nt DNA around the damage site including the sugar-phosphate backbone, followed by DNA synthesis using the undamaged strand as a template (reviewed in (SCHARER 2013)).

1.1.3.3 Mismatch repair Mismatch repair (MMR) is the primary repair mechanism for errors made during DNA replication. These errors can include incorporation of an incorrect DNA base, or insertion/deletion of sequence due to DNA secondary structure or DNA polymerase slippage. Repair involves exonucleolytic removal of newly-synthesized bases including the mispaired base(s), followed by DNA synthesis (reviewed in (LI 2008)).

1.1.3.4 Homologous recombination Homologous recombination (HR) is a mechanism to repair DNA double-strand breaks (DSBs). Repair involves resection of DNA flanking the break to create a 3' overhang that invades homologous DNA to use as a template for DNA synthesis. Depending on how the structure formed during HR is resolved, genetic information can be exchanged between the DNA molecules. Because a homologous DNA sequence is used as a

repair template, HR is considered a high-fidelity mechanism for repairing DSBs (reviewed in (KREJCI *et al.* 2012)).

1.1.3.5 Non-homologous end-joining Non-homologous end-joining (NHEJ) is another mechanism to repair DSBs. In contrast to HR, repair of DSBs by NHEJ does not require the presence of a homologous DNA template. Instead, the broken DNA ends are ligated back together with minimal processing. Because there is no undamaged homologous DNA to serve as a correct template, repair by NHEJ can result in errors, such as insertions/deletions (LIEBER 2010). Variations on NHEJ include alternative-NHEJ, which relies on microhomology at the terminal ends and can occur independently of the classical NHEJ factors (BENNARDO *et al.* 2008; LIEBER 2010).

1.1.3.6 Translesion synthesis Translesion synthesis (TLS) is a form of damage tolerance, which allows a cell to avoid death as a result of unrepaired DNA damage. Upon encountering DNA damage during DNA replication, specialized DNA polymerases insert nucleotides opposite the DNA lesion, leaving the lesion in place. Depending on the affinity of the translesion DNA polymerase for the specific lesion, TLS can be error-free or error-prone. Alternatively, damage can be tolerated by template switching (TS), in which the stalled nascent strand uses the newly-synthesized sister strand as a template to replicate past the lesion (reviewed in (BI 2015)).

1.1.4 Induction of apoptosis

In *C. elegans* germ cells, there are at least two forms of apoptosis: physiological death, which occurs under normal conditions and is hypothesized to serve a "nurse cell" function to non-

apoptotic oocytes by providing extra macromolecules required for oocyte growth (GUMIENNY *et al.* 1999); and DNA damage-induced germ cell death, which relies on the same core apoptotic machinery as physiological germ cell death but has distinct genetic triggers (GARTNER *et al.* 2000; GARTNER *et al.* 2008). CEP-1, the *C. elegans* homolog of p53, is uniquely required for DNA damage-induced apoptosis (DERRY *et al.* 2001; SCHUMACHER *et al.* 2001) through the transcriptional induction of *egl-1* following DNA damage (HOFMANN *et al.* 2002). EGL-1, in turn, binds to CED-9, freeing CED-4 to activate the caspase CED-3, thereby inducing apoptosis (CONRADT AND HORVITZ 1998; DOERFLINGER *et al.* 2015). HUS-1 is also required for CEP-1-dependent *egl-1* expression, though HUS-1 is not uniquely required for DNA damage-induced apoptosis (HOFMANN *et al.* 2002).

Although unrepaired DSBs from IR (or other exogenous sources of damage) and unrepaired DSBs from failure to complete meiotic HR have similar outcomes, there appears to be a genetic distinction between DNA damage-induced apoptosis in response to IR and apoptosis induced by persistent/unrepaired recombination intermediates. *chk-2* is not required for the former scenario; it is required for the latter (MACQUEEN AND VILLENEUVE 2001). Failure to complete meiotic HR, whether by defects in chromosome pairing, synapsis, or the process of DSB repair itself, also triggers apoptosis.

1.1.5 Consequences of deficiencies in the DNA damage response

1.1.5.1 Somatic cells Deficiencies in DNA repair capacity are overwhelmingly associated with cancer in mammals (NEGRINI *et al.* 2010; O'DRISCOLL 2012; DIETLEIN *et al.* 2014). Some disorders resulting from defective responses to DNA damage induce degrees of accelerated aging, such as XFE progeria, Cockayne syndrome, Werner syndrome, Bloom syndrome,

Rothmund-Thomson syndrome, trichothiodystrophy, Hutchinson-Gilford progeria syndrome, and ataxia telangiectasia (O'DRISCOLL 2012; ZHANG *et al.* 2014).

In *C. elegans*, somatic cells neither exhibit checkpoint signaling nor undergo apoptosis in response to DNA damage, although they do retain the ability to repair damaged DNA (GARTNER *et al.* 2000; VERMEZOVIC *et al.* 2012). The imbalance in DNA damage-induced checkpoint signaling between somatic and germ cells in *C. elegans* may reflect an evolutionary strategy to invest resources in reproductive capacity, as germ cells continue to proliferate in adulthood (HIRSH *et al.* 1976; VERMEZOVIC *et al.* 2012). Consequently, this dissertation will focus on DNA damage-induced signaling and repair in germ cells only.

1.1.5.2 Germ cells Germ cells are a specialized class of cells that are involved in reproduction. Germ cells are diploid and self-renew through mitosis, but they can also give rise to haploid gametes through meiosis. During meiosis, chromosomes undergo one round of DNA replication followed by two cell divisions. In the first cell division (meiosis I), homologous chromosomes segregate to opposite poles in a reductional division. In the second cell division (meiosis II), the sister chromatids segregate to opposite poles in an equational division. The end result is four products that contain half of the genetic material needed for that particular organism. During sexual reproduction, haploid gametes from each parent combine their genetic material to create the full genetic complement needed for life. Errors in germ cell DNA, then, can be passed on to offspring. The effect can be innocuous, such as a random mutation that does not alter gene function, to fatal, if essential genes or parts of chromosomes are disrupted.

Ironically, maintaining genome integrity in germ cell DNA requires DNA damage. During meiosis I, homologous chromosomes pair and exchange genetic information in a process called crossing over. Crossover (CO) formation initiates with a DSB purposefully induced by the

topoisomerase-like SPO-11 (KEENEY *et al.* 1997; DERNBURG *et al.* 1998), followed by HR repair. COs increase genetic diversity by mixing maternal and paternal genes; but more importantly, COs create a physical link between homologous chromosomes required for proper alignment on the metaphase plate and subsequent separation into daughter cells (COLE *et al.* 2010). Failure to faithfully form COs can result in aneuploidy in resultant gametes, which has few viable outcomes (HASSOLD AND HUNT 2001). Thus, the process of CO formation during meiosis I is highly regulated, with factors ensuring that each chromosome pair receives at least one DSB and repairs it as a CO.

Unsurprisingly, HR factors are critical to forming meiotic COs; indeed, many DNA repair mutants are also sterile (MUKHERJEE *et al.* 2010; GUNES *et al.* 2015; OKTAY *et al.* 2015). However, additional classes of factors are involved in CO assurance – factors involved in homolog pairing and synapsis, DSB formation and damage sensing, and chromatin factors – and deficiencies in such factors result in similar phenotypic outcomes (BAILLET AND MANDON-PEPIN 2012). Thus, any factor that insures faithful DNA repair and accurate segregation of chromosomes during meiosis I can be said to maintain genome stability.

1.2 *CAENORHABDITIS ELEGANS* AS A MODEL SYSTEM

1.2.1 General advantages of *C. elegans* as a model system

The free-living nematode *Caenorhabditis elegans* was developed into a genetic model nearly 50 years ago by Sydney Brenner, who wanted to use eukaryotic molecular biology to better understand development, particularly that of the nervous system (BRENNER 1974). His work

established a legacy of a strong community of researchers, with more than a thousand laboratories using *C. elegans* as a model organism today (CORSI *et al.* 2015).

C. elegans offers several key advantages for research. Adults are small (1 mm in length) and easily maintained on agar plates seeded with a non-pathogenic strain of *Escherichia coli*. Their life cycle progresses from egg through 4 larval stages to fertile adult in approximately 3.5 days at 20°C, and all developmental stages can be viewed under a dissecting microscope. The *C. elegans* genome was the first metazoan genome to be completely sequenced (CONSORTIUM 1998), and can be modified both randomly by chemical mutagenesis (BRENNER 1974; KUTSCHER AND SHAHAM 2014) and purposefully by CRISPR/Cas9 (DICKINSON *et al.* 2013) to identify key genes involved in a variety of biological processes (CORSI *et al.* 2015). More than 7,000 *C. elegans* genes have human orthologs, including those associated with human disease, making *C. elegans* an attractive genetic model with applications to human physiology (CULETTO AND SATTELLE 2000; KALETTA AND HENGARTNER 2006; SHAYE AND GREENWALD 2011).

1.2.2 Organization of the *C. elegans* germ line

The initial appeal of *C. elegans* as a model system was due to their relatively low number of neurons compared to other model organisms (BRENNER 1974). However, the organization of the *C. elegans* germ line also makes it an advantageous model for studying meiosis (Figure 2). The germ line is housed in two symmetrical U-shaped gonad arms that take up most of the *C. elegans* body. The germ line is spatially and temporally organized such that the stages of meiotic prophase I – and integrity thereof – can be readily distinguished by DNA morphology. The zones of the germ line and their corresponding stages of meiotic prophase are described in more detail below (for a full review, see (LUI AND COLAIACOVO 2013)).

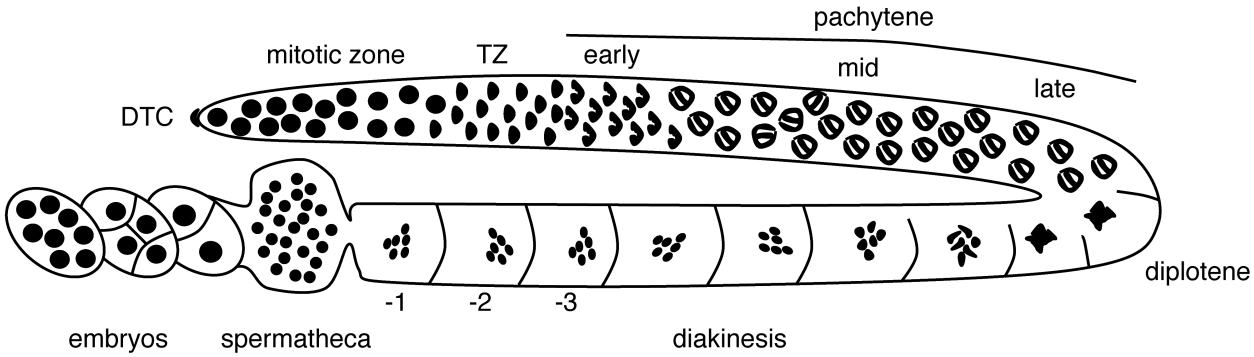

Figure 2. Organization of the *C. elegans* germ line: Schematic showing one gonad arm of an adult hermaphrodite. The nuclei are represented as they appear when stained with 4'-6-diamidino-2-phenylindole (DAPI) and visualized by compound microscopy. The germ line exhibits distal-proximal polarity; the mitotic zone marks the distal end of the germ line, while diakinesis marks the proximal end. Stages of meiotic prophase I beginning with the transition zone (TZ) are indicated, and described in more detail in the text. Diakinesis oocytes closest to the spermatheca are the most mature. Following diakinesis, the oocytes are fertilized, complete meiosis, and begin embryogenesis.

1.2.2.1 Mitotic Zone The most distal end of the germ line contains a population of stem cells. Here, the somatic distal tip cell (DTC) promotes nearby germ cells to proliferate mitotically via GLP-1/Notch signaling (KIMBLE AND WHITE 1981; KIMBLE AND SIMPSON 1997; CRITTENDEN *et al.* 2003).

Nuclei immediately adjacent to the transition zone are in meiotic S phase, which is distinct from mitotic S phase in several ways: first, meiotic S is estimated to take twice as long as mitotic S (JARAMILLO-LAMBERT *et al.* 2007); second, the meiosis-specific cohesion and axis factors, including REC-8 and HIM-3, respectively, are loaded onto chromosomes during meiotic S (ZETKA *et al.* 1999; PASIERBEK *et al.* 2001; JARAMILLO-LAMBERT *et al.* 2007); third, meiotic S appears to be coupled to programmed DSB formation (JARAMILLO-LAMBERT *et al.* 2007).

1.2.2.2 Transition Zone The transition zone (TZ) encompasses the leptotene and zygotene stages of meiotic prophase I, the entry of which is marked by GLD-1-dependent repression of *glp-1* expression (MARIN AND EVANS 2003). Transition zone nuclei are easily identified by the crescent-shaped appearance their DNA makes as chromosomes cluster at the nuclear periphery and establish connections to both the cytoplasmic microtubule network via the nuclear membrane-spanning SUN/KASH domain proteins and to their homolog through pairing centers (ZICKLER AND KLECKNER 1998; MACQUEEN *et al.* 2005; SATO *et al.* 2009). Polymerization of the synaptonemal complex (SC) begins at or near pairing centers and extends along the length of the paired chromosomes (ROG AND DERNBURG 2015). Programmed DSB formation initiated by SPO-11 begins in this stage, evidenced by a few (1-2) RAD-51 foci in some TZ nuclei (DERNBURG *et al.* 1998; ALPI *et al.* 2003). Unlike other organisms, SC assembly is independent of SPO-11 activity (DERNBURG *et al.* 1998).

1.2.2.3 Pachytene Pachytene can be further subdivided into three stages – early, mid, and late. Nuclei are identified by progression from crescent-shaped to thread-shaped as chromosomes continue to thicken and distribute themselves more evenly throughout the nucleus. SPO-11-induced DSB formation peaks in early- to mid-pachytene based on RAD-51 foci dynamics (ALPI *et al.* 2003). Although the process of homologous recombination will be discussed in detail in a later section (Section 1.3), it should be noted here that one DSB per chromosome pair must be repaired by HR during pachytene in a way that results in a crossover (CO). By the onset of pachytene, chromosomes are fully synapsed, though the SC begins to disassemble in late pachytene around the CO (MACQUEEN *et al.* 2005; NABESHIMA *et al.* 2005).

1.2.2.4 Diplotene Diplotene corresponds to the loop formed as the gonad arm swings inward toward the vulva. Chromosomes condense, and undergo structural remodeling around the CO formed on every homolog pair. Because COs preferentially occur on the terminal thirds of the chromosomes (BARNES *et al.* 1995; WAGNER *et al.* 2010; MENEELY *et al.* 2012), this reconfiguration results in a cruciform structure with long arms that are marked by axis components REC-8 and HIM-3, and short arms that retain SC markers (NABESHIMA *et al.* 2005). Approximately half of all germline nuclei are culled by physiological germ cell death at this point (GUMIENNY *et al.* 1999).

1.2.2.5 Diakinesis The most proximal end of the germ line corresponds to diakinesis, the final stage of meiotic prophase I. As the developing oocytes move toward the spermatheca and fertilization, the chromosomes condense further until they are maximally condensed at the most mature (-1) oocyte (Figure 2). Here, we can determine how well HR and CO formation went by examining the number and appearance of DAPI-staining bodies. In wild-type germ lines, we expect to see six DAPI-staining bodies corresponding to six pairs of homologous chromosomes held together by their chiasma (bivalents). If a pair of homologous chromosomes has not formed a chiasma, they will separate from one another and appear as two smaller DAPI-staining bodies (univalents).

1.2.3 Indicators of genome instability in *C. elegans*

Populations of *C. elegans* exist primarily as self-fertilizing hermaphrodites with two X chromosomes; rare nondisjunction of the X chromosome (<0.2% in wild type) results in viable

males with a single X chromosome (XO). Nondisjunction of autosomes, by contrast, is lethal in most cases and can be ascertained by the presence of unhatched eggs (HODGKIN *et al.* 1979; HODGKIN 1987).

The morphology of chromosomes at diakinesis coupled with the hatching and male frequencies of a strain provide readouts of DSB formation and the quality of repair (Figure 3). Diakinesis nuclei can be analyzed by confocal microscopy in whole-mounted worms that have been fixed in Carnoy's solution (66% ethanol, 33% acetic acid, 1% chloroform) and stained with 4'-6-diamidino-2-phenylindole (DAPI) (KAPUSCINSKI 1995).

When every chromosome pair receives at least one programmed DSB (complete DSB formation), and one DSB per chromosome pair is repaired as an interhomolog CO, the result is six DAPI-staining bodies corresponding to six pairs of homologous chromosomes (five pairs of autosomes and one pair of sex chromosomes) held together by chiasma at diakinesis (bivalents). Nearly all eggs laid by such hermaphrodites will hatch and develop into normal hermaphrodites (Figure 3, green box).

When programmed DSB formation is absent, such as in a *spo-11* mutant, no COs are formed, resulting in 12 DAPI-staining bodies corresponding to unpaired homologous chromosomes (univalents). Nearly all eggs laid by such hermaphrodites will fail to hatch due to random chromosome segregation (Figure 3, red box), although a small percentage of embryos will be viable since *C. elegans* only has six pairs of chromosomes to segregate.

When programmed DSB formation is incomplete (i.e. not every chromosome pair receives a DSB), a mix of univalents and bivalents are observed at diakinesis. Progeny survival depends on the chromosomes affected: if the unpaired chromosome is an autosome, some embryos will be aneuploid and will not hatch (Figure 3, orange box); if the unpaired

chromosome is the X chromosome, embryos will hatch but some will develop as males (Figure 3, blue box), while a much smaller percentage be XXX, slightly Dumpy hermaphrodites (CORTES *et al.* 2015).

It is important to note that observing univalents at diakinesis does not automatically imply failure in DSB formation. For example, SC mutants (*syp-1*, *syp-2*, *syp-3*, *syp-4*) have wild-type competency for DSB formation, yet exhibit near-total embryonic lethality due to an inability to form interhomolog COs (MACQUEEN *et al.* 2002; COLAIACOVO *et al.* 2003; SMOLIKOV *et al.* 2007a; SMOLIKOV *et al.* 2009). Introduction of exogenous DSBs by low doses of IR permits discrimination between univalents resulting from lack of DSB formation and univalents resulting from failure to repair DSBs as COs. In the former case, IR-induced DSBs will restore bivalent formation, suggesting that programmed DSB formation is deficient but downstream CO-promoting factors are functional; in the latter case, IR-induced DSBs will fail to restore bivalent formation, suggesting that CO formation is defective downstream of programmed DSB formation. In more complicated instances, the observation of chromatin abnormalities at diakinesis following IR-induced DSB formation suggests involvement for a factor in both promoting DSB formation and HR repair. Due to the lack of DSB-specific markers in *C. elegans*, such as γH2AX (SEDELNIKOVA *et al.* 2002), it is difficult to conclusively determine if factors are required for DSB formation or RAD-51 loading following DSB formation. However, a comparison of RAD-51 foci with DSBs labeled by the TUNEL assay showed nearly complete overlap during pachytene (METS AND MEYER 2009), suggesting a strong propensity for most (if not all) DSBs to be shuttled into HR-mediated repair.

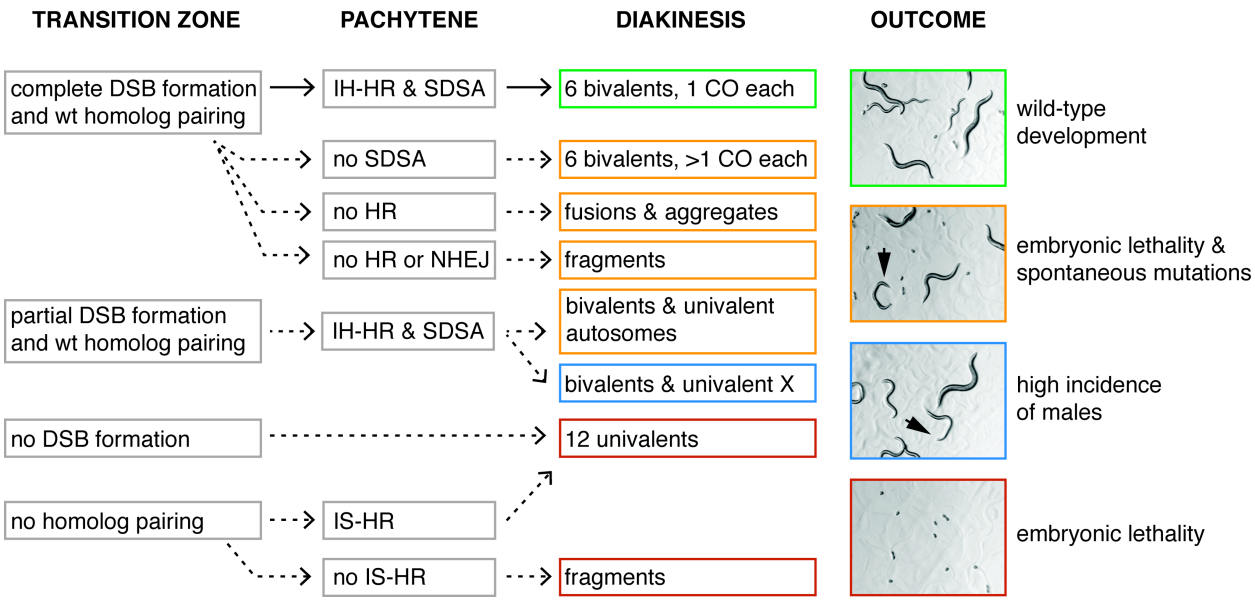

Figure 3. Indicators of genome instability in meiosis I prophase: Diagram depicting the consequences of defects in homolog pairing, DSB formation, and DNA repair during different stages of meiotic prophase I. Note that not all combinations are shown. Solid arrows represent wild-type progression of all processes. Homologous chromosome pairing and DSB induction occurs in the transition zone. During pachytene, DSB repair by IH-HR (interhomolog homologous recombination) and SDSA (synthesis-dependent strand annealing) yields 6 bivalents held together by one CO at diakinesis, resulting in normal hatching and development (green box). Dashed arrows depict deviations from wild type. In the absence of SDSA, additional COs are formed by IH-HR, which can lead to genome instability (orange box, (Ward et al. 2010)). Incomplete DSB induction or deficiencies in DSB repair manifest as increased embryonic lethality and the appearance of spontaneous mutations (orange box, arrow). However, failure of the X chromosome to receive a CO results in a viable *h*igh *i*ncidence of *m*ales phenotype (blue box, arrow). Defects in either DSB formation or homolog pairing result in near-total embryonic lethality due to aneuploidy, evidenced by unhatched eggs (red box). Figure adapted from (Lans and Vermeulen 2015). Photos taken by TB McClendon.

Defects in DSB repair, or utilization of non-HR repair pathways, such as NHEJ, can manifest as decondensed chromatin, DNA fragments, and chromosome aggregates in diakinesis nuclei. Progeny survival will be low, and progeny that do hatch may exhibit overt spontaneous mutations (e.g. appearance, movement) (Figure 3, orange box).

1.3 HOMOLOGOUS RECOMBINATION IN *C. ELEGANS* MEIOSIS I

1.3.1 Overview

This section will discuss specific steps of HR as pertains to *C. elegans* meiosis. Worm-specific factors and functions are used when possible. A model of HR is shown in Figure 4.

1.3.2 Programmed DSB formation

The initial step in HR is the induction of a DSB by the topoisomerase-like SPO-11 (KEENEY *et al.* 1997; DERNBURG *et al.* 1998). A pair of SPO11 monomers attacks the phosphodiester backbone of each DNA strand in a reaction that covalently links the protein and the 5' terminal strand and generates a 3' OH terminus (DE MASSY *et al.* 1995; KEENEY AND KLECKNER 1995; LIU *et al.* 1995; KEENEY *et al.* 1997). The nuclease MRE-11 has also been implicated in meiotic DSB formation (CHIN AND VILLENEUVE 2001; RINALDO *et al.* 2002). Other factors required for DSB formation in various roles include *him-17* (REDDY AND VILLENEUVE 2004), *dsb-1* (STAMPER *et al.* 2013) and *dsb-2* (ROSU *et al.* 2013), *rad-50* (HAYASHI *et al.* 2007) and *htp-3*

(GOODYER *et al.* 2008). Interestingly, two factors, *xnd-1* and *him-5*, seem to be required for DSB formation specifically on the X chromosome (WAGNER *et al.* 2010; MENEELY *et al.* 2012).

1.3.3 Resection and commitment to homologous recombination repair

Following DSB induction, DNA flanking the break is resected by MRE-11, an action that may also remove SPO-11 (CHIN AND VILLENEUVE 2001; LEMMENS *et al.* 2013; YIN AND SMOLIKOVE 2013). Studies in yeast have suggested that MRE11 creates a single-stranded DNA nick up to 300 bp downstream of the 5'-end of the DSB, then resects 3'→5' toward the DSB (GARCIA *et al.* 2011). COM-1 channels meiotic DSBs into HR by blocking Ku activity (a heterodimer encoded by *cku-70* and *cku-80*), which promotes repair by NHEJ (LEMMENS *et al.* 2013). The 5'→3' exonuclease EXO-1 is proposed to have a lesser, or redundant, role in resection, as *exo-1* mutants are competent for bivalent formation so long as MRE-11 and COM-1 are functional (LEMMENS *et al.* 2013). Resection exposes 3' single-stranded (ss) DNA overhangs, which are first coated by RPA, then replaced by RAD-51 in a BRC-2-dependent manner (MARTIN *et al.* 2005; PETALCORIN *et al.* 2007).

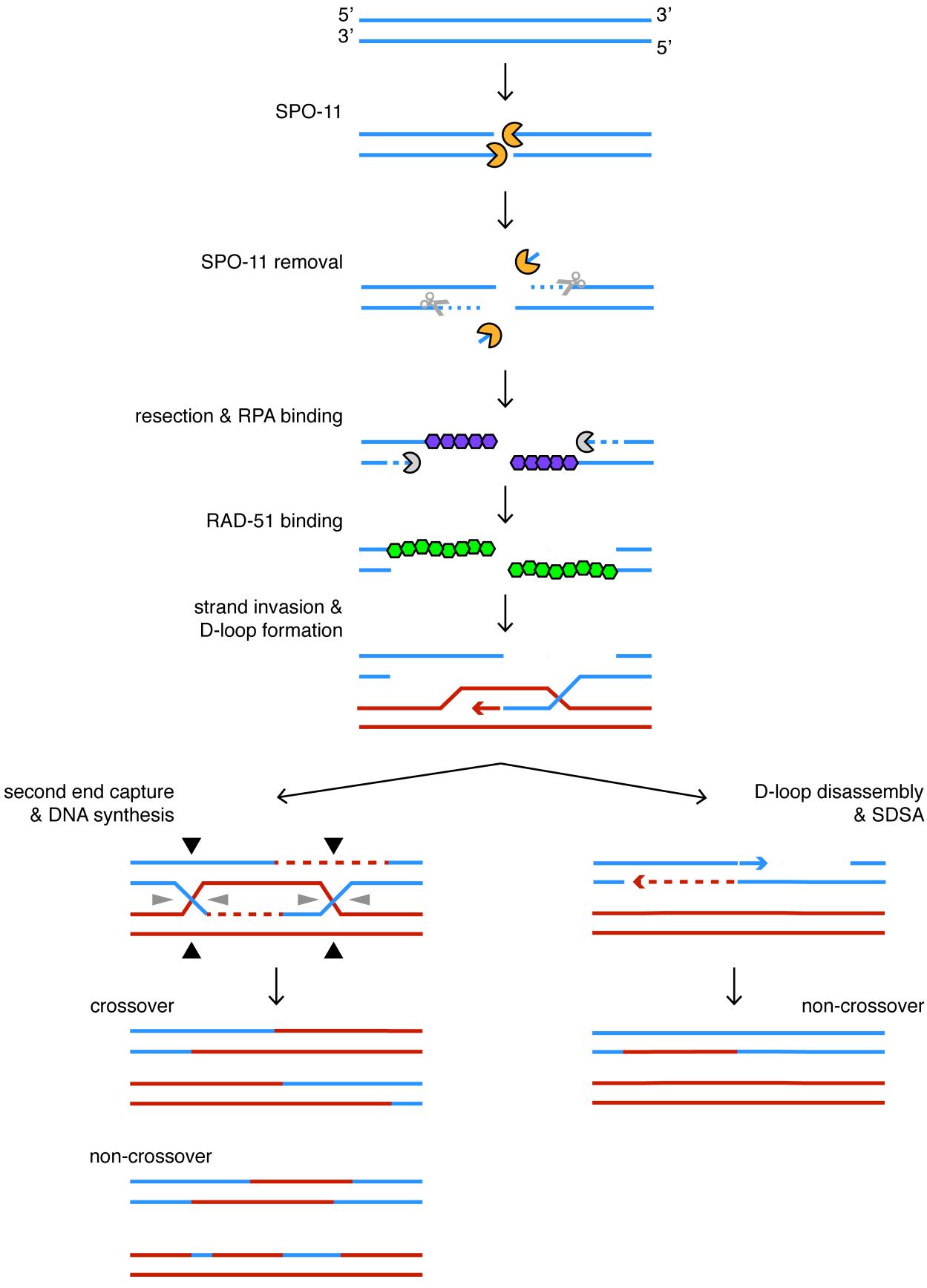
5’
3’
3’
5’
SPO-11
SPO-11 removal
resection & RPA binding
RAD-51 binding
strand invasion &
D-loop formation
second end capture
& DNA synthesis
D-loop disassembly
& SDSA
crossover
non-crossover
non-crossover

Figure 4. Homologous recombination during meiosis I: Model depicts the process of homologous recombination during meiosis I prophase. Maternal and paternal homologous chromosomes are shown in blue and red. A DSB is formed by SPO-11 nuclease (gold sector). MRE-11 (scissors) creates a ssDNA nick for SPO-11 removal. Resection of the DNA flanking the break (gray sector) creates 3' ssDNA overhangs that are coated with RPA (purple hexagons), then RAD-51 (green hexagons). RAD-51 is removed following strand invasion, though not shown here for simplicity. If the D-loop is displaced, repair continues by synthesis-dependent strand annealing (SDSA). If the D-loop is not displaced, DNA synthesis proceeds to second-end capture, forming a double Holliday junction (dHJ). The actions of dHJ resolvases (black and gray arrowheads) determine whether the end product will be a crossover (CO) or non-crossover (non-CO).

1.3.4 Strand invasion

RAD-51 forms nucleoprotein filaments on 3' ssDNA overhangs and engages in homology search and strand invasion. Although RAD-51 is capable of carrying out these tasks alone *in vitro* (GAINES *et al.* 2015; TAYLOR *et al.* 2015), it is unable to do so *in vivo* and is assisted by additional factors that bear structural resemblance to RAD-51 and are referred to as RAD-51 paralogs. In *C. elegans*, there are two known RAD-51 paralogs, *rfs-1* and the recently discovered *rip-1* (WARD *et al.* 2007; TAYLOR *et al.* 2015). Although not a RAD-51 paralog itself, *helq-1* functions in at least partially overlapping roles with *rfs-1* and *rip-1* in early steps of HR (WARD *et al.* 2010; TAYLOR *et al.* 2015). RAD-51 filaments are "trapped" in a *rad-54* mutant, suggesting that, like its yeast ortholog, RAD-54 is required for strand exchange activity (METS AND MEYER 2009; MAZIN *et al.* 2010). The invading RAD-51 filament displaces the non-template homologous strand, forming a displacement loop (D-loop). DNA synthesis begins using the non-displaced strand as a template (SZOSTAK *et al.* 1983).

The placement of *rfs-1*, *rip-1*, and *helq-1* function in relation to RAD-51-mediated strand invasion is not yet clear. Biochemical data with purified proteins suggest that RFS-1 and RIP-1 do not promote RAD-51 filament formation, as the RAD51 paralogs in *S. cerevisiae* do (SASANUMA *et al.* 2013; GAINES *et al.* 2015); rather, RFS-1 and RIP-1 remodel the RAD-51 pre-synaptic filament to a more flexible conformation necessary for strand invasion (TAYLOR *et al.* 2015). However, genetic analysis with the anti-recombinase *rtel-1* suggests that both *helq-1* and *rfs-1* function post-strand invasion (WARD *et al.* 2010). Based on the binding affinities of RFS-1/RIP-1 and HELQ-1 for ss- and dsDNA, respectively (WARD *et al.* 2010; TAYLOR *et al.* 2015), it is possible that RFS-1/RIP-1 hand off the RAD-51 filament to HELQ-1 at the strand invasion step.

In *S. cerevisiae*, mice, and humans, a complex comprised of RAD51 paralogs and a SWIM domain-containing protein (the Shu complex) promotes HR by stimulating RAD51 filament formation and strand invasion (GODIN *et al.* 2013; GAINES *et al.* 2015). Evolutionary analysis of the SWIM domain led to the identification of *C. elegans sws-1*, predicted to be the homolog of *S. cerevisiae* Shu2 (GODIN *et al.* 2015). Research concerning the putative role of *sws-1* in HR is discussed in Chapter 2.

1.3.5 Crossover designation

Failure to form one CO between homologous chromosomes is detrimental to maintaining proper ploidy in gametes; however, studies in *S. cerevisiae* RecQ helicase mutant *sgs1* suggest that too many COs are harmful as well (WATT *et al.* 1995). More DSBs are made than will ultimately become COs (MARTINEZ-PEREZ AND COLAIACOVO 2009; METS AND MEYER 2009; COLE *et al.* 2010). Therefore, additional factors are needed to select which DSBs will be committed to CO

repair, and which DSBs will be repaired as non-COs. In *C. elegans*, nearly all COs are formed using a MSH-4-MSH5 (MutS)-dependent pathway (ZALEVSKY *et al.* 1999). MSH-5 foci first appear in mid-pachytene in excess of eventual COs, then decrease to 6 foci per nucleus (YOKOO *et al.* 2012), suggesting that MutS stabilizes select recombination intermediates consistent with the proposed role of human MSH4-MSH5 (COLAIACOVO *et al.* 2003; SNOWDEN *et al.* 2004). Proper localization of MSH-5 to a single focus per chromosome is interdependent on two other CO designation factors, ZHP-3 and COSA-1; consequently, *msh-5*, *zhp-3*, and *cosa-1* mutants share meiotic phenotypes (ZALEVSKY *et al.* 1999; KELLY *et al.* 2000; JANTSCH *et al.* 2004; YOKOO *et al.* 2012). ZHP-3 localization is initially non-uniformly distributed along the length of the SC in early- and mid-pachytene, and becomes restricted to a single focus per chromosome in late pachytene/early diplotene (BHALLA *et al.* 2008). COSA-1 localizes to 6 foci beginning in late pachytene and persists through diplotene; COSA-1 does not colocalize with RAD-51, suggesting that COSA-1 is loaded after RAD-51 disassembly from DNA (YOKOO *et al.* 2012). The changing localization patterns of MSH-5 and ZHP-3 and eventual colocalization with COSA-1 suggest that the CO site is chosen by the end of mid-pachytene (YOKOO *et al.* 2012).

The decision to repair a DSB as a non-CO can be made early in the repair process. Following D-loop formation, DNA synthesis continues until the second end of the break is captured, forming a double Holliday junction (dHJ) (LUI AND COLAIACOVO 2013). If the D-loop is dissociated prior to second-end capture, repair is completed by synthesis-dependent strand annealing (SDSA), in which the extended single-strand is annealed to the other break end, followed by DNA synthesis to fill the gap (SUNG AND KLEIN 2006). RTEL-1 dissociates D-loops *in vitro*; *in vivo*, *rtel-1* mutants exhibit increased CO frequency consistent with its conserved role as an anti-recombinase (BARBER *et al.* 2008; YOUDS *et al.* 2010). *rtel-1* mutants also have

reduced broods (WARD *et al.* 2010), supporting the notion that too many COs are detrimental. *him-6*, the *C. elegans* homolog of RECQ helicase *BLM*, has D-loop dissociation activity *in vitro*; however, its *in vivo* role suggests a more complicated role in promoting CO formation (SCHVARZSTEIN *et al.* 2014).

1.3.6 Double Holliday junction resolution

The last step of meiotic HR is resolution of the dHJ by structure-specific endonucleases to yield either a CO or non-CO product. In *C. elegans*, genetic data has suggested that there are two redundant pathways for dHJ resolution, both of which require the function of the scaffold factor *him-18/slx-4*: nucleases *mus-81* and *slx-1* operate in one pathway, and nucleases *xpf-1* and *him-6* operate in the other (SAITO *et al.* 2009; AGOSTINHO *et al.* 2013; SAITO *et al.* 2013). Consistent with their roles in dHJ resolution, nuclease mutants exhibit chromatin bridges associated with unresolved recombination intermediates that are more pronounced when multiple nucleases are absent (AGOSTINHO *et al.* 2013; O'NEIL *et al.* 2013; SAITO *et al.* 2013). Although *gen-1* has resolvase activity *in vitro*, its phenotype is mild unless combined with deficiencies in other nucleases (BAILLY *et al.* 2010; SAITO *et al.* 2013). COs still form even in the absence of *mus-81;slx-1;xpf-1;gen-1* mutants, suggesting that there are still unidentified dHJ-resolvases in the *C. elegans* germ line (SAITO *et al.* 2013).

1.3.7 The role of chromatin in meiotic HR

It is simplistic to consider DNA-dependent processes outside of the context of chromatin, a complex of DNA and proteins. The fundamental unit of chromatin is the nucleosome, composed

of a histone octamer (two each of histones H2A, H2B, H3, and H4) and ~146 bp of DNA (KORNBERG 1974; LUGER *et al.* 1997). Histones are highly basic proteins with flexible N-terminal "tails" that can be covalently modified by a variety of post-translational modifications (PTM, histone marks), including acetylation, methylation, phosphorylation, sumoylation, ubiquitylation, ADP ribosylation, deamination, and proline isomerization (KOUZARIDES 2007). The type, placement, and abundance of these marks confers exquisite variation in regulating DNA-dependent processes (JENUWEIN AND ALLIS 2001).

There is evidence that chromatin structure influences DSB formation. *cra-1* promotes global histone acetylation by antagonizing the acetyl-CoA hydrolase ACER-1 (GAO *et al.* 2015). *cra-1* mutants exhibit decreased DSBs evidenced by fewer RAD-51 foci during pachytene that is reversed by injection of Trichostatin A (TSA), a histone deacetylase inhibitor (GAO *et al.* 2015). Interestingly, *xnd-1* mutants, which exhibit an increase in acetylation of lysine 5 on histone H2A specifically (H2AK5ac), form fewer DSBs based on RAD-51 focus formation, as well as change where recombination occurs on the chromosomes (WAGNER *et al.* 2010; MENEELY *et al.* 2012; GAO *et al.* 2015). Loss of *him-17* affects normal accumulation of histone H3 dimethylation at lysine 9 (REDDY AND VILLENEUVE 2004), though it is unclear how this modification is linked to DSB formation (BESSLER *et al.* 2010). In yeast and mice, DSB formation occurs at specific regions of the genome called hotspots that are enriched with histone H3 trimethylation at lysine 4 (H3K4me3), a mark that is also associated with transcriptionally-active chromatin (BORDE *et al.* 2009; BUARD *et al.* 2009; SMAGULOVA *et al.* 2011). In mice, an additional level of hotspot determination is conferred by the histone H3 methyltransferase PRDM9, which directs recombination away from promoter-associated H3K4me3 (BRICK *et al.* 2012; WU *et al.* 2013). Despite a propensity for recombination in the terminal thirds of the chromosome arms (BARNES

et al. 1995; MENEELY *et al.* 2002), there is not conclusive evidence for DSB hotspots in the *C. elegans* germ line (KAUR AND ROCKMAN 2014).

DSB formation induces a multitude of changes in the chromatin structure. Very little is known about how histone PTMs affect HR in the *C. elegans* germ line. It has been shown that failure to demethylate H3K4me2 following DSB induction is associated with decreased survival (NOTTKE *et al.* 2011). Another study has suggested that H2AK5ac is removed in pachytene nuclei after IR exposure, and then replaced following repair (COUTEAU AND ZETKA 2011).

In contrast, the role of histone PTMs in HR has been extensively studied in other organisms (reviewed in (LUIJSTERBURG AND VAN ATTIKUM 2011; DEEM *et al.* 2012)). Chromatin undergoes decondensation both locally and globally in response to DSBs (BAKKENIST AND KASTAN 2003; KRUHLAK *et al.* 2006; DELLAIRE *et al.* 2009). The relaxed chromatin structure facilitates the activation and recruitment of ATM, which phosphorylates the histone variant H2AX on serine 139 to form γH2AX (ROGAKOU *et al.* 1999; BURMA *et al.* 2001). In turn, γH2AX triggers histone acetylation and chromatin remodeling at the DSB site to promote amplification of the DNA damage response (DEEM *et al.* 2012). Both histone ubiquitylation and methylation are key for recruitment of 53BP1, which mediates the DNA damage response by facilitating checkpoint signaling (DEEM *et al.* 2012). In addition, histone ubiquitylation recruits a complex containing BRCA1. BRCA1 promotes the recruitment of BRCA2, which may promote the recruitment of RAD51 (DEEM *et al.* 2012).

Removal of the histone proteins from the area flanking the DSB (up to a few kilobases) permits access to DSB processing and repair factors. Following repair, histones must be reassembled onto DNA; additionally, the modifications associated with the DNA damage response need to be lost from the repair site in order to turn off DNA damage signaling and re-

enter the cell cycle (DEEM *et al.* 2012). Acetylation of lysine 56 on histone H3 (H3K56ac) is enriched at sites of completed repair in both yeast and humans (DEEM *et al.* 2012). Interestingly, yeast that fail to acetylate H3K56 are unable to inactivate the DNA damage checkpoint, suggesting that DNA repair alone is insufficient to turn off the DNA damage response (CHEN *et al.* 2008). Histone modifications associated with the DNA damage response can be lost during nucleosome disassembly during resection or exchanged for unmodified histones by chromatin remodelers (DEEM *et al.* 2012). Taken together, regulation of chromatin structure is essential during HR for activating the DNA damage response, recruiting DNA repair factors, providing access to DNA for repair, and inactivating the DNA damage response.

2.0 SWS-1 FUNCTIONS WITH THE RAD-51 PARALOGS TO PROMOTE HOMOLOGOUS RECOMBINATION IN *CAENORHABDITIS ELEGANS*

Homologous recombination (HR) repairs cytotoxic DNA double-strand breaks (DSBs) with high fidelity. Deficiencies in HR result in genome instability. A key early step in HR is the search for and invasion of a homologous DNA template by a single-stranded RAD-51 nucleoprotein filament. The Shu complex, comprised of a SWIM domain-containing protein and its interacting RAD51 paralogs, promotes HR by regulating RAD51 filament dynamics. Despite Shu complex orthologs throughout eukaryotes, our understanding of its function has been most extensively characterized in budding yeast. Evolutionary analysis of the SWIM domain identified *Caenorhabditis elegans sws-1* as a putative homolog of yeast Shu complex member, Shu2. Using a CRISPR-induced nonsense allele of *sws-1*, we show that *sws-1* promotes HR in mitotic and meiotic nuclei. *sws-1* mutants exhibit sensitivity to DSB-inducing agents and fail to form RAD-51 foci following treatment with camptothecin. Phenotypic similarities between *sws-1* and the two RAD-51 paralogs, *rfs-1* and *rip-1,* suggest they function together. Indeed, we detect direct interaction between SWS-1 and RIP-1 by yeast-two-hybrid that is mediated by the SWIM domain in SWS-1 and the Walker B motif in RIP-1. Furthermore, RIP-1 bridges an interaction between SWS-1 and RFS-1, suggesting RIP-1 facilitates complex formation with SWS-1 and RFS-1. We propose that SWS-1, RIP-1, and RFS-1 comprise a *C. elegans* Shu complex. Our work provides a new model for studying Shu complex disruption in the context of a multicellular

organism that has important implications as to why mutations in the human RAD51 paralogs are associated with genome instability.

2.1 INTRODUCTION

DNA double-strand breaks (DSBs) are extremely cytotoxic lesions that threaten genome integrity. DSBs arise from both endogenous sources such as replicative damage, or exogenous sources such as ionizing radiation (IR) and chemotherapeutic agents. To ensure the maintenance of the genome, DSBs need to be repaired by high-fidelity repair pathways, the most robust of which is homologous recombination (HR), in which DNA from a sister chromatid or homologous chromosome provides a repair template. Initial processing of DSB ends by resection forms 3' single-stranded DNA (ssDNA) overhangs that are coated with the ssDNA-binding protein RPA. The exchange of RPA for the recombinase enzyme RAD51 facilitates the homology search and strand invasion of homologous DNA templates to form displacement loop structures. Subsequent stabilization of HR intermediates then requires removal of RAD51 from the double-stranded DNA to allow access to the DNA polymerization machinery. Given the central role of the RAD51 filament in HR, its assembly and disassembly are tightly regulated to ensure the fidelity of repair (KREJCI *et al.* 2012; JASIN AND ROTHSTEIN 2013; HEYER 2015).

Key mediators of RAD51 filament assembly are the RAD51 paralogs. In humans, there are six RAD51 paralogs: RAD51B, RAD51C, RAD51D, XRCC2, XRCC3, and the newly identified SWSAP1 (LIU *et al.* 2011; KARPENSHIF AND BERNSTEIN 2012; PRAKASH *et al.* 2015). The RAD51 paralogs form multiple sub-complexes including a novel complex containing SWSAP1 and its binding partner SWS1 (MILLER *et al.* 2002; LIU *et al.* 2011). Mutations in the

RAD51 paralogs are associated with cancer predisposition and, in some cases, Fanconi anemia-like syndromes (VAZ *et al.* 2010; WANG *et al.* 2015), underscoring the importance of these proteins in maintaining genome stability. Nevertheless, progress in understanding the roles of these complexes in metazoans has been hampered by the embryonic lethality observed in mouse knockouts and the difficulty in attaining purified proteins for biochemical studies (DEANS *et al.* 2000; THACKER 2005; KUZNETSOV *et al.* 2009; SUWAKI *et al.* 2011).

Much of our understanding of the RAD51 paralogs comes from studies in budding yeast in which the Rad51 paralogs form two sub-complexes, the Shu complex (also called the PCSS complex) and the Rad55-Rad57 complex. The Shu complex is an obligate hetero-tetramer comprised of Psy3, Csm2, Shu1, and Shu2 which facilitates HR-mediated DSB repair by stimulating Rad51 filament formation (SHOR *et al.* 2005; MANKOURI *et al.* 2007; BALL *et al.* 2009; GODIN *et al.* 2013; HONG AND KIM 2013; SASANUMA *et al.* 2013; GAINES *et al.* 2015; GODIN *et al.* 2015). Csm2 and Psy3 are Rad51 paralogs whereas Shu2 is a member of the SWS1 protein family, defined by a highly conserved SWIM domain (MAKAROVA *et al.* 2002; MARTIN *et al.* 2006; GODIN *et al.* 2015). Yeast with Shu complex disruptions exhibit sensitivity to the alkylating agent methyl methanesulfonate (MMS), increased mutations, decreased meiotic crossover (CO) formation, and reduced spore viability (SHOR *et al.* 2005; HONG AND KIM 2013; SASANUMA *et al.* 2013; GODIN *et al.* 2015). Unlike yeast and humans, only two RAD-51 paralogs, RFS-1 and RIP-1, are known in *C. elegans*. Both paralogs function in HR, mediating repair of DNA lesions in the mitotic and meiotic regions of the worm germ line (WARD *et al.* 2007; YANOWITZ 2008; WARD *et al.* 2010; TAYLOR *et al.* 2015). Nevertheless, the relationship of the RAD-51 paralogs to a worm Shu complex remains largely unknown.

Although Shu complex function was thought to be conserved throughout eukaryotes, the poor amino acid conservation across species precluded identification of functional paralogs in other systems until recently. Evolutionary analyses of the SWIM domain led to the identification of *C. elegans sws-1* as the homolog of *S. cerevisiae* Shu2 (GODIN *et al.* 2015). *C. elegans* provides several advantages for probing the function of *sws-1*. The germ line is spatially and temporally organized such that the stages of meiotic prophase I – and integrity thereof – can be readily distinguished by DNA morphology (visualized by DAPI). The germ line is a reliable source of programmed DSBs induced by the topoisomerase-like SPO-11 (KEENEY *et al.* 1997), and HR is the favored repair mechanism due to the need to form crossovers between homologous chromosomes (COLE *et al.* 2010). Populations of *C. elegans* exist primarily as self-fertilizing hermaphrodites with two X chromosomes; rare nondisjunction of the X chromosome (<0.2% in wild type) results in viable males with a single X chromosome (XO). Nondisjunction of autosomes, by contrast, is lethal in most cases and can be ascertained by the presence of unhatched eggs (HODGKIN *et al.* 1979). Thus, progeny viability and male frequency (*h*igh *i*ncidence of *m*ales phenotype) can intimate meiotic HR repair defects, although those phenotypes are not sufficient indicators on their own.

Using CRISPR/Cas9, we created a nonsense allele of *sws-1* in *C. elegans* and probed the role of this conserved DNA repair factor in both mitotic and meiotic germline nuclei. We find that *sws-1* is the functional homolog of *S. cerevisiae* Shu2, showing that: 1. *sws-1* mutants exhibit DNA damage sensitivity; 2. disruption of *sws-1* results in reduced RAD-51 foci formation following camptothecin (CPT) treatment; and 3. SWS-1 interacts with the known *C. elegans* RAD-51 paralogs RFS-1 and RIP-1 (WARD *et al.* 2007; TAYLOR *et al.* 2015). Our

findings show for the first time the mitotic and meiotic role of *sws-1* in the context of a metazoan and expand upon the known RAD-51 paralog-interacting proteins in worms.

2.2 MATERIALS AND METHODS

2.2.1 Culture and strains

For all experiments, worms were cultured on NGM plates seeded with OP50 and grown at 20°C unless otherwise noted (BRENNER 1974). Mutant strains used in this study were: LG I, *syp-3(ok758)*, *dog-1(gk10)*; LG III, *rip-1(tm2948)*, *rfs-1(ok1372), helq-1(tm2134)*; LG V, *sws-1(ea12)* (generation of strain described in Section 2.2.2); LG X, *unc-58(e665)*. *rip-1*, *rfs-1 rip-1*, and *helq-1* were kindly provided by Simon Boulton; *syp-3* by Sarit Smolikove; and *dog-1* by Ann Rose. Other strains were provided by the Caenorhabditis Genetics Center. Double and triple mutants generated for this work were done so using standard genetic techniques and are listed in Table 1. *helq-1;sws-1* double mutants were maintained as heterozygotes due to lack of suitable genetic balancers and were genotyped in all experiments to confirm homozygosity of markers. Control animals used in this study are the homozygous wild-type self-progeny of an *sws-1* heterozygote and did not differ phenotypically from our N2 stock (Table 3, rows A and B).

Table 1. Strains generated for Chapter 2.

Strain	Genotype	Reference in text
QP1203	*helq-1(tm2134)* III;*sws-1(ea12)* V	*helq-1;sws-1*
QP1204	*rfs-1(ok1372)* III;*sws-1(ea12)* V	*rfs-1;sws-1*
QP1205	*rip-1(tm2948)* III;*sws-1(ea12)* V	*rip-1;sws-1*
QP1206	*rfs-1(ok1372),rip-1(tm2948)* III;*sws-1(ea12)* V	*rfs-1,rip-1;sws-1*
QP1208	*sws-1(ea12)* V	*sws-1*
QP1179	*sws-1(ea12)* V;*unc-58(e665)* X	*sws-1;unc-58*
QP1234	*dog-1(gk10)* I;*sws-1(ea12)* V	*dog-1;sws-1*
QP1263	*syp-3(ok758)* I;*sws-1(ea12)* V	*syp-3;sws-1*

2.2.2 Generation of *sws-1(ea12)*

Unique CRISPR guides near the start and stop codons of *sws-1* were selected using the CRISPR design tool at crispr.mit.edu (see Table 2 for sequences of the primers used in sgRNA design). Primers were inserted into pDD162 (P*eft-3::Cas9::tbb-2* 3' UTR) using the Q5 Site-Directed Mutagenesis Kit (NEB) as described (DICKINSON *et al.* 2013). DNA from positive clones was isolated using the PureLink®HQ Mini Plasmid DNA Purification kit (Invitrogen) and sequenced to verify the insertion. An injection mix consisting of 30 ng/µl *dpy-10(cn64)* repair oligo (ARRIBERE *et al.* 2014) and 50 ng/µl each gRNA in pDD162 (one for *dpy-10*, two for *sws-1*) diluted in PureLink EB buffer (Invitrogen) was prepared and injected into N2 day 1 adult hermaphrodites. Roller progeny (*dpy-10(cn64)*/+) of injected hermaphrodites were isolated and allowed to lay eggs before being lysed in buffer for DNA isolation (0.1 M Tris pH 8.5, 0.1 M

NaCl, 0.05 M EDTA, 1% SDS, 0.1 μg/mL proteinase K). A region ~300 bp around each Cas9 target site was amplified by PCR and resolved on a 2-3% agarose gel to identify products differing in size from an uninjected control (Table 2, Figure 5A-B). This approach yielded one candidate founder strain with an insertion near the start codon; we did not detect any mutations near the stop codon (data not shown). PCR product from the founder strain was purified (NucleoSpin Gel and PCR Clean-up kit, Macherey-Nagel), sequenced, and aligned with wild-type sequence to identify mutations. The candidate allele was outcrossed to N2 multiple times to lose the *dpy-10(cn64)* allele and any potential (though unanticipated) off-target mutations (PAIX *et al.* 2014).

2.2.3 Gene expression

A population of approximately 1000 day 1 adult hermaphrodites were washed thrice in 1x M9 buffer (3 g/L KH_2PO_4, 6 g/L Na_2HPO_4, 5 g/L NaCl, 1 mM $MgSO_4$), resuspended in Trizol (Invitrogen) and vortexed for ~60 seconds before being flash frozen and stored at -80°C. Worms were further disrupted by 3 freeze-thaw cycles in which samples were thawed in cold water, vortexed 30 seconds, and refrozen at -80°C. RNA was isolated by chloroform extraction and isopropanol precipitation, and resuspended in nuclease-free water. Genomic DNA was removed using the DNaseI kit (Sigma-Aldrich, AMPD1-1KT) according to manufacturer's instructions. RNA quality was measured by a spectrophotometer.

Reverse transcription was performed using the TaqMan High Capacity RNA-to-cDNA kit (Applied Biosystems) according to manufacturer's instructions. Comparative C_T experiments were performed according to manufacturer's instructions using TaqMan Fast Universal No AmpErase UNG PCR Master Mix and TaqMan gene expression assays for CELE_Y39B6A.40

Table 2. Primers used in Chapter 2.

Primer	Sequence (5'→3')
sws-1 5' gRNA	AAGTAGTCATCTGAGCTGCGTTTTAGAGCTAGAAATAGCAAGT
sws-1 3' gRNA	AGTGTAAATCCGAAATAGTGTTTTAGAGCTAGAAATAGCAAGT
1	AGCGGGAATTTGAAGATG
2	AGCTGGAAACTCTGAAAC
3	CCCATATTTCCAGTCAACC
4	GTGCCTGGAGTTGGAAAA
SWS-1.C133S.F	CATTATTGTACATCTCCATACTTTCAATC
SWS-1.C133S.R	GATTGAAAGTATGGAGATGTACAATAATG
SWS-1.A156T.F	GTGTTCATATTTTAACTTACTATTTTGC
SWS-1.A156T.R	GCAAAATAGTAAGTTAAAATATGAACAC
RIP-1.F	GCGGGATCCATGTCAGAATCGTGCAATTC
RIP-1.R	GCGGTCGACGAAAATTCATTTAATAAAAACC
RIP-1.D131A.F	GGTCGTCGTGATTGCTTTGAGAGATGAT
RIP-1.D131A.R	ATCATCTCTCAAAGCAATCACGACGACC
RFS-1.F	GCGAATTCATGGATCCTTCTGAGAATGTATTC
RFS-1.R	GAAGATCTTCATTCCACTGCTTTGAGTC

(*sws-1*) and reference gene *rpl-32* (HOOGEWIJS *et al.* 2008) (Thermo Fisher Scientific). Reactions were run in triplicate and analyzed with Applied Biosystems Fast PCR System and StepOne Software using the comparative C_T method (SCHMITTGEN AND LIVAK 2008).

2.2.4 Brood size/lethality/Him frequency

L4 hermaphrodites of a given genotype were individually plated and transferred to a clean plate every 12 hours until egg-laying ceased. After transfer, the number of eggs and L1s on the plate was counted and recorded. Three to four days later, each plate was scored for the number of adult hermaphrodites and males. Timepoint data from each individual parent was combined to give total eggs, total adult brood, and total males. Percent hatching was calculated by dividing total adults by total eggs and multiplying by 100. Percent lethality was then calculated by subtracting this value from 100. Percent lethality is normalized to N2 to account for 3% error in egg counts. To calculate male frequency, the total number of males was divided by the total number of adults. The data are presented as the mean ± SEM from isogenic parents.

2.2.5 Developmental arrest assay

Developmental arrest in unstressed larvae was assayed as previously described (CRAIG *et al.* 2012). Briefly, 100 L1 larvae of a given genotype were plated onto center-seeded 3-cm dishes in triplicate. After 48-60 hours, the number of adult, L3-L4, and L1-L2 worms on each plate was counted. To calculate larval arrest, the number of worms in each developmental stage was divided by the total number of worms counted.

2.2.6 Mutation frequency

Mutation frequency of *sws-1(ea12)* was assessed as described previously (HARRIS *et al.* 2006). Briefly, *sws-1(ea12);unc-58(e665)* and *unc-58(e665)* homozygotes were grown on 40 6-cm plates until starvation, then transferred by chunking to approximately 100 10-cm plates containing a streak of OP50 opposite the agar chunk. Plates were scored by eye for the presence of Unc revertants that could reach the OP50. Mutation frequency was calculated as described (HARRIS *et al.* 2006). Mutation frequency of *sws-1(ea12)* in the *dog-1* background was assessed as described previously (YOUDS *et al.* 2006). Briefly, generation-matched (F3) *dog-1(gk10)* and *dog-1(gk10);sws-1(ea12)* day 1 adults were individually lysed in buffer for DNA isolation. The poly G/C tract of *vab-1* was amplified by PCR (primers and conditions described in (YOUDS *et al.* 2006)) and resolved on a 1.5% agarose gel. The presence of one or more bands below the expected product size signified a deletion event.

2.2.7 Genotoxin Sensitivity Assays

Details for each genotoxin exposure are described below. In all assays, the number of eggs and L1s were counted at the end of the collection window. Three to four days later, each plate was scored for the number of adult progeny. Survival was calculated as the number of adult progeny divided by the number of eggs/L1s relative to untreated worms ± SEM from 22-50 adults over two trials.

2.2.7.1 Ionizing Radiation (IR) L4 hermaphrodites were plated on each of 4 6-cm plates with 30-100 worms/plate depending on genotype and IR dose. The following day, worms were

exposed to 0, 10, 50, or 100 Gy of IR from a ^{137}Cs source (Gammacell®1000 Elite, Nordion International Inc.). Twelve hours post-irradiation, worms were plated (2 worms per 3-cm dish) and allowed to lay for 12 hours before removal and egg counts.

2.2.7.2 Methyl Methanesulfonate (MMS) L4 hermaphrodites were incubated in 0%, 0.0025%, 0.005%, and 0.01% MMS (50-9480886, Fisher Healthcare) dissolved in 1x M9 buffer for 12 hours at room temperature with mild agitation. Following exposure, worms were washed, transferred to plates, and allowed to recover for 12 hours. Post recovery, worms were plated (2 worms per 3-cm dish) and allowed to lay for 12 hours before removal and egg counts.

2.2.7.3 Camptothecin (CPT) CPT exposure was performed as described with minor alterations (KESSLER AND YANOWITZ 2014). Briefly, young adult hermaphrodites were incubated in 0 nM, 250 nM, 500 nM, and 1000 nM CPT (ICN15973250, Fisher Healthcare) dissolved in 1x M9 pH 6.0 buffer and 0.2% DMSO for 18 hours at room temperature with mild agitation. Following exposure, worms were washed, transferred to plates, and allowed to recover for three hours. Post recovery, worms were plated (5 worms per 3-cm dish) and allowed to lay for 4 hours before removal and egg counts.

To assess DNA damage-induced apoptosis in response to CPT, young adult hermaphrodites were treated, washed, and allowed to recover as described above. Post recovery, worms were exposed to acridine orange (AO, Invitrogen A3568) as previously described (LANT AND DERRY 2014). Worms that were verified to have taken up the stain were mounted in levamisole and observed on a compound microscope with fluorescence. Cells in the pachytene-diplotene region of the germ line that retained AO were scored as apoptotic. The data are presented as mean AO-positive nuclei ± SEM from 25 germ lines.

2.2.7.4 Hydroxyurea (HU) Hydroxyurea (H8627, Sigma-Aldrich) was dissolved in approximately 60°C NGM to final concentrations of 0 mM, 8 mM, 12 mM, and 25 mM, poured into 3-cm dishes to solidify, and used within 24 hours. Plates were seeded with heat-killed OP50 (KESSLER AND YANOWITZ 2014) and dried for 45-60 minutes under a fume hood. L4 hermaphrodites were incubated on HU plates for 20 hours at 20°C. Following exposure, worms were moved to plates with drug-free NGM and live OP50 (2-4 worms per 3-cm dish) and allowed to lay for 12 hours before removal and egg counts.

2.2.8 Immunofluorescence

Day 1 adult hermaphrodites were dissected in PBS/levamisole and fixed in 0.5% triton/1% PFA for 5 minutes in a humid chamber. Slides were freeze-cracked and briefly immersed in methanol. Following fixation, slides were washed in PBST and incubated in primary antibody (α-RAD-51, kindly provided by Verena Jantsch, 1:5000; α-XND-1 (WAGNER *et al.* 2010), 1:2000) overnight at 4°C. Next day, slides were washed and incubated in secondary antibody (α-rabbit 568, 1:2000; α-guinea pig 633, 1:2000) for 2 hours at room temperature in the dark. Slides were mounted in Prolong Gold with DAPI (Life Technologies) and imaged on a Nikon A1r confocal microscope using a 63x Plan Fluor objective with 0.2 μm step sizes. Images were analyzed using Volocity 3D software (PerkinElmer). RAD-51 foci were quantified by dividing the region from leptotene (transition zone) through the pachytene/diplotene border into 6 even zones (based on physical distance in μm), and individually scoring RAD-51 foci in each nucleus by scrolling through the images in the Z-dimension. RAD-51 counts were confirmed by examining 3D renderings of nuclei. Graphs represent the averages of three germ lines for each genotype.

2.2.9 Yeast-two- and three-hybrid plasmid construction

A population of predominately adult N2 hermaphrodites were washed thrice in 1x M9 buffer, flash frozen in RNAzol (Invitrogen), and stored at -80°C. RNA was isolated by chloroform extraction and isopropanol precipitation, and resuspended in DEPC water. Purity was verified by spectrophotometry. cDNA synthesis was performed as described previously (FUKUSHIGE AND KRAUSE 2012). cDNA was diluted 1:15 in deionized water prior to further use.

Yeast-two-hybrid (Y2H) plasmids were created from pGAD-C1 and pGBD-C1. The additional plasmid used in yeast-three-hybrid (Y3H) analysis was created from pRS-ADH-416. pGAD-SWS-1 was synthesized by Genewiz (Genewiz Inc., Gene Synthesis Services, South Plainfield, NJ) using a codon-optimized sequence for expression in *S. cerevisiae*. pGBD-SWS-1 was created by subcloning SWS-1 into pGBD using 5'SmaI and 3'BglII restriction sites. SWIM domain mutants were made by site-directed mutagenesis of the pGAD-SWS-1 plasmid for SWS-1-C133S (SWS-1.C133S.F and SWS-1.C133S.R) and SWS-1-A156T (SWS-1.A156T.F and SWS-1.A156T.R) (Table 2). pGAD-RIP-1 and pGAD-RFS-1 were constructed using standard restriction digestion and ligation techniques. First, PCR amplification was used for the coding regions of both *rip-1* and *rfs-1* genes from N2 cDNA using oligonucleotide pairs RIP-1.F/RIP-1.R and RFS-1.F/RFS-1.R, respectively (Table 2). *rip-1* was subcloned into pGBD and pRS-ADH-416 using 5'BamHI and 3'SalI restriction sites. Walker B motif mutant was made by site-directed mutagenesis (RIP-1.D131A.F and RIP-1.D131A.R, Table 2) of pGBD-RIP-1. *rfs-1* was subcloned into pGBD using 5'EcoRI and 3'BglII restriction sites. All other plasmids were constructed as previously described (GODIN *et al.* 2015).

2.2.10 Yeast-two- and three-hybrid assays

Yeast strains, media, and Y2H assays were performed as previously described (GODIN *et al.* 2015) with the following modifications. For Y2H analysis, pGAD and pGBD plasmids were co-transformed into the PJ69-4A Y2H strain (JAMES *et al.* 1996) and 1 mM histidine competitive inhibitor, 3-Amino-1,2,4-triazole (3AT) was used to detect more stringent Y2H interactions (SC-LEU-TRP-URA+3AT; Sigma Aldrich). For Y3H analysis, pGAD, pGBD, and pRS-ADH-416 (with URA selection maker) plasmids were co-transformed into the PJ69-4A Y2H strain. Yeast were selected for expression by growth on SC-LEU-TRP (Y2H) or SC-LEU-TRP-URA (Y3H) solid medium. Plates were grown for 2-4 days at 30°C and photographed.

2.3 RESULTS

2.3.1 *sws-1* contributes to germline HR repair

We generated an *sws-1* allele using CRISPR/Cas9 mediated genome engineering (Figure 1A-B, Materials and Methods) (DICKINSON *et al.* 2013; ARRIBERE *et al.* 2014). Using this approach, we identified a founder strain with a 3 bp deletion/83 bp insertion in exon 2 just downstream of the predicted Cas9 cleavage site, designated as *ea12* (Figure 5A-B and Figure 6). Interestingly, the *dpy-10(cn64)* repair oligo donated most of the sequence for the insertion. *sws-1(ea12)* (hereafter referred to as *sws-1*) is predicted to produce the first 19 amino acids of the wild-type SWS-1 protein followed by 32 frameshifted amino acids prior to truncation (Figure 5C). Given the substantial truncation of the protein including the conserved SWIM domain encoded in exon 4

(Figure 5A), and that disruption of the SWIM domain in *S. cerevisiae* Shu2 results in a non-functional protein (GODIN *et al.* 2015), we expect *ea12* to be a null allele. Consistent with the presence of a premature stop codon, which triggers nonsense mediated mRNA decay, we detect approximately 5-fold less *sws-1* mRNA in *sws-1(ea12)* hermaphrodites compared to wild type (Figure 5D).

sws-1 homozygotes are viable, although they exhibit decreased survival compared to their wild-type counterparts ($p=0.0399$, Mann-Whitney) (Table 3, rows B-C). This decrease in survival is not solely attributable to embryonic lethality, as we found a small but significant percentage of *sws-1* homozygotes fail to develop past the L2 stage ($p<0.001$ vs. wt, Fisher's exact test) (Figure 5E). We also observed a four-fold increase in male frequency compared to their wild-type counterparts ($p=0.0114$, Mann-Whitney) (Table 3, rows B-C). These results suggest that *sws-1* is required for both normal development and X chromosome disjunction.

In other eukaryotes, such as *S. cerevisiae*, the Rad51 paralogs and a SWIM domain-containing protein form the Shu complex and share HR phenotypes (SHOR *et al.* 2005; MANKOURI *et al.* 2007). Therefore, we asked whether *sws-1* mutants would exhibit similar phenotypes to RAD-51 paralog mutants in worms. In *C. elegans*, the two known RAD-51 paralogs, *rfs-1* and *rip-1*, confer reduced survival and Him phenotypes (WARD *et al.* 2007; YANOWITZ 2008; TAYLOR *et al.* 2015). Importantly, the reduced survival and Him phenotypes of *sws-1* resembled those of *rfs-1* and *rip-1* (Table 3, rows D and F), suggesting *sws-1* may have an analogous role in HR repair.

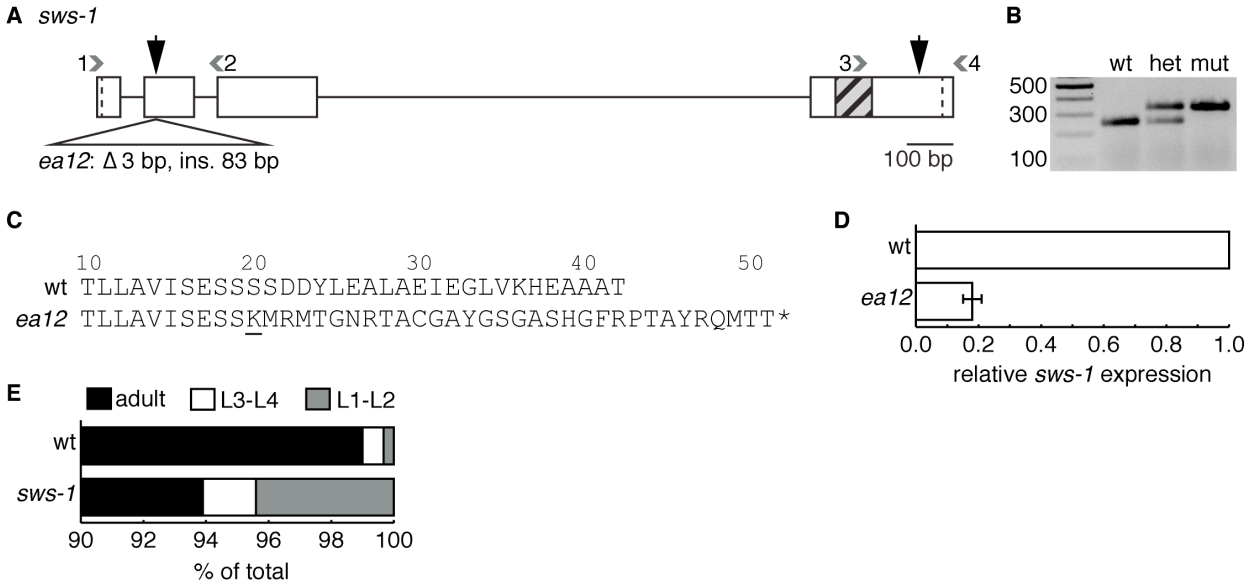

Figure 5. ***sws-1(ea12)*** **is an insertion/deletion that results in an early stop codon: A. Diagram of** ***sws-1*** **coding region. Boxes and straight lines represent exons and introns, respectively. Start and stop codons demarcated by dotted lines. Gray hatched box shows DNA encoding the SWIM domain. Large black vertical arrows mark predicted Cas9 cleavage sites for each injected gRNA; small gray numbered arrowheads represent primers used for screening (primer sequences listed in Table 2).** ***ea12*** **is a 3 bp deletion/83 bp insertion in exon 2. B. Representative image of** ***ea12*** **genotyping using primer combination 1 and 2 as shown in (A). The mutant allele is readily detected as the slower migrating band on a 2% agarose gel. C. Predicted protein sequence of exon 2 of wt (top) and** ***ea12*** **(bottom) SWS-1.** ***sws-1(ea12)*** **is predicted to produce the first 19 amino acids of the wild-type SWS-1 protein followed by 32 frameshifted amino acids prior to truncation (underlined text marks beginning of frameshift). D. Expression of** ***sws-1*** **mRNA in wt and** ***sws-1(ea12)*** **hermaphrodites. The data are presented as the mean expression of** ***sws-1*** **relative to reference gene** ***rpl-32*** **± SEM for 2 biological replicates. E. Developmental progression of wt and** ***sws-1*****. For each genotype, 100 L1s were plated in triplicate and scored 50 hours later as L1-L2, L3-L4, or adult. The results shown are the percent of total worms in each developmental stage. A subset of** ***sws-1*** **mutants arrested as L1-L2 larvae ($p<0.001$ vs. wt, Fisher's exact test).**

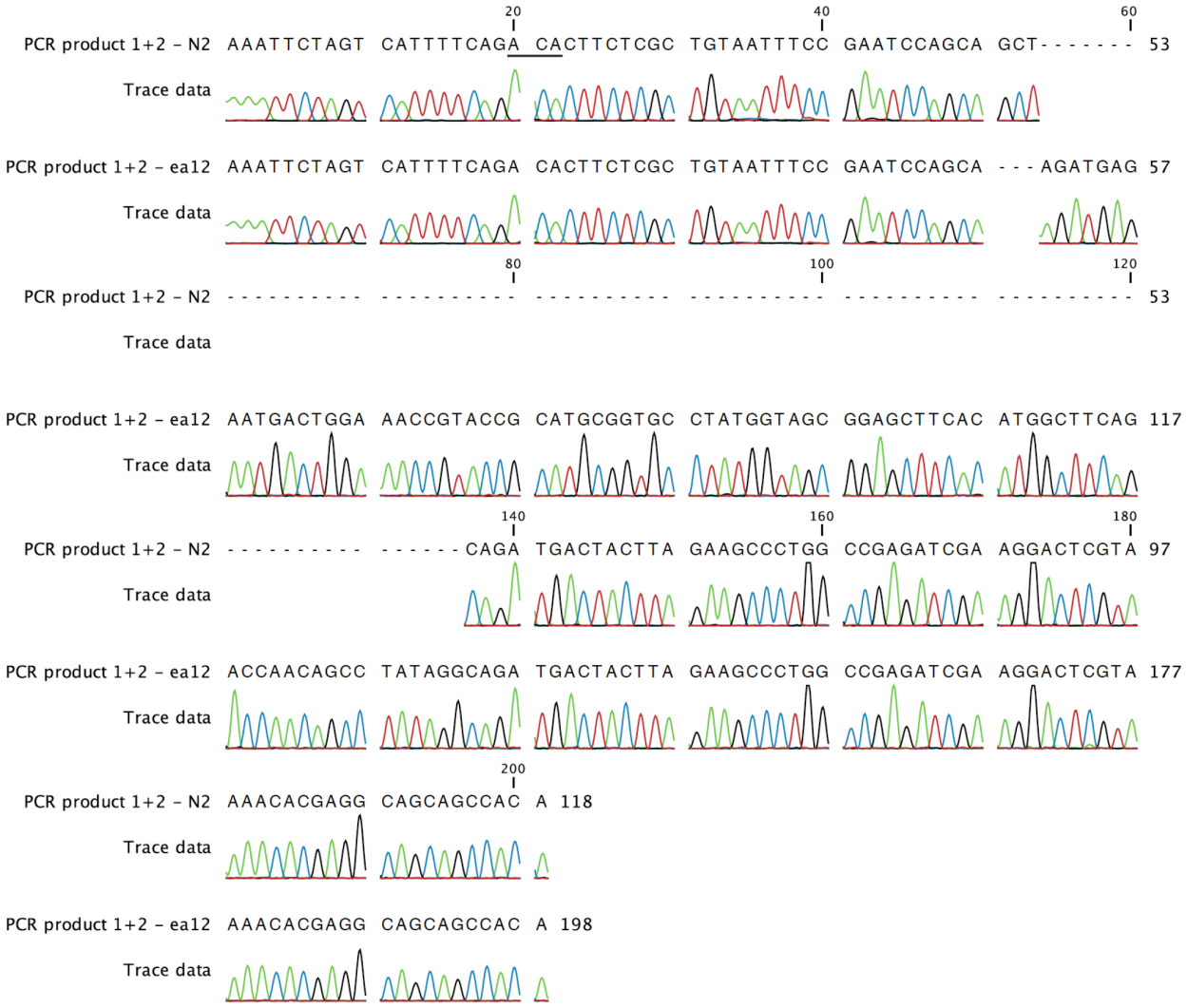

Figure 6. Alignment of *sws-1* exon 2 in N2 and *ea12*: Sequencing data for exon 2 of *sws-1* in N2 and *sws-1(ea12)* worms. PCR products were amplified with primers 1 and 2 and purified as described in Section 2.2.2. Line marks both beginning of exon 2 and establishes translation frame.

Table 3. General characteristics of strains used in Chapter 2: Brood size, lethality, and male frequency were collected as described in Section 2.2.4 (n=number of worms). % lethal ± SEM is normalized to N2 (row A) to account for counting error. Differences between wild type and *sws-1* were assessed by Mann-Whitney (* p<0.05); differences in lethality and male frequency among genetic combinations of *sws-1*, *rip-1*, and *rfs-1* were assessed using one-way ANOVA with multiple comparisons (Tables 5 and 6).

	Genotype	n	Avg. Brood ± SEM	% lethal ± SEM	% male ± SEM
A	N2	12	232.42 ± 5.97	0.00 ± 0.67	0.07 ± 0.05
B	wild type	6	227.17 ± 9.28	0.56 ± 1.49	0.16 ± 0.16
C	*sws-1*	25	203.84 ± 10.35	8.45 ± 2.05*	0.63 ± 0.08*
D	*rip-1*	6	265.33 ± 8.02	6.33 ± 1.11	1.78 ± 0.72
E	*rip-1;sws-1*	16	268.00 ± 9.72	2.59 ± 0.49	0.87 ± 0.10
F	*rfs-1*	10	212.90 ± 7.59	9.36 ± 1.48	2.22 ± 0.31
G	*rfs-1;sws-1*	13	206.77 ± 9.59	7.84 ± 2.00	1.78 ± 0.26
H	*rfs-1,rip-1*	11	177.00 ± 9.00	8.47± 1.29	2.20 ± 0.31
I	*rfs-1,rip-1;sws-1*	22	164.23 ± 9.97	12.33 ± 1.94	2.43 ± 0.29

To test this, we analyzed the viability and cytology of *helq-1;sws-1* double mutants. *helq-1* encodes a conserved DNA helicase that functions in HR-mediated repair during replication stress and meiosis (MUZZINI *et al.* 2008; WARD *et al.* 2010). In meiosis, *helq-1* exhibits synthetic lethality with both *rfs-1* and *rip-1* due to persistent HR intermediates, suggesting *helq-1* and *rfs-1/rip-1* perform overlapping roles in DSB repair (WARD *et al.* 2010; TAYLOR *et al.* 2015). Whereas *helq-1* single mutants exhibited low levels of lethality (~3.6%), *helq-1;sws-1* double mutants displayed ~63% lethality in the F2 generation (Figure 7A). Analysis of diakinesis-stage

nuclei in *helq-1;sws-1* hermaphrodites revealed chromatin abnormalities associated with impaired DSB repair – including decondensed chromatin, DNA fragments, and chromosome aggregates – in nearly all nuclei scored (Figure 7B-C). The redundancy with *helq-1* indicates that *sws-1* functions in HR repair and the raises the possibility that *sws-1* functions with the RAD-51 paralogs in this role.

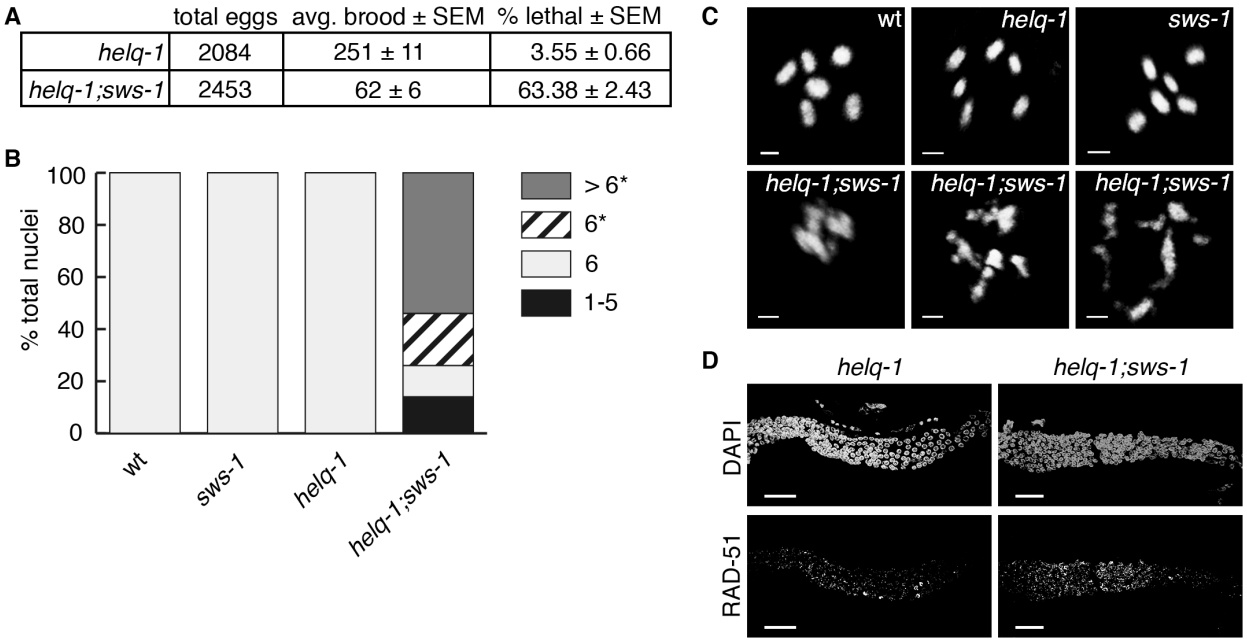

Figure 7. *sws-1* is synthetic lethal with *helq-1*: A. Brood size and viability of *helq-1* and *helq-1;sws-1* mutants. B. Quantification of the number of DAPI-staining bodies at diakinesis in wt, *sws-1*, *helq-1*, and *helq-1;sws-1* germ lines. Only the -1 oocyte was used for analysis (n=20 for wt and *helq-1*; n=50 for *sws-1* and *helq-1;sws-1*). Asterisk indicates chromosomal abnormalities. C. Representative images of -1 oocytes analyzed as described in (B). Scale bar is 2 µm. D. Representative images of RAD-51 foci from the transition zone (left) to late pachytene (right) in *helq-1* and *helq-1;sws-1* germ lines. Scale bar is 20 µm.

We reasoned that, if *sws-1* is required for HR repair during meiosis, we might observe a change in RAD-51 dynamics compared to wild type. We quantified RAD-51 foci in wild-type and *sws-1* germ lines from the onset of leptotene (transition zone, TZ) through pachytene, the time during which SPO-11 induced DSBs breaks are made and repaired (Figure 8). In wild-type germ lines, RAD-51 foci first appear in the TZ, peak during early-pachytene, then disappear by late-pachytene as HR progresses ((ALPI *et al.* 2003) and Figure 8 (wt)). Similar to wild type, most *sws-1* nuclei had no RAD-51 foci upon entry to meiosis (Figure 8, zone 1) and RAD-51 foci slowly accumulated as nuclei progressed into pachytene. However, in later stages of pachytene, a greater proportion of *sws-1* nuclei had 7 or more RAD-51 foci than their wild-type counterparts (Figure 8A, $p<0.05$ for 7-8 foci in zone 3, $p<0.0001$ for 9+ foci in zone 3, $p<0.05$ for 9+ foci in zone 4, Student's t-test). Although this may be explained by increased formation of DSBs, the exclusively mid- to late-pachytene persistence of RAD-51 foci suggests that *sws-1* nuclei were delayed in removing RAD-51 foci. At the late-pachytene/diplotene border, the proportion of nuclei containing RAD-51 foci was again similar to wild type (Figure 8, zone 6), indicating that all DSBs are eventually repaired.

The observation that RAD-51 foci eventually resolve in *sws-1* germ lines (Figures 7B and 8A) left us curious about the cause of lethality in *sws-1* mutants. *C. elegans* exhibits strong CO control such that only one DSB per chromosome pair becomes an interhomolog CO (BARNES *et al.* 1995; MENEELY *et al.* 2002; HILLERS AND VILLENEUVE 2003). One possible explanation for the lethality, then, is that *sws-1* mutants are deficient in HR repair of DSBs not designated to be repaired as interhomolog COs. To test this hypothesis, we analyzed the competency of *sws-1* mutants for intersister HR by examining the cytology of diakinesis-stage oocytes in *syp-3;sws-1* double mutants (Figure 9). *syp-3* is a component of the synaptonemal complex

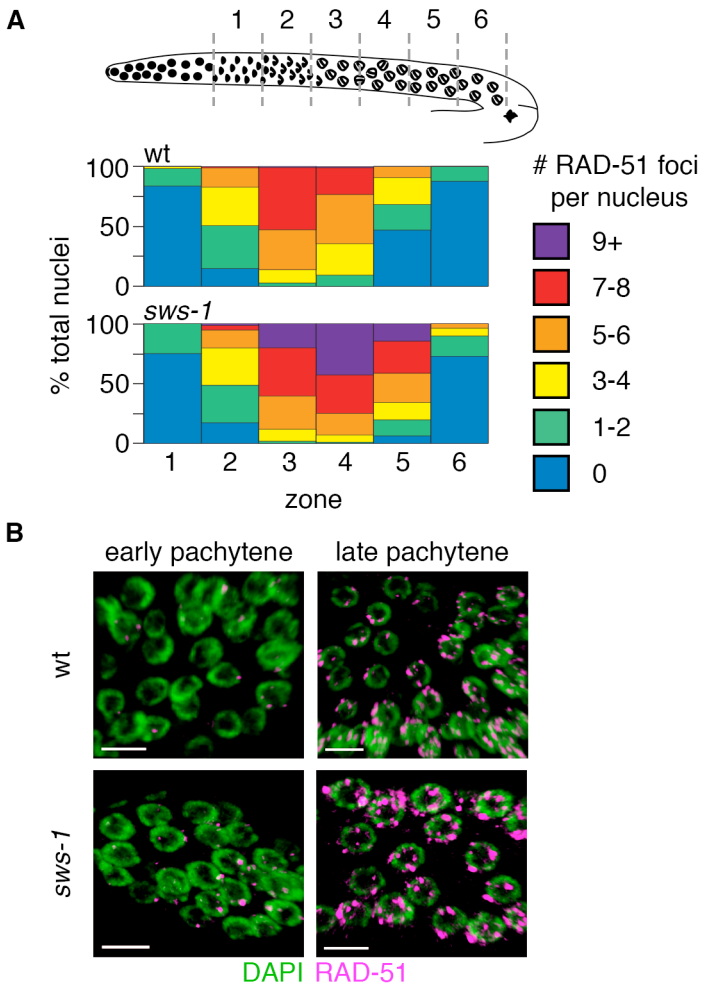

Figure 8. *sws-1* alters meiotic RAD-51 dynamics: A. Quantitative analysis of RAD-51 foci during meiotic prophase. Diagram depicts organization of the hermaphrodite germ line with meiotic prophase prior to diplotene divided into six equal-sized zones (gray dashed lines) based on physical distance. The heat map shows percent of total nuclei per zone with the indicated number of RAD-51 foci from wt (top) and *sws-1* (bottom) germ lines (color code, legend). B. Representative images of early and late pachytene nuclei in wt (top) and *sws-1* (bottom) showing higher levels of RAD-51 foci (magenta) on DNA (green) in late pachytene. Scale bar is 5 µm.

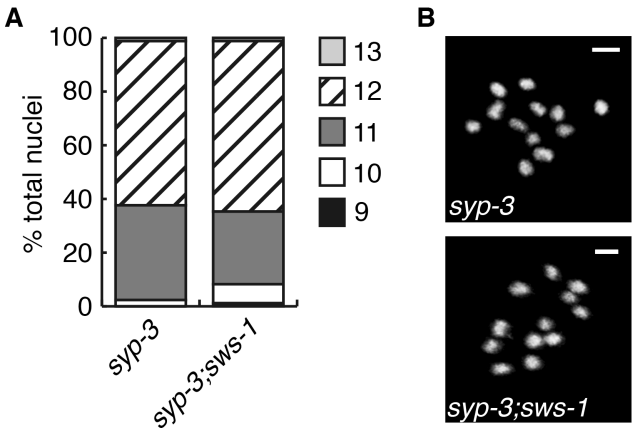

Figure 9. *sws-1* is competent for intersister HR: A. Quantification of the number of DAPI-staining bodies at diakinesis in *syp-3* and *syp-3;sws-1* germ lines. The -1 and -2 oocytes were used for analysis (n=85 nuclei for both *syp-3* and *syp-3;sws-1*). B. Representative images of -1 oocytes showing 12 condensed univalents. Scale bar is 2 µm.

(SC) that holds homologs together during meiosis. In the absence of the SC, HR repair between homologous chromosomes cannot occur and DSBs are repaired from the sister chromatids. Consequently, *syp-3* mutants exhibit an average of 11.6 condensed DAPI-staining bodies at diakinesis (Figure 9 and (SMOLIKOV *et al.* 2007a; SMOLIKOV *et al.* 2007b)). We did not observe a significant change in either number or morphology of DAPI-staining bodies at diakinesis between *syp-3* and *syp-3;sws-1* mutants (Figure 9), suggesting that *sws-1* mutants are competent for intersister HR.

A second possibility is that *sws-1* mutants have an increased reliance on error-prone DSB repair pathways. If this is the case, *sws-1* might be expected to show an increase in spontaneous mutation rate, which can be assessed by the reversion to wild-type movement of *unc-58(e665)*, a missense gain-of-function mutation that confers paralysis (HARRIS *et al.* 2006). Although not significantly different from controls, *sws-1;unc-58* mutants exhibited a trend towards increased

mutation rate with an approximately 3-fold increase in reversion to non-Unc offspring compared to *unc-58* alone (Table 4, p=0.4058, Student's t-test). These observations are consistent with what has been reported for *rfs-1* mutants (YANOWITZ 2008), and may suggest that HR factors are not critical for correction of mismatches during DNA replication. However, HR factors – including *rfs-1* – have been shown to be important for maintaining the integrity of poly G/C tracts in the absence of the helicase *dog-1*, which prevents the formation of deletions in G/C-rich DNA by unwinding secondary DNA structures that hinder replication fork progression (CHEUNG *et al.* 2002; YOUDS *et al.* 2006; WARD *et al.* 2007). We observed increased deletion frequency in *dog-1;sws-1* mutants compared to *dog-1* alone (Figure 10, p=0.0386, Fisher's exact test), suggesting increased reliance on mutagenic repair pathways in the absence of *sws-1*. Collectively, these results suggest that *sws-1* functions in HR, and is important for maintaining genome integrity during DNA replication.

Table 4. Spontaneous revertant frequencies of *unc-58(e665)*: *unc-58* reversion assay carried out as described in Section 2.2.6. Mutation frequency was calculated by dividing the proportion of plates with reversion events by the number of haploid genomes per plate. The data are presented as the mean mutation frequency ± SEM for four trials.

unc-58 background	Trial	Plates with revertants/ total plates	Mutation frequency ± SEM
wild type	1	0/40	$7.06 \times 10^{-7} \pm 7.06 \times 10^{-7}$
	2	1/38	
	3	0/39	
	4	0/36	
sws-1	1	2/41	$2.00 \times 10^{-6} \pm 1.26 \times 10^{-6}$
	2	0/40	
	3	0/37	
	4	1/39	

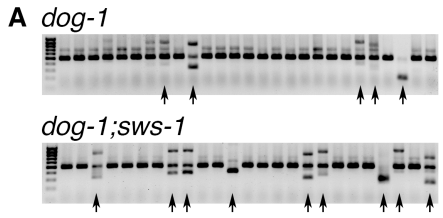

B

	n	# animals with deletions
wt	95	0
sws-1	96	1
dog-1	191	35
dog-1;sws-1	192	53*

Figure 10. *sws-1* maintains G/C tract stability in the absence of *dog-1*: A. Amplification of the *vab-1* G/C tract in *dog-1* (top) and *dog-1;sws-1* (bottom) mutants. Deletions in the amplified region are observed as faster-migrating bands on a 1.5% agarose gel (black arrows). B. Quantification of deletion frequency in wt, *sws-1*, *dog-1*, and *dog-1;sws-1* mutants. Number of individual animals with one or more deletions in the *vab-1* G/C tract as described in (A) is indicated. * $p<0.05$, Fisher's exact test.

2.3.2 *sws-1* mutants are sensitive to genotoxins that induce HR substrates

In *C. elegans*, both *rfs-1* and *rip-1* mutants display sensitivity to DSB-inducing agents, especially those that obstruct replication fork progression (WARD *et al.* 2007; TAYLOR *et al.* 2015). To further investigate the role of *sws-1* in HR repair, we exposed hermaphrodites to a subset of genotoxins that create HR repair substrates: gamma irradiation (IR), methyl methanesulfonate (MMS), hydroxyurea (HU), or camptothecin (CPT). The survival of the offspring laid post-exposure reflects the repair capacity in the hermaphrodite germ line. As shown in Figure 11, we observed a modest, but statistically significant, increased sensitivity of *sws-1* mutants to IR, MMS, and HU compared to their wild-type counterparts (Figure 11A-C). By contrast, *sws-1* mutants were dramatically more sensitive than wild type to CPT (Figure 11D). The reduced

progeny survival following CPT treatment was accompanied by a 2-fold increase in apoptotic germline nuclei (Figure 12), indicating that *sws-1* meiotic nuclei were unable to repair CPT-induced DSBs. This increased sensitivity to CPT may suggest that *sws-1* plays a more prominent role in the repair of a specific subset of DSB-inducing lesions.

The *S. cerevisiae* Shu complex has been shown in vitro to promote Rad51-mediated repair in concert with Rad52 and the Rad55-Rad57 heterodimer by stimulating Rad51 loading onto ssDNA and stabilizing it thereafter (GAINES *et al.* 2015). Further studies in *S. cerevisiae* suggest that the Shu complex promotes Rad51 assembly on meiotic chromosomes in vivo based on a reduced number of Rad51 foci in Shu mutants (SASANUMA *et al.* 2013). In *C. elegans*, the RAD-51 paralogs *rfs-1* and *rip-1* stabilize RAD-51 foci in response to cisplatin, nitrogen mustard, and UV (WARD *et al.* 2007; TAYLOR *et al.* 2015). We reasoned that the increased sensitivity of *sws-1* mutants to CPT might stem from a failure to stabilize RAD-51 presynaptic filaments at damage sites. To test this hypothesis, we visualized RAD-51 foci by immunofluorescence (Figure 13). In wild-type and *sws-1* germline nuclei under normal conditions, RAD-51 foci were rarely – if at all – seen in the mitotic zone (Figure 13A). In response to CPT treatment, RAD-51 foci were readily visible throughout the mitotic zone nuclei in wild-type germ lines, indicative of ongoing HR repair (compare Figure 13A and 13C). In contrast, we observed a striking absence of RAD-51 foci in the mitotic zone of *sws-1* germ lines following CPT exposure (compare Figure 13B and 13D). These results suggest that the sensitivity of *sws-1* mutants to CPT may be due to a failure to undergo HR repair.

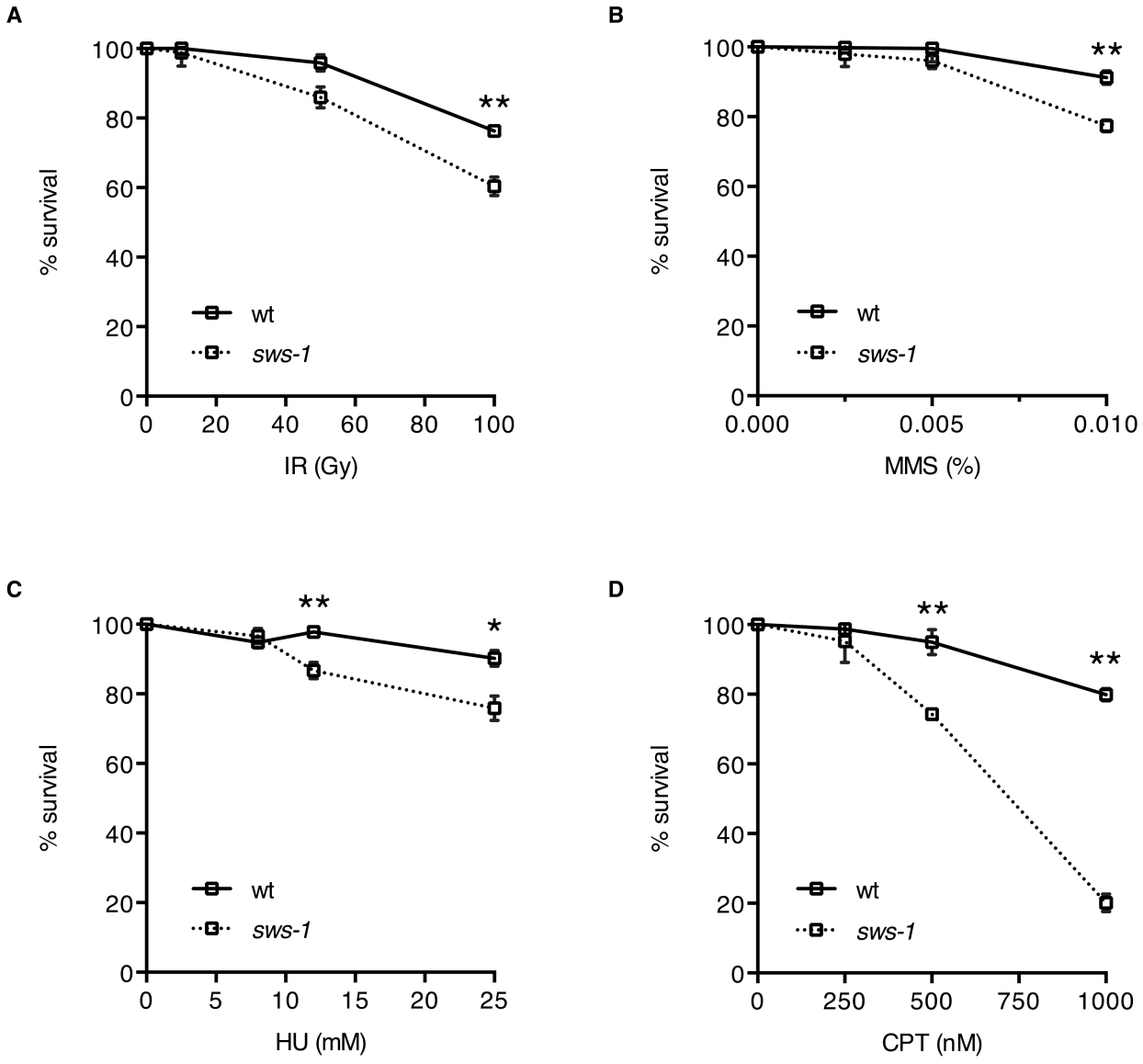

Figure 11. ***sws-1*** **mutants are sensitive to genotoxins that induce HR repair substrates: Progeny survival of hermaphrodites treated with IR (A), MMS (B), HU (C), or CPT (D) as described in Section 2.2.7. Survival was calculated as the number of adult progeny divided by the number of eggs and L1s relative to untreated worms ± SEM from at least 22 adults over two trials. Statistical analysis was performed using Student's t-test (* p<0.01, ** p<0.0001).**

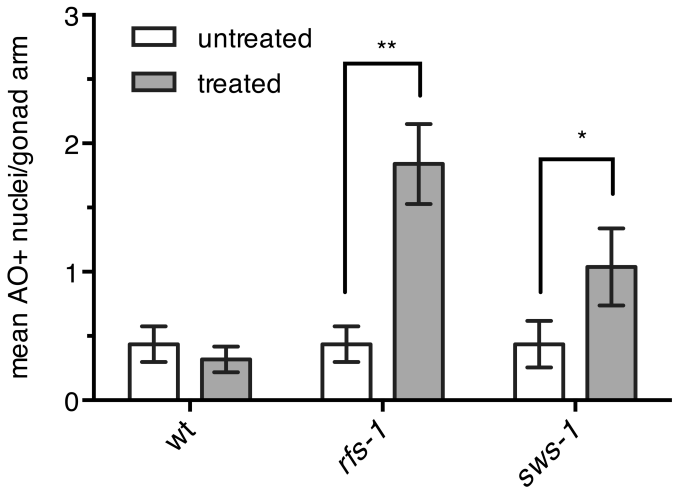

Figure 12. Apoptosis increases in response to CPT in *rfs-1* and *sws-1* germ lines: Apoptosis in wt, *rfs-1*, and *sws-1* germ lines as determined by retention of acridine orange (AO) staining. Young adult hermaphrodites were treated with 0 (untreated) or 500 nM (treated) CPT and stained with AO in the timeframe corresponding to assessment of progeny survival (Figure 11) as described in Section 2.2.7.3. The data are presented as mean AO-positive nuclei per gonad arm ± SEM for 25 hermaphrodites. * $p<0.05$, ** $p<0.001$, Mann-Whitney.

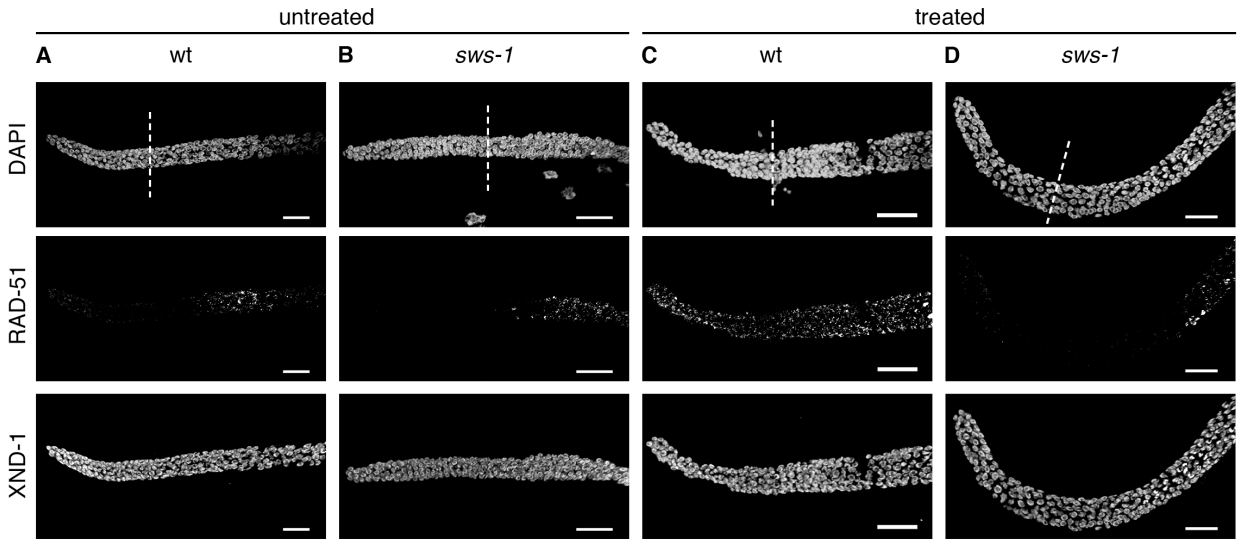

Figure 13. *sws-1* fails to form mitotic RAD-51 foci following CPT treatment: Immunofluorescence of RAD-51 with or without CPT exposure in germ lines of wt (A, C) and *sws-1* (B, D) hermaphrodites. Treated worms were exposed to 500 nM CPT as described in Section 2.2.7.3 and dissected at the end of the recovery period. Immunostaining conditions described in Section 2.2.8. White dashed line marks beginning of transition zone. XND-1 immunofluorescence serves as a staining control. Scale bar is 20 µm.

2.3.3 RIP-1 interacts with SWS-1 by yeast-two-hybrid and bridges an interaction between SWS-1 and RFS-1 by yeast-three-hybrid

The HR repair defects of *sws-1* mutants, including synthetic lethality with *helq-1*, resemble those of RAD-51 paralogs *rfs-1* and *rip-1* (WARD *et al.* 2007; WARD *et al.* 2010; TAYLOR *et al.* 2015). To further explore if these factors act in the same pathway, we compared the lethality and male frequency of double and triple mutant combinations of *sws-1*, *rfs-1*, and *rip-1* (Table 3, rows C-I). We observed that the incidence of lethality was statistically unchanged between the *rfs-1,rip-1;sws-1* triple mutant and any of the single mutants (ANOVA, $p>0.05$). Curiously, the lethality of *rip-1;sws-1* double mutants exhibited reduced lethality compared to the *rfs-1,rip-1;sws-1*

triple mutant ($p<0.05$, Tukey's test, Table 5), although there was no statistical difference in lethality between *rip-1;sws-1* and either *rfs-1;sws-1* or *rfs-1,rip-1* double mutants. Furthermore, the lethality of the *rfs-1,rip-1;sws-1* triple mutant is well below the additive value predicted from each single mutant, suggesting the cause of lethality is shared. The male frequency of *rfs-1,rip-1;sws-1* triple mutants was unchanged from either *rfs-1* or *rip-1* single mutants, but significantly increased compared to *sws-1* single mutants ($p<0.05$, Tukey's test, Table 6). This result is consistent with the observation in yeast that *psy3* or *csm2* mutants exhibit more severe phenotypes compared to *shu1* or *shu2* mutants (SASANUMA *et al.* 2013; GODIN *et al.* 2015), and highlights the importance of the RAD-51 paralogs in Shu complex function.

In yeast and human cells, Shu2/SWS1 is found in complexes with the Rad51 paralogs Csm2-Psy3 and SWSAP1, respectively (MARTIN *et al.* 2006; LIU *et al.* 2011; GODIN *et al.* 2013; GODIN *et al.* 2015). To determine if SWS-1 similarly interacts with the known RAD-51 paralogs in *C. elegans*, we performed yeast-two-hybrid (Y2H) analysis, fusing SWS-1, RFS-1, or RIP-1 to the GAL4 activation domain (pGAD) and the GAL4 DNA-binding domain (pGBD). By Y2H, SWS-1 interacted directly with RIP-1 but not RFS-1 in both configurations (Figure 14A and Figure 15). Since yeast Shu2 interacts with the other Shu complex members Shu1 and Psy3, and human SWS1 directly interacts with SWSAP1, we next examined if worm SWS-1 could interact with the any other member of the yeast Shu complex or with human SWSAP1 by Y2H. We were unable to detect a cross-species Y2H interaction between worm SWS-1 and the other yeast or human Shu complex members (Figure 16 and data not shown). These data make it unlikely that the yeast Shu complex members are bridging an interaction between SWS-1 and RIP-1. Rather, these data support the conclusion that SWS-1 and RIP-1 directly interact and comprise core components of the worm Shu complex.

Based on the known Y2H interaction between RIP-1 and RFS-1 ((TAYLOR *et al.* 2015) and Figure 7A), we hypothesized that RIP-1 may bridge an interaction between SWS-1 and RFS-1. To test this possibility, we performed a yeast-three-hybrid (Y3H) assay in which SWS-1 was again expressed as a fusion with the GAL4 activation domain and RFS-1 as a fusion with the GAL4 DNA-binding domain, but in this case a third, untagged vector expressing RIP-1 or an empty vector was co-expressed (pRS416-RIP-1 or pRS416, respectively) (Figure 7B). By Y3H, we find that in the presence of RIP-1, but not the empty vector control, SWS-1 and RFS-1 confer growth on the Y3H medium suggesting that these proteins are now able to interact (Figure 7B). Together, these studies suggest that RIP-1 facilitates ternary complex formation with SWS-1 and RFS-1.

Table 5. One-way ANOVA multiple comparisons of lethality among genetic combinations of *sws-1*, *rfs-1*, and *rip-1*: Tukey's test performed simultaneously with one-way ANOVA. Asterisks indicate multiplicity adjusted p values (p<0.01).**

Comparison	Mean Diff.	95% CI of Diff.	p<0.05
sws-1 vs. rip-1;sws-1	5.867	-1.328 to 13.06	No
sws-1 vs. rip-1	2.121	-8.095 to 12.34	No
sws-1 vs. *rfs-1,rip-1*	-0.02070	-8.152 to 8.111	No
sws-1 vs. *rfs-1,rip-1;sws-1*	-3.880	-10.45 to 2.689	No
sws-1 vs. *rfs-1*	-0.9106	-9.319 to 7.498	No
sws-1 vs. *rfs-1;sws-1*	0.6105	-7.074 to 8.295	No
rip-1;sws-1 vs. *rip-1*	3.746	-7.013 to 14.50	No
rip-1;sws-1 vs. *rfs-1,rip-1*	-5.888	-14.69 to 2.915	No
rip-1;sws-1 vs. *rfs-1,rip-1;sws-1*	-9.748	-17.13 to -2.363	Yes**
rip-1;sws-1 vs. *rfs-1*	-6.778	-15.84 to 2.282	No
rip-1;sws-1 vs. *rfs-1;sws-1*	-5.257	-13.65 to 3.135	No
rip-1 vs. *rfs-1,rip-1*	-2.142	-13.55 to 9.264	No
rip-1 vs. *rfs-1,rip-1;sws-1*	-6.002	-16.35 to 4.349	No
rip-1 vs. *rfs-1*	-3.032	-14.64 to 8.574	No
rip-1 vs. *rfs-1;sws-1*	-1.511	-12.60 to 9.581	No
rfs-1,rip-1 vs. *rfs-1,rip-1;sws-1*	-3.860	-12.16 to 4.439	No
rfs-1,rip-1 vs. *rfs-1*	0.8899	-8.930 to 10.71	No
rfs-1,rip-1 vs. *rfs-1;sws-1*	-0.6312	-9.838 to 8.576	No

Table 5 (continued)

rfs-1,rip-1;sws-1 vs. *rfs-1*	-2.970	-11.54 to 5.601	No
rfs-1,rip-1;sws-1 vs. *rfs-1;sws-1*	-4.491	-12.35 to 3.371	No
rfs-1 vs. *rfs-1;sws-1*	1.521	-7.932 to 10.97	No

Table 6. One-way ANOVA multiple comparisons of male frequency among genetic combinations of *sws-1*, *rfs-1*, and *rip-1*: Tukey's test performed simultaneously with one-way ANOVA. Asterisks indicate multiplicity adjusted p values (* p<0.05, ** p<0.01, *** p<0.001, ****p<0.0001).

Comparison	Mean Diff.	95% CI of Diff.	p<0.05
sws-1 vs. *rip-1;sws-1*	-0.2374	-1.177 to 0.7025	No
sws-1 vs. *rip-1*	-1.151	-2.486 to 0.1833	No
sws-1 vs. *rfs-1,rip-1*	-1.568	-2.630 to -0.5058	Yes***
sws-1 vs. *rfs-1,rip-1;sws-1*	-1.798	-2.656 to -0.9398	Yes****
sws-1 vs. *rfs-1*	-1.583	-2.681 to -0.4846	Yes***
sws-1 vs. *rfs-1;sws-1*	-1.152	-2.156 to -0.1480	Yes*
rip-1;sws-1 vs. *rip-1*	-0.914	-2.319 to 0.4914	No
rip-1;sws-1 vs. *rfs-1,rip-1*	-1.331	-2.480 to -0.1808	Yes*
rip-1;sws-1 vs. *rfs-1,rip-1;sws-1*	-1.561	-2.525 to -0.5961	Yes****
rip-1;sws-1 vs. *rfs-1*	-1.346	-2.529 to -0.1622	Yes*
rip-1;sws-1 vs. *rfs-1;sws-1*	-0.9145	-2.011 to 0.1817	No
rip-1 vs. *rfs-1,rip-1*	-0.4167	-1.907 to 1.073	No
rip-1 vs. *rfs-1,rip-1;sws-1*	-0.6467	-1.999 to 0.7054	No
rip-1 vs. *rfs-1*	-0.4317	-1.948 to 1.084	No
rip-1 vs. *rfs-1;sws-1*	-0.0005128	-1.449 to 1.448	No
rfs-1,rip-1 vs. *rfs-1,rip-1;sws-1*	-0.23	-1.314 to 0.8541	No
rfs-1,rip-1 vs. *rfs-1*	-0.015	-1.298 to 1.268	No
rfs-1,rip-1 vs. *rfs-1;sws-1*	0.4162	-0.7865 to 1.619	No

Table 6 (continued)

rfs-1,rip-1;sws-1 vs. *rfs-1*	0.215	-0.9046 to 1.335	No
rfs-1,rip-1;sws-1 vs. *rfs-1;sws-1*	0.6462	-0.3808 to 1.673	No
rfs-1 vs. *rfs-1;sws-1*	0.4312	-0.8037 to 1.666	No

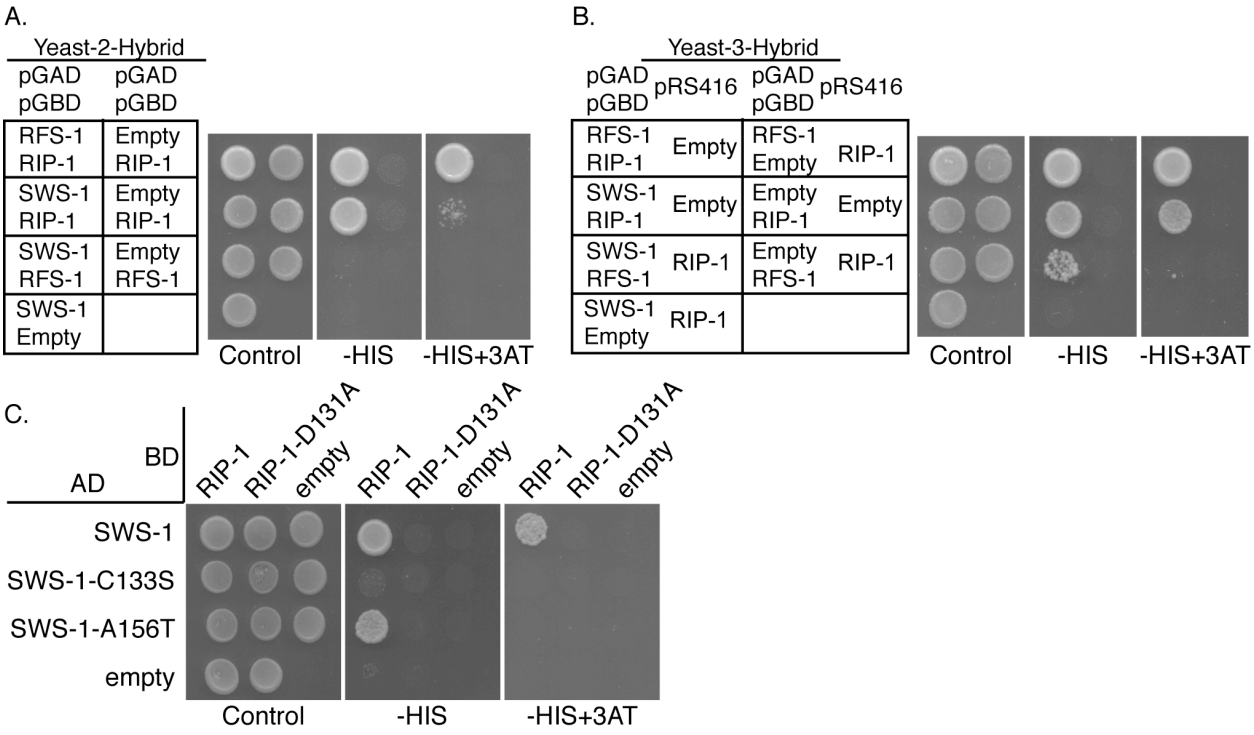

Figure 14. RIP-1 interacts with SWS-1 and bridges an interaction between SWS-1 and RFS-1: Y2H (A, C) and Y3H (B) panels from left to right show plating controls on SC-LEU-TRP or SC-LEU-TRP-URA respectively with the additional dropout of histidine (-HIS) and histidine with 3-amino-1,2,4-triazole (-HIS+3AT) indicating interaction a Y2H or Y3H interaction. Within each panel, the left column shows potential interactions between two proteins and the right column shows an empty vector control. RIP-1 interacts with both SWS-1 and RFS-1. SWS-1 and RFS-1 do not interact (A). With constitutive expression of RIP-1, SWS-1 and RFS-1 promote growth on SC-LEU-TRP-URA-HIS indicating a Y3H interaction (row 3, B). Two SWIM domain mutations were created in SWS-1, C133S and A156T. SWS-1-C133S disrupts interaction with RIP-1 (row 2, C). SWS-1-A156T decreases interaction with RIP-1 on –HIS+3AT (row 3, C). A Walker B motif mutation was introduced into RIP-1 that disrupts interaction with SWS-1, SWS-1-C133S, and SWS-1-A146T (column 2, C). Performed by MR Sullivan.

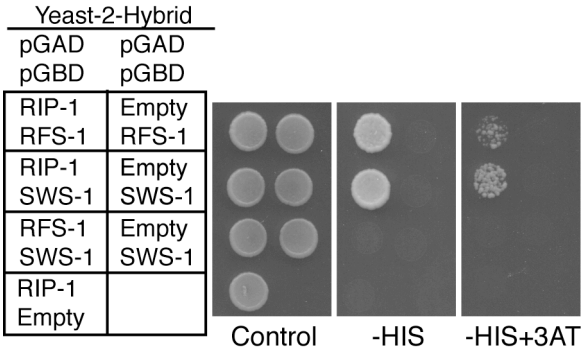

Figure 15. SWS-1, RIP-1, RFS-1 Y2H interactions are also observed when the genes are cloned into the opposite pGAD or pGBD vectors shown in Figure 14: SWS-1 interacts with RIP-1 when RIP-1 is expressed in the pGAD plasmid and SWS-1 is expressed in the pGBD plasmid. SWS-1 does not interact with RFS-1 when RFS-1 is expressed in the pGAD plasmid and SWS-1 is expressed in the pGBD plasmid. Performed by MR Sullivan.

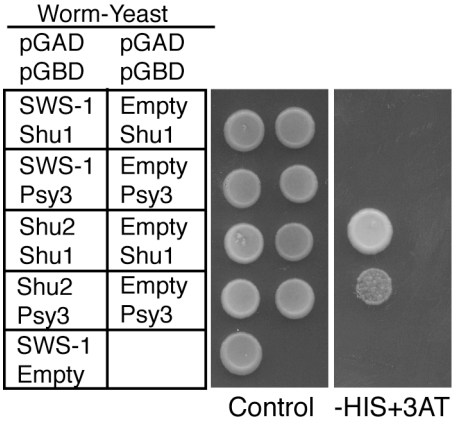

Figure 16. Y2H of SWS-1 with yeast Shu complex components: Interactions between worm SWS-1 and yeast Shu1 or Psy3 were not detected. Controls show known interactions between the yeast SWS1 family member, Shu2, and its binding partners Shu1 and Psy3 on –HIS+3AT. Performed by MR Sullivan.

2.3.4 The SWIM domain in SWS-1 and the Walker B motif in RIP-1 are important for their yeast-two-hybrid interaction

We originally identified SWS-1 because of its invariant SWIM domain, a zinc-finger binding-like motif ($CxCx_nCxHxxA$, n being 6-25 residues), which we found to be important for Sws1 protein family Y2H interactions with the Rad51 paralogs in yeast and humans (GODIN *et al.* 2015). Therefore, we wondered whether the SWIM domain of SWS-1 would be important for its interaction with RIP-1. We mutated the second cysteine of the SWIM motif to serine (*sws-1-C133S*) in the Y2H expression vector and retested the functionality of this protein to support growth on SC-HIS medium or the more stringent SC-HIS+3AT medium, where 3AT is a competitive inhibitor of histidine. As shown in Figure 14, *sws-1-C133S* abrogated the Y2H interaction between SWS-1 and RIP-1 (Figure 14C). Previously we identified a cancer-associated mutation in human SWS1 on the COSMIC database where the invariant alanine was mutated to a threonine (GODIN *et al.* 2015). Therefore, we made the analogous mutation in SWS-1 and found that *sws-1-A156T* maintains its interaction with RIP-1 at lower stringencies but exhibited reduced Y2H interaction upon more stringent conditions (Figure 14C; plating on SC–HIS medium vs. SC–HIS+3AT). Together these results suggest that the SWIM domain in SWS-1 is important for its interaction with RIP-1.

RIP-1 is defined as a RAD-51 paralog by the presence of a conserved Walker B-like motif. Therefore, we next asked whether the Walker B motif is important for its interaction with SWS-1. By Y2H, expression of a RIP-1 Walker B mutant, *rip-1-D131A*, disrupts interaction with both wild-type SWS-1 and the SWS-1 SWIM domain mutants (C133S and A156T) (Figure 14C). Interestingly, *rip-1-D131A* was found to maintain its Y2H interaction with RFS-1 under

the same conditions (TAYLOR *et al.* 2015). Therefore, RIP-1 interacts with SWS-1 through its Walker B-like motif.

2.4 DISCUSSION

2.4.1 SWS-1 functions in HR with RFS-1 and RIP-1

C. elegans sws-1 was identified as a putative Shu2 homolog based on the presence of a conserved SWIM domain, although no functional analysis was performed (GODIN *et al.* 2015). Using a nonsense allele of *sws-1* (Figure 5), we show that *sws-1* is involved in HR in the germ line. *sws-1* mutants exhibit mild reduction in viability and increased male frequency compared to wild type (Table 3). The mildness of these phenotypes belies the importance of *sws-1* when worms are further compromised by loss of *helq-1*. *helq-1;sws-1* double mutants exhibit synthetic lethality and diakinesis oocytes with severe chromosomal abnormalities (Figure 7). These results indicate functional redundancy of *sws-1* and *helq-1* for meiotic HR repair. Impaired meiotic HR functions become obvious in *sws-1* single mutants based on the sensitivity to DSB-inducing agents (Figure 11), and perhaps most significantly, increased accumulation of RAD-51 in mid- to late- pachytene nuclei (Figure 8).

The clear substrate preference for SWS-1 at replication forks implicates a mitotic role: first, *sws-1* is needed to maintain poly G/C tract stability in the absence of *dog-1* (Figure 10), which is predicted to function during DNA replication (YOUDS *et al.* 2006); second, *sws-1* mutants are most sensitive to CPT, which induces DSBs by blocking replication forks (Figure 11); third, RAD-51 foci were notably absent in *sws-1* mitotic nuclei following CPT treatment

(Figure 13). However, the timing of our genotoxin exposure assays is consistent with assessing repair capacity of meiotic nuclei (JARAMILLO-LAMBERT *et al.* 2007; KESSLER AND YANOWITZ 2014). Consistent with this, we observed a 2- and 4-fold increase in germline apoptosis following treatment with CPT in *sws-1* and *rfs-1* hermaphrodites, respectively (Figure 12). Collectively, these results suggest that *sws-1* promotes HR by stabilizing RAD-51 at specific HR substrates in both mitosis and meiosis, as has been shown for *rfs-1* and *rip-1* (WARD *et al.* 2007; TAYLOR *et al.* 2015). Using this cell biological approach, we cannot distinguish if SWS-1 promotes RAD-51 loading or stabilizes RAD-51 after it has loaded onto ssDNA, as previous work with RFS-1 and RIP-1 has suggested (TAYLOR *et al.* 2015).

The similar phenotypes of *sws-1* and the RAD-51 paralogs, *rfs-1* and *rip-1* (WARD *et al.* 2007; WARD *et al.* 2010; TAYLOR *et al.* 2015), prompted us to examine whether these genes function together in HR repair. The lack of additive lethality among double and triple mutant combinations strongly suggests that they function together (Table 3 and Table 5). In support of this notion, we observe a direct interaction between SWS-1 with RIP-1 and RFS-1 by Y2H (Figure 14). Taken together, our results suggest that SWS-1, RIP-1, and RFS-1 form a conserved complex to promote RAD-51-dependent HR (Figure 17). We note that *rfs-1* mutants have a higher male frequency than *sws-1*, which likely contributes to the increased male frequency in the triple mutants (Table 3 and Table 6). While we cannot rule out that *rfs-1* may have additional roles outside of the Shu complex, it may be that mutation of *rfs-1* may have more severe consequences than other members of the complex because it directly mediates an interaction with RAD-51 (WARD *et al.* 2010; TAYLOR *et al.* 2015).

2.4.2 The *C. elegans* Shu complex is composed of SWS-1, RIP-1, and RFS-1

Budding and fission yeast as well as the human Shu complexes have been defined as consisting of an SWS1 protein family member and its associated RAD51 paralog interacting partners (SHOR *et al.* 2005; MARTIN *et al.* 2006; LIU *et al.* 2011). Using this definition, we propose that *C. elegans* contains a Shu complex comprised of SWS-1, RIP-1, and RFS-1 (Figure 17). Previously, we have shown that yeast Shu2 is most closely related to SWS-1 in *C. elegans* using sequence homology to the conserved SWIM domain; however, it remained unknown whether this conservation was limited to its sequence or if it extended to SWS-1 protein function (GODIN *et al.* 2015). Given the embryonic lethality observed in the knockout models of the mouse RAD51 paralogs (DEANS *et al.* 2000; THACKER 2005; KUZNETSOV *et al.* 2009; SUWAKI *et al.* 2011), our work in *C. elegans* provides a unique opportunity to study Shu complex disruption in a multicellular organism. Here we demonstrate the first evidence for a functional worm Shu complex consisting of SWS-1 and RIP-1, which likely directly interact through the SWIM domain of SWS-1 and the Walker B motif of RIP-1. Note that it is possible that the *sws-1* SWIM domain mutants may not be properly folded or expressed. Additionally, RIP-1 bridges an interaction between SWS-1 and RFS-1 (Figures 14 and 17). Unlike yeast and humans, only two RAD-51 paralogs have been identified in worms (WARD *et al.* 2007; TAYLOR *et al.* 2015). One possibility is that the worm RAD-51 paralogs, RFS-1 and RIP-1, are sufficient to perform all the various functions of the RAD-51 paralogs described in other eukaryotes. Alternatively, additional RAD-51 paralogs have yet to be identified in *C. elegans*. Importantly, the budding yeast Csm2 and Psy3 proteins were only shown to be Rad51 paralogs upon crystallization as their sequence conservation to Rad51 is extremely poor (SHE *et al.* 2012; TAO *et al.* 2012; SASANUMA *et al.* 2013). Further, the poor sequence conservation of Rad51 paralogs between

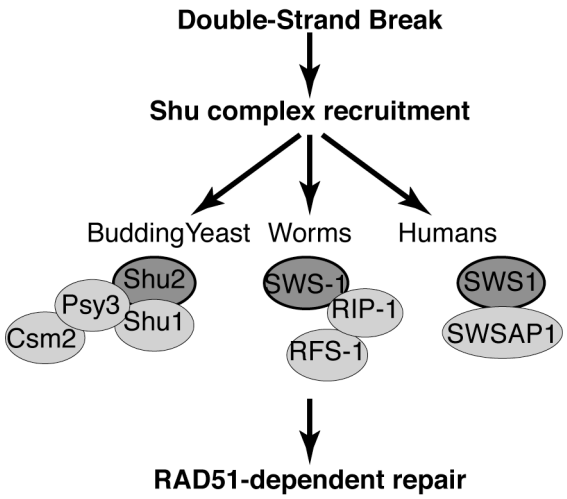

Figure 17. Model of Shu complex function in promoting Rad51-mediated repair: After a double-strand break occurs, the Shu complex in budding yeast, worms, or humans, is recruited to sites of DNA damage where it subsequently promotes RAD51-dependent repair. In budding yeast, the Shu complex is composed of a SWIM domain containing protein, Shu2, the Rad51 paralogs Csm2-Psy3, and Shu1. In humans the exact components of the Shu complex are not completely known but consist of the SWIM domain containing protein, SWS1, and its associated RAD51 paralog, SWSAP1. Here we define the worm Shu complex to consist of SWS-1 and the RAD-51 paralogs, RFS-1 and RIP-1, where SWS-1 directly interacts with RIP-1 through the SWIM domain of SWS-1 and the Walker-B motif of RIP-1. RIP-1 bridges an interaction between SWS-1 and RFS-1 suggesting that it can interact with both proteins simultaneously. SWS1 family members are depicted by dark gray circles with a black outline and the other Shu complex components by light gray circles.

species and our inability to complement yeast harboring disruptions of the Shu complex genes with worm proteins also makes direct comparisons between the individual Rad51 paralogs challenging (data not shown). Therefore, further studies will be important for determining whether additional RAD-51 paralogs exist in worms and which RAD-51 paralogs correlate with the functions attributed to the equivalent human and yeast proteins.

2.4.3 Substrate specificity of the worm Shu complex

We find that *sws-1* mutants are most sensitive to the DNA damaging agent CPT (Figure 11). In contrast, budding yeast containing a deletion of the *sws-1* ortholog, *shu2*Δ, exhibits a more pronounced sensitivity to MMS (SHOR *et al.* 2005; MANKOURI *et al.* 2007; BALL *et al.* 2009). Therefore, it is possible that the different DNA damage sensitivities observed for the Shu complex members relative to other more general HR factors may indicate a specialized role of SWS-1 in repair of specific types of DNA lesions. CPT is a topoisomerase I inhibitor which would specifically become covalently modified on the ssDNA end and would therefore be converted into a DSB upon replication fork progression. It is intriguing to speculate that perhaps the specific sensitivity of *sws-1* worms to CPT provides a framework for determining the types of DNA structures created during meiosis. Studies in yeast have shown that the Shu complex is important for driving homolog bias during meiosis, where the homologous chromosome is made the preferred partner for repair over the sister chromatid (HONG AND KIM 2013; HONG *et al.* 2013; SASANUMA *et al.* 2013). Therefore, further studies to delineate the specific lesions that the worm Shu complex are needed to resolve will shed light on their function during both mitotic and meiotic repair. Importantly, our work on the worm Shu complex provides a new way in which to study disruption in the Shu complex in the context of a multicellular organism that will

help us to determine why mutations in the human RAD51 paralogs are associated with cancer predisposition and in some cases Fanconi anemia.

2.5 ACKNOWLEDGEMENTS

We are grateful to Tyler Machovina for performing injections and initial screening. We thank Simon Boulton, Ann Rose, and Sarit Smolikov for strains, Verena Jantsch for the anti-RAD-51 antibody, and Francis Gandhi for guidance with qPCR. Some strains were provided by the Caenorhabditis Genetics Center, which is funded by NIH Office of Research Infrastructure Programs (P40 OD010440). Sequencing of CRISPR constructs and of *sws-1* was performed in the Genomics Research Core at the University of Pittsburgh. This work was supported by the National Institutes of Health grants to K.A.B. (ES024872) and J.L.Y. (GM1040070).

A modified version of this paper has been accepted at *Genetics*:

Promotion of Homologous Recombination by SWS-1 in Complex with RAD-51 Paralogs in *Caenorhabditis elegans*

***McClendon TB**, *Sullivan MR, Bernstein KA, Yanowitz JL.

* Denotes equally contributing authors

3.0 X CHROMOSOME CROSSOVER FORMATION AND GENOME STABILITY IN *CAENORHABDITIS ELEGANS* ARE INDEPENDENTLY REGULATED BY *XND-1*

Maintenance of genome integrity is important for both individual survival and species propagation. During meiosis I, different classes of genes maintain genome stability, from induction and repair of programmed double-strand breaks by homologous recombination, to modulation of chromatin structure through histone modifications – which can affect DNA accessibility and regulate DNA-dependent processes through recruitment of effector molecules. We show here that *xnd-1*, known to have roles in ensuring X chromosome CO formation and germline development, also regulates genome stability. *xnd-1* mutants exhibit a mortal germ line, high embryonic lethality, *h*igh *i*ncidence of *m*ales, and sensitivity to ionizing radiation. However, the nature of genome instability in *xnd-1* mutants is unknown. A reported increase in acetylation of H2A lysine 5 in *xnd-1* germ lines prompted us to examine the histone acetyltransferase *mys-1*, whose homolog TIP60 acetylates H2AK5. Here we show that a hypomorphic allele of *mys-1* increases fecundity and fitness in *xnd-1* mutants and rescues *xnd-1* IR sensitivity, all of which may be mediated through H2AK5 acetylation. Our data suggests *mys-1* functions independently of DNA damage checkpoint factors *hus-1* and *cep-1*, and parallel to *atm-1*. Interestingly, decreased *mys-1* function does not affect the *h*igh *i*ncidence of *m*ales phenotype in *xnd-1* mutants and can instead be attributed to *him-5*, which is under expressed in *xnd-1* germ lines. Our work

provides *xnd-1* as a model in which to study the link between chromatin factors, gene expression, and genome stability.

3.1 INTRODUCTION

Genome stability encompasses the mechanisms that ensure the integrity of DNA is kept intact amidst constant insults, the most toxic of which are DNA double-strand breaks (DSBs). DSBs emanate from both endogenous sources such as replication stress and the action of nucleases, or exogenous sources such as ionizing radiation (IR). Despite their toxicity, the formation and repair of DSBs in the germ line is essential for the establishment of crossovers (COs) between homologous chromosomes during meiosis I. DSBs are purposefully created as the first step in meiotic CO formation by the topoisomerase-like enzyme Spo11 (KEENEY *et al.* 1997; DERNBURG *et al.* 1998). To maintain genome integrity, two events must occur: first, at least one DSB per chromosome pair must be repaired by interhomolog homologous recombination (HR) and resolved as a CO; second, other DSBs must be repaired by HR with a non-CO outcome. Defects in either event are associated with genome instability, either from aneuploidy due to chromosome missegregation, or through inappropriate DNA repair. Accordingly, numerous factors ensure the appropriate execution of meiotic HR, including those involved in DSB formation, DNA damage sensing and repair, and chromatin structure (LUI AND COLAIACOVO 2013).

DNA and its associated proteins together form chromatin, the fundamental unit of which is the nucleosome, comprised of ~146 bp of DNA wound around a histone octamer made up of two copies each of histones H2A, H2B, H3, and H4 (KORNBERG 1974; LUGER *et al.* 1997).

Histones are highly basic globular proteins with flexible N-terminal tails that can be covalently modified by a variety of post-translational modifications (PTMs). The type, placement, and abundance of these marks confers exquisite variation in regulating DNA-dependent processes (JENUWEIN AND ALLIS 2001), including meiotic DSB formation and HR repair.

During meiosis, programmed DSB formation occurs at specific regions of the genome called hotspots that are enriched with histone H3 trimethylation at lysine 4, a mark that is also associated with transcriptionally-active chromatin (BORDE *et al.* 2009; BUARD *et al.* 2009; SMAGULOVA *et al.* 2011). In mice, an additional level of regulation is conferred by the histone H3 methyltransferase PRDM9, which directs recombination away from promoter-associated H3K4me3 (BRICK *et al.* 2012; WU *et al.* 2013). In response to exogenous DSBs, chromatin undergoes decondensation both locally and globally (KRUHLAK *et al.* 2006; DELLAIRE *et al.* 2009). The relaxed chromatin structure facilitates the activation and recruitment of ATM, which initiates a signaling cascade leading to histone acetylation and additional chromatin remodeling at the DSB site to promote amplification of the DNA damage response, recruit repair factors, and provide accessibility to the repair machinery (DEEM *et al.* 2012). Following repair, the nucleosome is replaced and/or reassembled. In yeast, acetylation of lysine 56 on histone H3 is required to inactivate the DNA damage response (CHEN AND TYLER 2008).

In contrast, very little is known about how histone PTMs affect HR in the *C. elegans* germ line, though regulation of histone acetylation has been linked to both meiotic DSB formation and HR. *cra-1* promotes DSB formation through regulation of global histone acetylation (GAO *et al.* 2015). Another study has shown that acetylation of lysine 5 on histone H2A (H2AK5ac) is removed in pachytene nuclei in response to IR, then replaced following repair (COUTEAU AND ZETKA 2011). Interestingly, *xnd-1* germ lines exhibit an increase in

H2AK5ac and decreased DSB formation, especially on the X chromosome (WAGNER *et al.* 2010; GAO *et al.* 2015). Thus, the significance of histone acetylation in the germ line, particularly H2AK5ac, is not well understood.

Previously, we identified *xnd-1* as an autosomally-associated protein that regulates X chromosome CO formation through chromatin structure (WAGNER *et al.* 2010); additionally, we recently described a role for *xnd-1* in germline development (MAINPAL *et al.* 2015). The variability in severity of *xnd-1* phenotypes, including brood size, lethality, and sterility, suggested a broader role for *xnd-1* in maintaining genome stability. Here we show that *xnd-1* is a regulator of genome stability in the *C. elegans* germ line. *xnd-1* mutants exhibit a mortal germ line phenotype and are sensitive to ionizing radiation, consistent with a role in responding to DNA damage. Interestingly, a hypomorphic allele of the histone acetyltransferase *mys-1* completely rescued *xnd-1* IR sensitivity and improved fecundity, both of which appear to be mediated through H2AK5ac. Although *mys-1*-depdendent changes in chromatin structure had no effect on the male frequency (Himness) of *xnd-1* mutants, we find instead that the X chromosome CO defect in *xnd-1* mutants is due to low expression of *him-5*, which XND-1 appears to regulate transcriptionally. Our work provides *xnd-1* as a model in which to study the link between chromatin factors, gene expression, and genome stability.

3.2 MATERIALS AND METHODS

3.2.1 Culture and strains

For all experiments, worms were cultured on NGM plates seeded with OP50 at 20°C unless otherwise noted (BRENNER 1974). Mutant strains used in this study were: LG I, *hus-1(op244)*, *atm-1(gk186)*, *cep-1(gk138)*, *cep-1(lg12501)*; LG III, *xnd-1(ok709)*; LG IV, *ced-3(n717)*; LG V, *mys-1(n3681)*, *him-5(ok1896)*. Some strains were provided by the Caenorhabditis Genetics Center. *xnd-1(ok709)* was outcrossed multiple times for these studies due to long-term maintenance problems of the strain. Double and triple mutants were generated using standard genetic techniques and are listed in Table 7. Creation of transgenic animals is described in Section 3.2.9. N2 served as wild-type controls in this study. For strains containing either *xnd-1(ok709)* and/or an allele that must be balanced, F2 hermaphrodites were used unless otherwise noted. Due to some phenotypic differences between *xnd-1/qC1* and *xnd-1/hT2* populations, double and triple mutants were compared to the isogenic balancer strain (*xnd-1* F2 from *hT2*-balanced stock is described in Table 9; *xnd-1* F2 from *qC1*-balanced stock is described in Table 11).

Table 7. Strains generated for Chapter 3.

Strain	Genotype	Reference in text
QP810	*xnd-1(ok709)* III/qC1 [*dpy-19(e1259) glp-1(q339)* qIs26] III;*mys-1(n3681)* V	*xnd-1;mys-1*
QP1180	*hus-1(op244)* I;*xnd-1(ok709)* III/hT2 [*bli-4(3937) let-?(q782)* qIs48] (I;III)	*xnd-1;hus-1*
QP953	*atm-1(gk186)* I;*xnd-1(ok709)* III/hT2 [*bli-4(3937) let-?(q782)* qIs48] (I;III)	*xnd-1;atm-1*
QP1089	*xnd-1(ok709)* III/qC1 [*dpy-19(e1259) glp-1(q339)* qIs26] III;*ced-3(n717)* IV	*xnd-1;ced-3*
QP654	*cep-1(gk138)* I;*xnd-1(ok709)* III/hT2 [*bli-4(3937) let-?(q782)* qIs48]	*xnd-1;cep-1(gk)*
QP1181	*cep-1(lg12501)* I;*xnd-1(ok709)* III/hT2 [*bli-4(3937) let-?(q782)* qIs48]	*xnd-1;cep-1(lg)*
QP1182	*atm-1(gk186)* I/hT2 [*bli-4(3937) let-?(q782)* qIs48] (I;III);*mys-1(n3681)* V	*atm-1;mys-1*
QP1183	*atm-1(gk186)* I;*xnd-1(ok709)* III/hT2 [*bli-4(3937) let-?(q782)* qIs48] (I;III);*mys-1(n3681)* V	*xnd-1;atm-1;mys-1*
QP663	*unc-119(ed3)* III*;eaIs4*[*Phim-5::him-5::gfp::3xFLAG* + unc-119(+)] ?	*unc-119;eaIs4*

Table 7 (continued)

QP1176	*xnd-1(ok709)* III/qC1 [*dpy-19(e1259) glp-1(q339)* qIs26] III;*mys-1(n3681)* V;*eaIs4*[P*him-5::him-5::gfp::3xFLAG* + *unc-119(+)*] ?	*xnd-1;mys-1;eaIs4*
QP1016	*xnd-1(ok709)* III, *eaIs15*[*Ppie-1::him-5::gfp* + *unc-119*(+) III]/qC1 [*dpy-19(e1259) glp-1(q339)* qIs26] III	*xnd-1,eaIs15*
QP1042	*xnd-1(ok709)* III/qC1	*xnd-1*
QP964	*eaIs15*[*Ppie-1::him-5::gfp* + *unc-119*(+) III];*him-5(ok1896)* V	*him-5;eaIs15*
QP1030	*eaIs15*[*Ppie-1::him-5::gfp* + *unc-119*(+)]/qC1 [*dpy-19(e1259) glp-1(q339)* qIs26] III	*eaIs15*
QP1174	*xnd-1(ok709)* III/qC1 [*dpy-19(e1259) glp-1(q339)* qIs26] III;*eaIs4*[P*him-5::him-5::gfp::3xFLAG* + unc-119(+)] ?	*xnd-1;eaIs4*
QP1175	qC1 [*dpy-19(e1259) glp-1(q339)* qIs26] III;*mys-1(n3681)* V;*eaIs4*[P*him-5::him-5::gfp::3xFLAG* + unc-119(+)] ?	*mys-1;eaIs4*
QP1173	qC1 [*dpy-19(e1259) glp-1(q339)* qIs26] III;*eaIs4*[P*him-5::him-5::gfp::3xFLAG* + unc-119(+)] ?	*eaIs4*

3.2.2 Clutch size, brood size, lethality, Him frequency

L4 hermaphrodites of a given genotype were individually plated and transferred to a clean plate every 12 hours until egg-laying ceased. After transfer, the number of eggs and L1s on the plate were counted and recorded. Three to four days later, each plate was scored for the number of adult hermaphrodites and males. Timepoint data from each individual parent was combined to give total eggs, total adult brood, and total males. Percent hatching was calculated by dividing total adults by total eggs and multiplying by 100. Percent lethality was then calculated by subtracting this value from 100. Percent lethality is normalized to N2 to account for ~2% error in egg counts. To calculate percent male, the total number of males was divided by the total number of adults and multiplied by 100. The data are presented as the mean ± SEM from isogenic parents. Statistical tests used were Student's t-test or Mann-Whitney depending on whether or not the data were normally distributed based on the results of D'Agostino-Pearson normality test.

3.2.3 Sterility

All progeny from several hermaphrodite parents were plated individually. For strains containing either *xnd-1(ok709)* and/or an allele that must be balanced, F1 hermaphrodite parents were used; thus, F2 progeny were plated individually. Five days post-plating, each plate was scored for the presence or absence of eggs and/or progeny. Only plates in which the adult hermaphrodite was still present were included in analysis. Hermaphrodites failing to lay a single egg were scored as sterile. Data from isogenic worms were combined to give the total numbers of sterile worms and hermaphrodites scored. To calculate percent sterility, the total number of sterile worms was divided by the total number of hermaphrodites and multiplied by 100.

3.2.4 Microarray

Day 1 adult hermaphrodites were dissected in 1x sperm salts (50 mM PIPES, pH 7.0, 25 mM KCl, 1 mM $MgSO_4$, 45 mM NaCl, 2 mM $CaCl_2$) with 0.5 mM levamisole. Fifty distal gonads from both N2 and *xnd-1* were cleaved away from the maturing oocytes by cutting extruded gonads at the bend and collected in Trizol (Invitrogen) on ice. Samples were vortexed and frozen at -20°C prior to RNA isolation and cDNA synthesis, which were performed as previously described (FUKUSHIGE AND KRAUSE 2012). Microarrays were performed by Dr. Michael W. Krause (National Institute of Diabetes and Digestive Kidney Diseases) using the C. elegans Genome Array (Affymetrix).

3.2.5 Gene expression analysis

Approximately 1000 day 1 adults of a given genotype were washed thrice in 1x M9 buffer (3 g/L KH_2PO_4, 6 g/L Na_2HPO_4, 5 g/L NaCl, 1 mM $MgSO_4$), resuspended in Trizol (Invitrogen) and vortexed for ~60 seconds before being flash frozen and stored at -80°C. Once all the samples were collected, the samples were thawed on ice, sonicated, and RNA was isolated by chloroform extraction and isopropanol precipitation. Samples were treated with DNase (Sigma #AMPD1) and reverse transcribed into cDNA (Protoscript m-MuLV First Strand cDNA Synthesis kit, NEB #E6300S) according to manufacturer's instructions. Quantitative real-time PCRs were performed on the Applied Bio Systems 7300 Real Time PCR System using Sybr Green chemistry (SensiMix SYBR Hi-ROX kit, Bioline #QT-605) with transcript-specific primers designed using GETPrime (Table 8, (GUBELMANN *et al.* 2011). The reference genes *rpl-32* and Y45F10D.4 (HOOGEWIJS *et al.* 2008) were used for normalization across samples and gene expression was

analyzed using the ΔC_T method (LIVAK AND SCHMITTGEN 2001). Results are presented as the average of combined data from three independent biological replicates that in turn is comprised of three technical replicates each.

3.2.6 Ionizing radiation (IR) sensitivity

L4 hermaphrodites were plated on each of four 6-cm plates at 30-100 worms/plate. The following day, worms were exposed to 10, 50, or 100 Gy of IR from a ^{137}Cs source (Gammacell®1000 Elite, Nordion International Inc.). Twelve hours post-irradiation, worms were individually plated and allowed to lay for twelve hours, at which point the number of eggs and L1s on the plate were counted. Three to four days later, each plate was scored for the number of adult progeny. Survival was calculated as the number of adult progeny divided by the number of eggs/L1s relative to untreated worms ± SEM from 10-95 adults over two trials.

3.2.7 Immunofluorescence

Day 1 adult worms were dissected in 1x sperm salts 1 mM levamisole and fixed in 0.5% triton/1% PFA for 5 minutes in a humid chamber. Slides were then freeze-cracked and briefly immersed in 100% ethanol. Following fixation, slides were washed in PBST and incubated in primary antibody (rabbit α-H2AK5ac, Cell Signaling #2576, 1:2000; guinea pig α-SYP-1, 1:1000, (MACQUEEN *et al.* 2002)) overnight at room temperature. Next day, slides were washed and incubated in secondary antibody (α-rabbit 568, 1:2000; α-guinea pig 488, 1:2000) for 90 minutes at room temperature in the dark. Slides were mounted in Prolong Gold with DAPI (Life Technologies) and visualized by confocal microscopy.

Table 8. qPCR primers used in Chapter 3.

Primer	Sequence (5'→3')
gen-1 (F)	GGAAGCTTCGTTTACGACG
gen-1 (R)	TCGTAATTGCATTGTGTACGG
rad-51 (F)	GTATCACTGAGGTTTACGGAG
rad-51 (R)	TCGGCAATTGACACAAGAC
rad-54 (F)	GAAGATAAGGATCGAAAGGTGC
rad-54 (R)	AACACCATCTCTTTGATGCG
rpa-2 (F)	AGAAAGCCTGACTCGAAGG
rpa-2 (R)	AAAGTGCTCGATCAGATTGGA
rtel-1 (F)	GATTTCTCGGAGTGACACTG
rtel-1 (R)	TGTATTCGGTCTTCGAATTCTC
slx-4/him-18 (F)	TCAGCTTCCAGTACCAGTG
slx-4/him-18 (R)	CATTTCTTCCAAGGATACAGGT
him-5 (F)	CTTTCTATGCAAAGCTCCGG
him-5 (R)	TCGTCATTGGAGTCGACAG
rpl-32 (F)	GGATTTGGACATGCTCCTC
rpl-32 (R)	GATTCCCTTGCGGCTCTT
Y45F10D.4 (F)	TTCACTGTTCAATGCTCGC
Y45F10D.4 (R)	CTTAGGCCTTCTTAGTCTGCT

3.2.8 Western blotting

For each genotype, a population of primarily adult worms was transferred from 2-6 6-cm plates into a glass conical tube and washed thrice with 1x M9. The remaining liquid was removed and the worm pellet was transferred to a 1.5 mL tube and flash frozen in liquid nitrogen. Pellets were thawed on ice, mixed with an equal volume of Laemmli Sample Buffer (Bio-Rad #161-0737) with 5% β-mercaptoethanol (Amresco M131), sonicated in a water bath for 2 minutes, heated at 95°C for 10 minutes, then spun in a tabletop centrifuge for 5 minutes at maximum speed. Samples were resolved by 12% PAGE (TGX FastCast, Bio-Rad) and transferred to nitrocellulose in 20% methanol. Membrane was blocked in 5% nonfat milk/TBST (50 mM Tris-HCl, pH 7.4, 150 mM NaCl, 0.1% Tween-20) overnight at 4°C. Next day, membrane was washed in TBST and incubated in α-FLAG M2 (Sigma-Aldrich F1804, 1:5000 in 3% milk/TBST) for 2 hours at room temperature, followed by α-mouse HRP (1:50,000 in 3% milk/TBST) for 1 hour at room temperature. Product was visualized by enhanced chemiluminescence (ECL) (Invitrogen #WP20005) according to manufacturer's instructions. Membrane was stripped by washing in mild stripping solution (200 mM glycine, 3.5 mM SDS, 1% Tween-20, pH to 2.2 with HCl) twice for 10 minutes each, followed by washing in PBS twice for 10 minutes each, then washing twice in TBST for 5 minutes each and blocking overnight as before. Membrane was incubated in α-E7 (tubulin, Developmental Studies Hybridoma Bank, 1:2000 in 0.2% milk/TBST) for 1.5 hours at room temperature, followed by α-mouse HRP (1:3000 in 0.2% milk/TBST) for 1 hour at room temperature. Product was visualized by ECL.

3.2.9 Transgene construction

The *Ppie-1::him-5::gfp::pie-1* 3' UTR transgene (*eaIs15*) was constructed by subcloning the open reading frame of *him-5* into pJK7 (John G. White lab) using 5' SpeI and 3' MluI restriction sites. The *Phim-5::him-5::gfp* transgene (*eaIs4*) was constructed by recombineering 2xTY::GFP::3xFLAG into the fosmid clone WRM0634bF01 at the C-terminus of *him-5* coding sequence (MAINPAL *et al.* 2015). All transgenes were bombarded in the *unc-119(ed3)* strain using microparticle bombardment (PRAITIS *et al.* 2001) to produce transgenic worms.

3.3 RESULTS

3.3.1 *xnd-1* is required for maintaining genome stability

Initial studies identified *xnd-1* for its role in CO formation and meiotic chromosome segregation. Mutations in *xnd-1* increased embryonic lethality – approximately half of eggs failed to hatch – and increased the incidence of males compared to wild type, evidence of X chromosome nondisjunction (WAGNER *et al.* 2010). We confirmed these phenotypes by following F2 hermaphrodites throughout their reproductive lifespan, taking note of the total number of eggs laid by each animal (hereafter referred to as clutch size) and the subsequent brood, including the number of males. Despite substantial variation in the severity of each phenotype examined among *xnd-1* hermaphrodites, we observed an overall reduced clutch size of *xnd-1* hermaphrodites compared to wild type (Table 9, compare rows A and B), as well as a reduced brood size reflective of increased embryonic lethality. We noted an increased incidence

Table 9. General characteristics of strains used in Chapter 3: Data was collected as described in Section 3.2.2.

*** p<0.05 vs. *xnd-1*, ** p<0.01 vs. *xnd-1*.**

	Genotype	n	Avg. Clutch ± SEM	Avg. Brood ± SEM	% lethal ± SEM (NORM.)	% male ± SEM
A	N2	5	235.20±12.72	231.00 ± 13.48	0.00 ± 1.04	0.10 ± 0.104
B	*xnd-1*	23	103.13 ± 10.97	40.39 ± 8.06	67.71 ± 4.82	15.49±2.65*
C	*mys-1*	5	255.60 ± 21.73	226.20 ± 20.17	9.81 ± 1.24	0.00 ± 0.00
D	*xnd-1;mys-1*	32	151.53 ± 5.14**	114.03± 4.76**	23.57 ± 1.81**	13.00 ± 1.66
E	*hus-1*	8	230.75 ± 13.12	184.75 ± 12.46	18.63 ± 2.11	0.61 ± 0.19
F	*xnd-1;hus-1*	21	110.10 ± 12.56	32.71 ± 5.87	73.67 ± 3.83	26.17 ± 4.53*
G	*cep-1(gk)*	10	192.30 ± 19.81	170.00 ± 19.88	10.93 ± 2.58	0.43 ± 0.34
H	*xnd-1;cep-1(gk)*	26	102.15 ± 10.69	31.04 ± 4.85	70.77 ± 3.60	30.28±3.41**
I	*cep-1(lg)*	8	213.38 ± 13.10	191.13 ± 12.25	8.74 ± 1.18	1.04 ± 0.33
J	*xnd-1;cep-1(lg)*	22	119.50 ± 10.40	32.27 ± 5.88	75.65 ± 3.63	34.69±5.65**
K	*atm-1*	5	250.60 ± 10.17	239.60 ± 8.78	2.50 ± 0.63	0.08 ± 0.08
L	*xnd-1;atm-1*	21	135.86 ± 9.68*	67.67 ± 9.79*	51.88 ± 4.92*	10.23 ± 1.69
M	*ced-3*	8	257.38 ± 14.60	192.00 ± 14.30	24.47 ± 1.90	0.44 ± 0.21
N	*xnd-1;ced-3*	26	94.04 ± 5.32	19.77 ± 2.74	79.64 ± 2.25*	18.80 ± 2.48
O	*atm-1;mys-1*	18	174.83 ± 8.56	162.33 ± 8.37	5.57 ± 0.87	0.13 ± 0.07
P	*xnd-1;atm-1;mys-1*	23	119.26 ± 8.53	78.96 ± 7.39**	33.94 ± 3.13**	22.93 ± 2.27*

of males in *xnd-1* broods, albeit at a lower frequency than previously reported (WAGNER *et al.* 2010), which we attribute to outcrossing. Consistent with previous reports, a fraction of *xnd-1* hermaphrodites were completely sterile and failed to lay a single egg (13.95%, $p<0.0001$ vs. N2, Fisher's exact test (WAGNER *et al.* 2010; MAINPAL *et al.* 2015)).

The variability that is observed in *xnd-1* mutants was reminiscent of mutations that cause a mortal germ line phenotype (AHMED AND HODGKIN 2000). We therefore set out to determine if the sterility and brood sizes associated with *xnd-1* mutations become more severe upon passaging. The progeny of ten, independent F1 animals were used to start 12 lines that were passaged by picking the first L4 animals to a new plate each generation. If no progeny were present, the next generation was seeded by an immediate cousin. Populations were declared fully sterile when all twelve animals gave no progeny. As shown in Figure 18A, the average brood sizes decreased and incidence of sterility increased with progressive generation in *xnd-1* mutants. After six generations, however, the brood size appeared to level off to an average size of ~30 progeny per worm. The percentage of sterile animals, however, continued to increase over 30 generations. These differences may reflect different thresholds for *xnd-1*-dependent function in egg production versus offspring viability. Collectively, these results clearly indicate that *xnd-1* mutants exhibit a mortal germ line phenotype.

Close examination of brood dynamics also revealed periodic upswings and downswings in population sizes from single lines (Figure 18A and B). For example, a line may show progressive decrease in brood size over 5-10 generations, reach a size of fewer than 10 progeny, and then increase to over 100 progeny in the next generation. Such transitions were reminiscent of our prior studies of *rfs-1*, a gene required for homologous recombination (YANOWITZ 2008). We therefore set out to determine if *xnd-1* may have a role in responding to DNA damage.

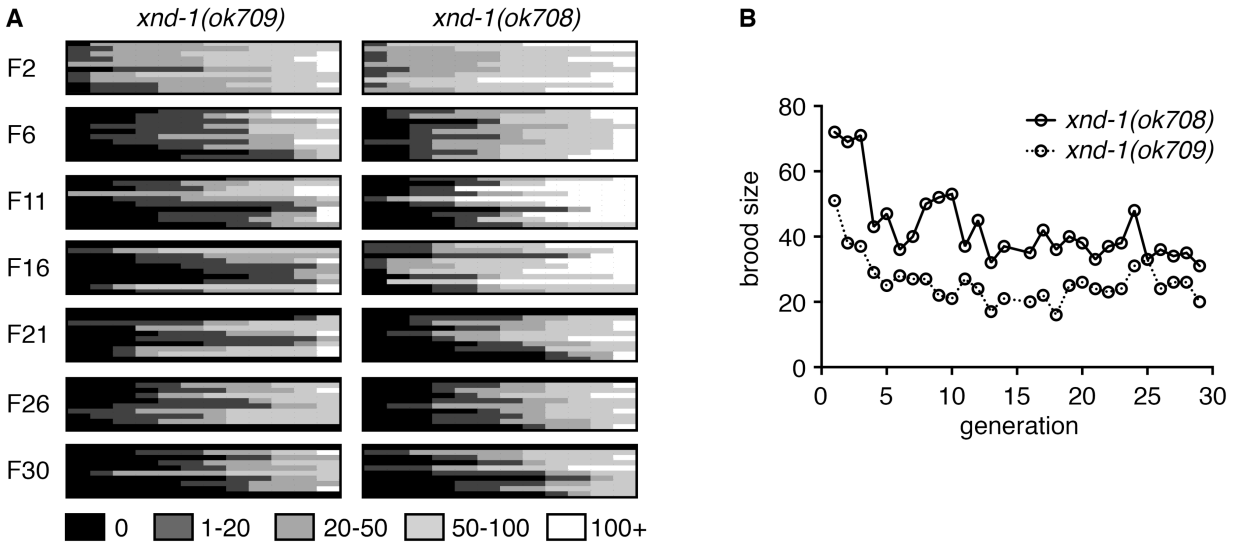

Figure 18. *xnd-1* exhibits a mortal germ line phenotype: A. Heat map depicts brood sizes (color, legend) of 12 lines (columns) from 10 independent *xnd-1* F1s (rows) for indicated generations. Assay was performed as described in text. B. Average brood sizes from fertile lines depicted in (A) over generations indicated. Both *ok708* and *ok709* alleles are presented and are phenotypically similar (WAGNER *et al.* 2010). Rest of analyses are performed with *ok709*.

To test this, we exposed *xnd-1* F2 hermaphrodites to increasing doses of ionizing radiation (IR), which induces DNA double-strand breaks (DSBs). The survival of progeny laid post-exposure reflects the repair capacity in the hermaphrodite germ line. Compared to wild type, survival of *xnd-1* progeny post-IR was significantly decreased compared to wild type at both 50 and 100 Gy (Figure 19A, $p<0.01$ vs. N2 at both doses, Student's t-test). Collectively, these results suggest that *xnd-1* is required for normal fertility, viability, and maintenance of genome stability.

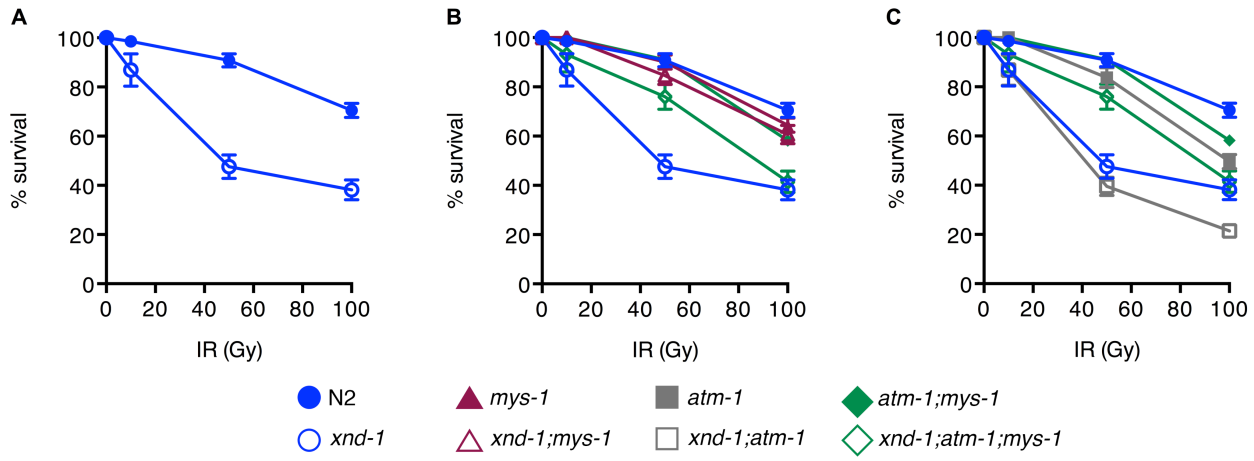

Figure 19. IR sensitivity of *xnd-1*, *mys-1*, and *atm-1* mutants: Progeny survival 12-24 hours post irradiation in wild type (N2, solid blue circles), *xnd-1* (open blue circles), *mys-1* (solid maroon triangles), *xnd-1;mys-1* (open maroon triangles), *atm-1* (solid gray squares), *xnd-1;atm-1* (open gray squares), *atm-1;mys-1* (solid green diamonds), and *xnd-1;atm-1;mys-1* (open green diamonds). The data are plotted as the percent surviving progeny relative to untreated ± SEM (error bars). For easier viewing, the data are divided into N2 and *xnd-1* (A), *mys-1* and related strains in (B), and *atm-1* and related strains in (C).

3.3.2 Genome instability in *xnd-1* mutants is probably not due to a defect in expression of DNA repair genes

We hypothesized that genome instability phenotypes in *xnd-1* mutants may stem from a defect in DSB repair. First, we analyzed diakinesis nuclei in *xnd-1* germ lines. The *C. elegans* germ line is a spatial and temporal organization of meiosis I prophase, and the quality of DSB repair can be assessed by DNA morphology at diakinesis as visualized by DAPI staining. In wild-type hermaphrodites, six condensed DAPI-staining bodies corresponding to six pairs of homologous chromosomes held together by chiasma are seen at diakinesis (Figure 20). Known DNA repair mutants, such as *rad-51*, exhibit decondensed chromatin and aggregates associated with a defect

in HR repair (TAKANAMI *et al.* 2000; RINALDO *et al.* 2002; ALPI *et al.* 2003). Interestingly, most *xnd-1* diakinesis nuclei observed showed either the wild-type complement of six DAPI-staining bodies, or seven DAPI-staining bodies consistent with non-exchange X chromosomes (~62% and ~17% respectively, Figure 20 and (WAGNER *et al.* 2010)). In most cases, chromatin appeared to be properly condensed. However, we observed chromatin abnormalities, including aggregation, decondensation, and DAPI bridges in ~12% of nuclei (Figure 20). We also observed what appeared to be several nuclei with pachytene-like morphology clustered together at the -1 oocyte position, which we called "clustered nuclei" (~10%, Figure 20 and (WAGNER *et al.* 2010)). Curiously, the frequency of abnormal oocytes and clustered nuclei are not sufficient to account for the lethality observed in *xnd-1* mutants (Table 9, row B).

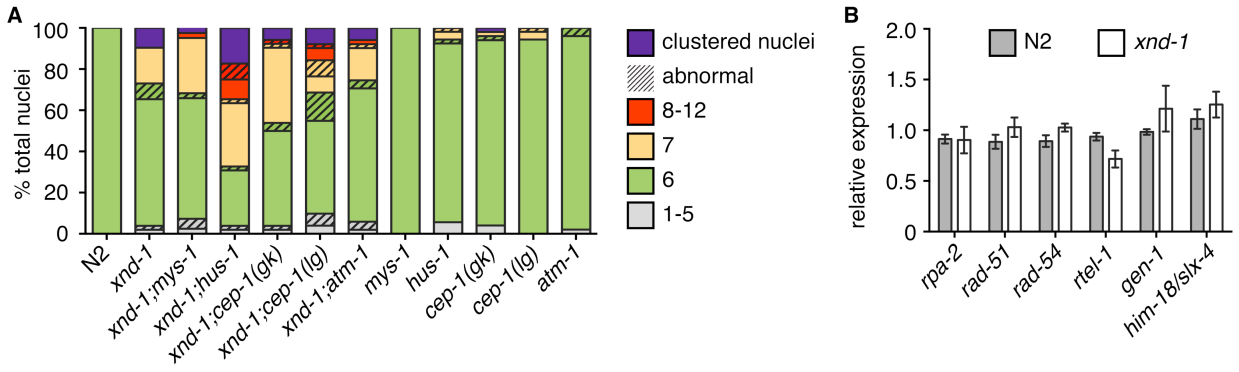

Figure 20. Bivalent formation and expression of select HR genes: A. Quantification of the number of DAPI-staining bodies at diakinesis for indicated genotypes. Only the -1 oocyte was used for analysis (n=40-52 nuclei). Color indicates number of DAPI-staining bodies; hatched lines on top of a color indicate chromatin abnormalities. B. Expression of selected DSB repair genes from Table 10 using cDNA from day 1 adult N2 or *xnd-1* hermaphrodites. Results are presented as average expression relative to reference genes from three biological replicates that in turn is comprised of three technical replicates ± SEM.

We next analyzed microarray data performed using RNA isolated from N2 or *xnd-1* germ lines, focusing on genes encoding factors known to be involved in HR-mediated DSB repair (reviewed in (LEMMENS AND TIJSTERMAN 2011)). We found 3 DSB repair genes – *rpa-2*, *gen-1*, and *slx-4/him-18* – that were significantly down-regulated in xnd-1 germ lines compared to wild type (threshold of 2-fold, $p<0.05$, Table 10). Consistent with their various roles in HR repair, all three factors exhibit sensitivity to DNA damaging agents (VAN HAAFTEN *et al.* 2004; SAITO *et al.* 2009; BAILLY *et al.* 2010). To verify the results of the microarray, we isolated RNA from a large pool of *xnd-1* and wild type day 1 adults and performed quantitative PCR using transcript-specific primers for *rpa-2*, *gen-1*, and *slx-4/him-18*, as well as key DSB repair factors *rad-51*, *rad-54*, and *rtel-1* as controls (LIVAK AND SCHMITTGEN 2001; GUBELMANN *et al.* 2011). Except for *rtel-1*, whose expression was slightly reduced compared to wild type ($p=0.037$, Student's t-test), all genes assayed expressed at wild-type levels in *xnd-1* mutants (Figure 20). As *rtel-1* mutants were reported to have greater numbers of crossovers (BARBER *et al.* 2008), and the overall number of crossovers in *xnd-1* mutants is unchanged on autosomes and reduced on the X (WAGNER *et al.* 2010), it is unlikely that *rtel-1* down-regulation contributes to any *xnd-1* phenotypes. Together, these results suggest that *xnd-1* mutants show phenotypes consistent with genome instability that do not seem to stem from misregulation of DNA repair genes.

Table 10. Fold change of HR gene transcripts in *xnd-1* germ lines vs. N2 as determined by microarray.

Gene ID	Gene	Fold-change vs. N2	p value
C36A4.8	*brc-1*	-1.362	0.003
T07E3.5	*brc-2*	-1.437	0.016
C44B9.5	*com-1*	-1.309	0.025
F43G6.1	*dna-2*	-1.201	0.230
F45G2.3	*exo-1*	-1.659	0.173
T12A2.8	*gen-1*	-2.606	0.027
Y55B1AL.3	*helq-1*	-1.431	0.079
T04A11.6	*him-6*	1.056	0.832
ZC302.1	*mre-11*	1.029	0.837
C43E11.2	*mus-81*	-1.401	0.005
T04H1.4	*rad-50*	-1.351	0.013
Y43C5A.6	*rad-51*	-1.102	0.428
W06D4.6	*rad-54*	-1.894	0.003
C30A5.2	*rfs-1*	-1.413	0.009
F18A1.5	*rpa-1*	-1.541	0.076
M04F3.1	*rpa-2*	-2.215	0.017
F59A3.5	*rpa-3*	-1.285	0.123
F25H2.13	*rtel-1*	-1.897	0.006
F56A3.2	*slx-1*	-1.884	0.002

Table 10 (continued)

T04A8.15	*slx-4/him-18*	-2.646	0.001
Y56A3A.27	*top-3*	1.549	0.150
C47D12.8	*xpf-1*	-1.787	0.147

3.3.3 A hypomorphic allele of *mys-1* improves *xnd-1* genome stability, but not male frequency

The ability of *xnd-1* mutants to form a CO on the X chromosome appears to be dependent on changes in the chromatin state (WAGNER *et al.* 2010). Previous studies have reported increased histone acetylation in *xnd-1* germ lines, specifically H2AK5ac (WAGNER *et al.* 2010; GAO *et al.* 2015). RNAi against *mys-1*, the *C. elegans* Tip60 homolog, decreased the amount of germline H2AK5ac, suggesting that H2AK5 is an acetylation target of MYS-1 in agreement with *in vitro* data for TIP60 (KIMURA AND HORIKOSHI 1998; WAGNER *et al.* 2010). Additionally, *mys-1(RNAi)* decreased the incidence of non-exchange X chromosomes at diakinesis in *xnd-1* mutants (WAGNER *et al.* 2010). We hypothesized that *mys-1* may be inappropriately active in *xnd-1* germ lines, resulting in both increased H2AK5ac and genome instability phenotypes. To test this, we generated *xnd-1;mys-1* double mutants. Because *mys-1(n4075)* homozygous mutants are sterile with no diakinesis nuclei, we used *mys-1(n3681)*, which encodes a missense mutation (G341R) in the acetyltransferase domain and results in viable homozygous progeny with at least a partially functional protein (CEOL AND HORVITZ 2004; COUTEAU AND ZETKA 2011).

Compared to *xnd-1* alone, *xnd-1;mys-1* hermaphrodites had significantly increased broods due to a combination of higher clutch sizes and reduced lethality, although these

phenotypes were not rescued to wild-type levels (Table 9, rows B and D). The incidence of sterility was dramatically decreased in *xnd-1;mys-1* mutants to less than 1% (0.69% sterile, $p<0.0001$ vs. *xnd-1*, Fisher's exact test). These results suggest that *mys-1* affects both fecundity and fitness in *xnd-1* mutants. Surprisingly, we did not observe the reduction in male frequency expected in *xnd-1;mys-1* mutants based on previous results with *mys-1(RNAi)* (15.49% in *xnd-1* vs. 13% in *xnd-1;mys-1*, p=0.5688 Mann-Whitney) (WAGNER *et al.* 2010), perhaps reflecting the weak loss-of-function nature of the *mys-1(n3681)* allele.

Human cell lines lacking Tip60 are sensitive to IR (KAIDI AND JACKSON 2013), suggesting that *mys-1* may also have a role in survival following genotoxic stress. We found that *mys-1(n3681)* mutants display wild-type sensitivity to IR (Figure 19B), indicating that *mys-1* either does not have a role in IR response or that its role is unaffected by the missense mutation in the acetyltransferase domain. Surprisingly, the IR sensitivity of *xnd-1* was restored to that of wild type by impairing *mys-1* function (Figure 19B), suggesting that the IR sensitivity phenotype of *xnd-1* mutants may be due to inappropriate *mys-1* function.

As the *n3681* allele encodes a missense mutation in the acetyltransferase domain of MYS-1, we hypothesized that the improved fitness we observed in *xnd-1;mys-1* mutants could be due to decreased germline H2AK5ac. We examined H2AK5ac in wild type, *xnd-1*, *mys-1*, and *xnd-1;mys-1* germ lines by immunofluorescence. Consistent with previous reports, we observed elevated H2AK5ac in the mitotic zone that decreased upon entry into meiosis in wild-type germ lines, yet remained elevated upon meiotic entry in *xnd-1* germ lines (Figure 21 and (WAGNER *et al.* 2010; GAO *et al.* 2015)). H2AK5ac was present in the mitotic zones of *mys-1* germ lines, but was nearly absent from meiotic nuclei, suggesting that H2AK5 may be an acetylation target of MYS-1 during meiotic prophase. Although H2AK5ac was still present in meiotic nuclei in *xnd-*

1;mys-1 germ lines, the intensity of H2AK5ac foci was markedly reduced in the pachytene region of germ line compared to *xnd-1* alone (Figure 21). From these data we infer that *n3681* hinders MYS-1 acetyltransferase activity. These data also suggest that either additional histone acetyltransferases function in mitotic nuclei and developing oocytes (data not shown), or that different thresholds of *mys-1* activity are required in distinct germ line regions. Collectively, these results suggest that the acetyltransferase domain of MYS-1 contributes to *xnd-1* germline development and IR sensitivity phenotypes, but does not seem to affect X chromosome nondisjunction based on unchanged male frequency.

3.3.4 Fecundity and progeny survival in *xnd-1* mutants partially depends on *atm-1*

Research has implicated TIP60 involvement in multiple levels of responding to DNA damage, including signaling (SQUATRITO *et al.* 2006). Studies in mammalian cells have shown that in response to either IR or treatment with Trichostatin A, which induces a histone hyperacetylation environment through inhibition of class I and II histone deacetylases, TIP60 acetylates and promotes activation of ATM kinase (SUN *et al.* 2005; SUN *et al.* 2009; KAIDI AND JACKSON 2013). We wondered, then, if the reduced fitness of *xnd-1* mutants could be explained by increased DNA damage signaling triggered by inappropriate accumulation of H2AK5ac. In the

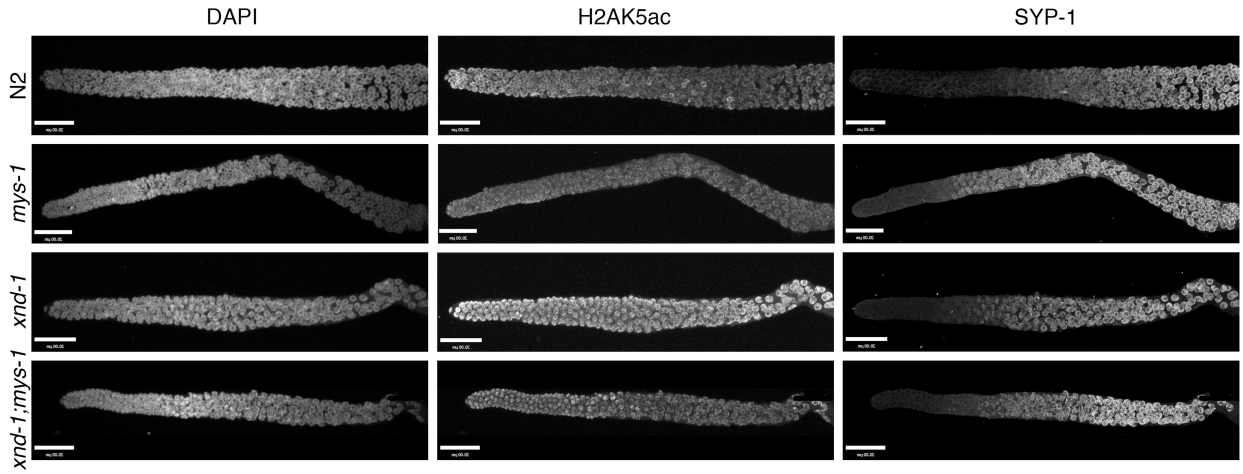

Figure 21. H2AK5 is an acetylation target of MYS-1: Immunofluorescence of H2AK5ac (middle column) and synaptonemal complex component SYP-1 (right column, control) in wild type (N2), *mys-1*, *xnd-1*, or *xnd-1;mys-1* hermaphrodite germ lines. Dissection and staining conditions are described in Section 3.2.7. The distal end of the germ line is oriented left, and SYP-1 staining marks meiotic entry. All images were taken with identical camera settings and processed identically. Scale bar is 20 µm.

germ line, mitotic proliferation arrest and increased apoptosis are responses to genotoxic stress and governed by checkpoint genes, which ultimately prevent a cell with damaged DNA from continuing through the cell cycle until either the damage is repaired, or apoptosis is initiated if the damage cannot be repaired (GARTNER *et al.* 2000). In *C. elegans*, both *atm-1* and *hus-1* are required for mitotic arrest following IR, possibly through parallel pathways (HOFMANN *et al.* 2002; GARCIA-MUSE AND BOULTON 2005; STERGIOU *et al.* 2007). Additionally, *hus-1* is required for DNA damage-induced apoptosis through CEP-1-dependent transcriptional activation of *egl-1* (HOFMANN *et al.* 2002). Both *atm-1* and *hus-1* mutants exhibit genome instability phenotypes including a mortal germ line, Himness, and spontaneous mutations (HOFMANN *et al.* 2002; JONES *et al.* 2012), suggesting that they have roles in responding to endogenous genotoxic stress.

We employed double mutant analysis to examine whether DNA damaged-induced checkpoint pathways were hyperactive in *xnd-1* hermaphrodite germ lines, leading to reduced fitness. Since *cep-1* is required for DNA damage-induced apoptosis, but not mitotic arrest (DERRY *et al.* 2001; SCHUMACHER *et al.* 2001), we reasoned that we could assess the effects of mitotic arrest and DNA damage-induced apoptosis on *xnd-1* fecundity through phenotypic differences between *atm-1*, *hus-1*, and *cep-1* double mutants. Compared to *xnd-1* alone, we observed no change in either the average clutch size of *xnd-1;hus-1* and *xnd-1;cep-1(gk)* hermaphrodites (Table 9, rows F and H), or the proportion of sterile hermaphrodites within these populations (15.79% sterile in *xnd-1;hus-1*, 18.87% sterile in *xnd-1;cep-1(gk)*). We observed similar results with a second allele of *cep-1*, *lg12501*, which also abrogates *egl-1* induction, although retains some function lost by the *gk138* allele (Table 9, row J, 8.33% sterile in *xnd-1;cep-1(lg)*, p=0.09 vs. *xnd-1*, Fisher's exact test (SCHUMACHER *et al.* 2005; WATERS *et al.* 2010)). In contrast, *xnd-1;atm-1* double mutants exhibited both an increase in average clutch size compared to *xnd-1* (Table 9, rows B and L, p=0.03), as well as a significant reduction in the proportion of sterile animals (7.41% sterile, p=0.0185 vs. *xnd-1*, Fisher's exact test). *xnd-1;atm-1* mutants also exhibited increased brood size and hatching compared to *xnd-1*, although male frequency remained unchanged (Table 9, rows B and L). These results suggest that neither *hus-1*-mediated DNA damage-induced mitotic arrest nor *cep-1*-mediated apoptosis contribute to fecundity of *xnd-1* hermaphrodites, but rather implicate *atm-1* activity as a factor partially mediating fecundity and fitness in *xnd-1* germ lines.

Interestingly, the frequency of male progeny in *xnd-1;hus-1*, *xnd-1;cep-1(gk)*, and *xnd-1;cep-1(lg)* populations were notably increased compared to *xnd-1* (Table 9, rows B, F, H, and J), which could implicate a role for *hus-1* and *cep-1* in DSB formation. If this were the case, we

would expect to observe a greater number of univalents indicative of achiasmate chromosomes in *xnd-1;hus-1*, *xnd-1;cep-1(gk)*, and *xnd-1;cep-1(lg)* diakinesis oocytes. Compared to *xnd-1*, both *xnd-1;hus-1* and *xnd-1;cep-1(gk)* exhibited an increase in 7 or more DAPI-staining bodies in the -1 oocyte (Figure 20A, p=0.009 for *xnd-1;hus-1* vs. *xnd-1* and 0.027 for *xnd-1;cep-1(gk)* vs. *xnd-1*, Z-test for proportions). Surprisingly, we did not observe a similar increase in univalents in *xnd-1;cep-1(lg)* diakinesis oocytes, although approximately 6% of -1 oocytes examined exhibited 8-12 DAPI-staining bodies (Figure 20A). The difference in diakinesis phenotypes between *xnd-1;cep-1(gk)* and *xnd-1;cep-1(lg)* could reflect differences in *cep-1* activity conferred by each allele.

One explanation for the increase in males in *xnd-1;hus-1* and *xnd-1;cep-1* mutants is that DNA damage-induced apoptosis selectively eliminates nuclei that failed to receive a CO on the X chromosome. To test this, we examined physiological germ cell death, a second apoptotic pathway that culls approximately 50% of germline nuclei under normal conditions (GUMIENNY *et al.* 1999). Both physiological and DNA damage-induced cell death pathways rely on the core apoptotic machinery encoded by *ced-3*, *ced-4*, and *ced-9* (GARTNER *et al.* 2000). We analyzed the male frequency of *xnd-1;ced-3* double mutants to determine if decreased apoptosis could account for the increased male frequency observed in *xnd-1;hus-1* and *xnd-1;cep-1* double mutants. We observed no change in male frequency between *xnd-1* and *xnd-1;ced-3* mutants (Table 9, rows B and N), ruling out that cell death selectively eliminates *xnd-1* oocytes with non-exchange X chromosomes. Thus, these data support a role for *hus-1* and *cep-1* in DSB formation (Mateo *et al*., accepted).

3.3.5 *mys-1* and *atm-1* function in independent mechanisms

Both *xnd-1;mys-1* and *xnd-1;atm-1* double mutants showed increased brood sizes and hatching rates compared to *xnd-1* mutants, though the improvement was more pronounced in *xnd-1;mys-1* double mutants ($p<0.0001$ *xnd-1;mys-1* vs. *xnd-1;atm-1* for both phenotypes, Mann-Whitney, Table 9, rows B, D, and L). Given the function of TIP60 in ATM kinase activation in mammalian cells (SUN *et al.* 2005; SUN *et al.* 2009; KAIDI AND JACKSON 2013), we hypothesized that *mys-1* and *atm-1* may be mediating genome stability in *xnd-1* germ lines through the same pathway. If this were the case, we would expect that *atm-1*, like *mys-1*, would also suppress the IR sensitivity of *xnd-1*. Strikingly, however, IR sensitivity of *xnd-1;atm-1* mutants resembled that of *xnd-1* single mutants up to 100 Gy, suggesting that the cause of IR sensitivity in *xnd-1* mutants is independent of *atm-1* (Figure 19C). At 100 Gy IR, the sensitivity of *xnd-1;atm-1* mutants was significantly lower than that of *xnd-1* alone ($p<0.01$, Student's t-test), suggesting that *atm-1* is required for survival following IR at high doses (>50 Gy) only. In support of this, we noted that the IR sensitivity of *atm-1* single mutants did not differ from that of wild-type worms until 100 Gy ($p=0.4804$ at 10 Gy, $p=0.2715$ at 50 Gy, $p=0.0001$ at 100 Gy).

The opposing IR sensitivities of *xnd-1;mys-1* and *xnd-1;atm-1* mutants provided an opportunity to examine an epistatic relationship between *mys-1* and *atm-1*. We generated an *xnd-1;atm-1;mys-1* triple mutant and assayed its sensitivity to IR (Figure 19B and C). We observed that, at up to 50 Gy IR, survival of *xnd-1;atm-1;mys-1* mutants resembled that of *xnd-1;mys-1* mutants, suggesting that the acetyltransferase domain of MYS-1 contributes to IR response independently of *atm-1*. However, at 100 Gy IR, survival of *xnd-1;atm-1;mys-1* mutants was significantly decreased compared to *xnd-1;mys-1* ($p<0.01$, Student's t-test), and matched that of *xnd-1* mutants. These results suggest that survival of *xnd-1;mys-1* mutants following IR is

independent of *atm-1* at low doses. Additionally, these results implicate a threshold IR dose at which *atm-1* is generally required for survival.

In mammalian cells, a missense mutation in the chromodomain of TIP60 abolished TIP60-dependent ATM activation in response to IR, yet left housekeeping acetylation functions of TIP60 intact (KAIDI AND JACKSON 2013). Therefore, we wondered if *mys-1* and *atm-1* might function in the same pathway apart from ones involved in survival following IR. To test this, we analyzed the clutch size, lethality, and male frequency of *xnd-1;atm-1;mys-1* triple mutants (Table 9, row P). The average clutch size of *xnd-1;atm-1;mys-1* triple mutants was significantly decreased from that of *xnd-1;mys-1* mutants but similar to *xnd-1;atm-1* mutants (Table 9, rows D, L, and P, $p<0.0029$ vs. *xnd-1;mys-1*, $p=0.2308$ vs. *xnd-1;atm-1*), suggesting *atm-1* may be epistatic to *mys-1* for this phenotype. However, we noticed a marked reduction in average clutch size between *atm-1;mys-1* double mutants and either single mutant (Table 9, rows C, K, and O, $p<0.001$ *atm-1;mys-1* vs. *atm-1* or *mys-1*), indicating that *atm-1* and *mys-1* function in parallel pathways in this regard. Lethality of *xnd-1;atm-1;mys-1* mutants fell between that of *xnd-1;mys-1* and *xnd-1;atm-1* mutants, and was statistically distinct from both ($p<0.01$ *xnd-1;atm-1;mys-1* vs. *xnd-1;mys-1* or *xnd-1;atm-1*). Surprisingly, the male frequency of *xnd-1;atm-1;mys-1* triple mutants was higher than that of either *xnd-1;mys-1* or *xnd-1;atm-1* mutants, although neither of the double mutants exhibited a change in male frequency compared to each other or to *xnd-1* (Table 9, rows B, D, L, and P, $p<0.001$ *xnd-1;atm-1;mys-1* vs. *xnd-1;mys-1* or *xnd-1;atm-1*, $p<0.05$ *xnd-1;atm-1;mys-1* vs. *xnd-1*). Taken together, these results suggest that *atm-1* and *mys-1* mediate genome stability phenotypes in *xnd-1* mutants through independent mechanisms.

3.3.6 *xnd-1* promotes X chromosome CO formation by regulating *him-5* independently of *mys-1*

One proposed explanation for the X chromosome CO defect in *xnd-1* mutants is that increased H2AK5ac changes the chromatin architecture such that the X chromosome is rendered inaccessible to DSBs. The previous observation that RNAi against *mys-1* increases X chromosome CO formation (WAGNER *et al.* 2010) supports this hypothesis, yet is confounded here by a similar male frequency (indicative of X chromosome nondisjunction) in both *xnd-1* and *xnd-1;mys-1* broods (Table 9, rows B and D). This discord could reflect differences in *mys-1* levels and activity between *mys-1(RNAi)* and *mys-1(n3681)*; alternatively, it could intimate a separate factor responsible for X chromosome CO formation.

A previous study has suggested *xnd-1* and *him-5* function in the same genetic pathway in regards to X chromosome CO formation (MENEELY *et al.* 2012). HIM-5 levels are diminished in *xnd-1* germline nuclei, yet XND-1 localization is normal in *him-5* germline nuclei, suggesting that *xnd-1* operates upstream of *him-5* (MENEELY *et al.* 2012). We observed dramatic reduction of *him*-5 expression in *xnd-1* mutants compared to wild type by quantitative RT-PCR (Figure 22A, $p<0.001$, Student's t-test), suggesting that regulation of *him-5* is XND-1-dependent. We hypothesized that reduced expression of *him-5* in *xnd-1* germ lines could be responsible for the X chromosome CO defect. Therefore, we separated *him-5* from its native regulatory elements in order to study its function in *xnd-1* germ lines. We integrated a transgene expressing *him-5::gfp* under *pie-1* regulatory elements (*Ppie-1::him-5::gfp::pie-1* 3' UTR, hereafter referred to as *eaIs15*) into the genome by bombardment (see Section 3.2.9). After verifying *eaIs15* rescued the X chromosome nondisjunction and lethality phenotypes of *him-5* mutants (Table 11), we crossed the transgene into *xnd-1* mutants and characterized the resultant strain. GFP fluorescence was

detectable throughout the germ line in live-mounted *xnd-1,eaIs15* animals, indicating expression of the transgene (data not shown). We observed a decrease in univalent X chromosomes in diakinesis nuclei (Figure 22B), suggesting that X chromosome CO formation was restored by the presence of *eaIs15*. Increased X chromosome CO formation was also reflected in a reduction in male progeny in *xnd-1,eaIs15* broods compared to *xnd-1* (Table 11). Collectively, these results indicate that one role of *xnd-1* in X chromosome CO formation is in regulating *him-5* expression.

Despite the rescue of the X chromosome CO defect, other *xnd-1* phenotypes persisted in *xnd-1,eaIs15* animals (Table 11 and Figure 22C). The average clutch and brood sizes of *xnd-1,eaIs15* mutants was indistinguishable from that of *xnd-1* mutants (Table 11). We observed a significant decrease in hatching in *xnd-1* mutants when *eaIs15* was present, although it appears additive with the small increase in lethality observed in wild type worms containing the transgene, suggesting it may be due to the site of integration of the transgene. The presence of *eaIs15* had no effect on the sensitivity of *xnd-1* mutants to IR (Figure 22C). Together these results reveal that decreased *him-5* expression accounts for only the X chromosome CO defect observed in *xnd-1* mutants. The failure of *eaIs15* to rescue other *xnd-1* phenotypes points to the involvement of multiple genes and/or pathways independent of *him-5*. Importantly, it also suggests that defects in meiotic DSB formation conferred by loss of *him-5* are not sufficient to explain the lethality observed in *xnd-1* mutants.

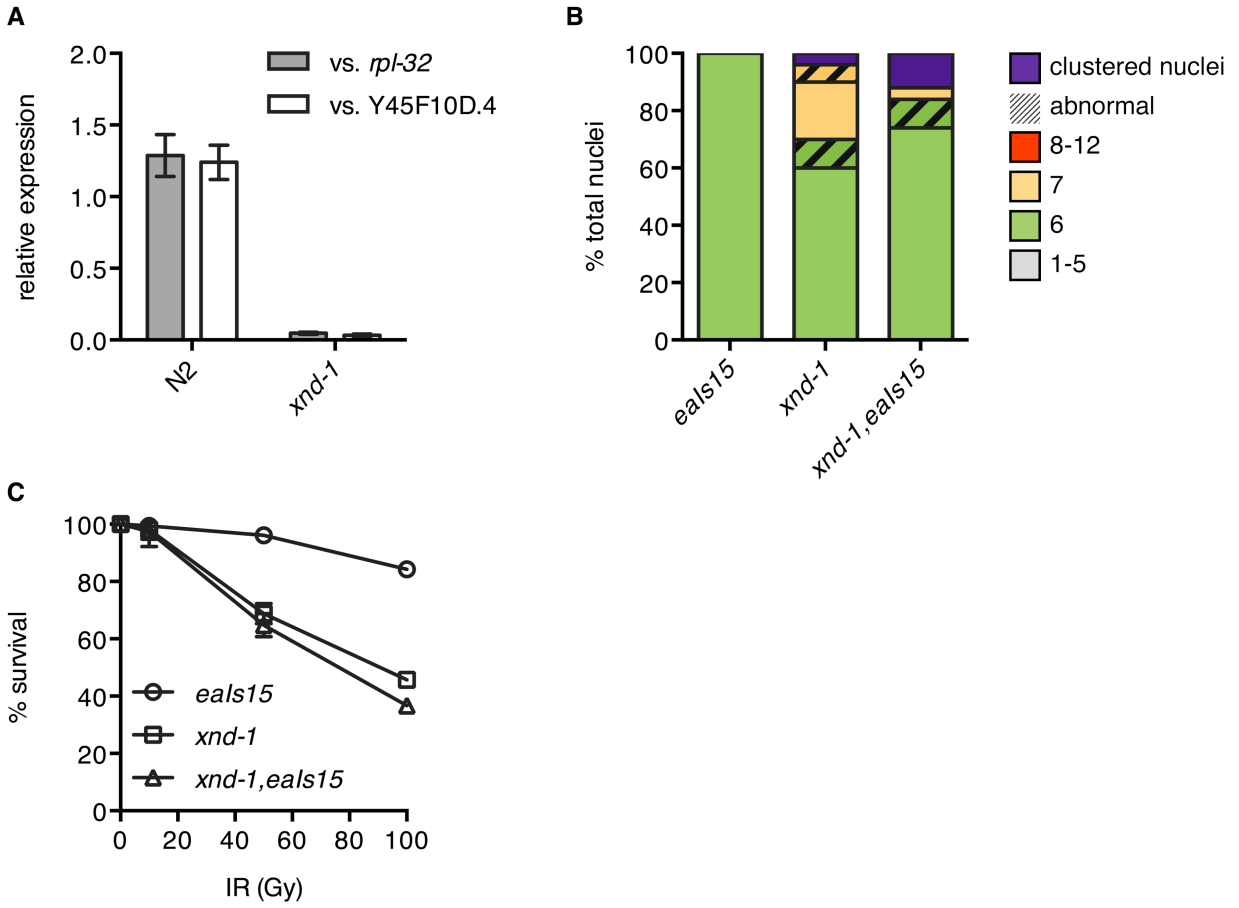

Figure 22. *xnd-1* X chromosome CO defect is due to down-regulation of *him-5*: A. Expression of *him-5* in wild type (N2) and *xnd-1* hermaphrodites as described in Section 3.2.5. Primers listed in Table 8. B. Quantification of the number of DAPI-staining bodies at diakinesis for indicated genotypes. Only the -1 oocyte was used for analysis (n=50 nuclei). Color indicates number of DAPI-staining bodies; hatched lines on top of a color indicate chromatin abnormalities. C. Progeny survival 12-24 hours post irradiation in *eaIs15* (wt, circle), *xnd-1* (square), *xnd-1,eaIs15* (triangle). The data are plotted as the percent surviving progeny relative to untreated ± SEM (error bars).

Table 11. General characterization of *eaIs15* in *him-5* and *xnd-1*: Data was collected as described in Section 3.2.2. ‡ p<0.01 vs. *him-5*, ** p<0.01 vs. *xnd-1*.

	Genotype	n	Avg. Clutch ± SEM	Avg. Brood ± SEM	% lethal ± SEM (NORM.)	% male ± SEM
A	*eaIs15*	6	228.17 ± 33.41	212.67 ± 30.96	4.69 ± 1.72	0.00 ± 0.00
B	*him-5*	9	253.33 ± 15.20	170.00 ± 9.58	31.25 ± 1.91	31.87 ± 0.98
C	*him-5;eaIs15*	8	247.75 ± 12.33	228.63 ± 11.55	5.88 ± 0.78‡	0.30 ± 0.17‡
D	*xnd-1*	26	109.69 ± 4.97	55.00 ± 3.60	49.71 ± 2.24	17.26 ± 2.05
E	*xnd-1;eaIs15*	24	87.79 ± 10.27	31.71 ± 5.15	71.14 ± 3.81	0.09 ± 0.08**

Having established that transgenic expression of *him-5* under *pie-1* regulatory elements is sufficient to restore wild-type X chromosome CO formation in *xnd-1* mutants, we wanted to test if *mys-1*-dependent changes in chromatin state affected *him-5* expression. We constructed a *him-5::gfp* transgene driven by its native regulatory elements (*Phim-5::him-5::gfp::3xFLAG*, hereafter referred to as *eaIs4*) and integrated it as a fosmid into the genome by bombardment (see Section 3.2.9). Expression of *eaIs4* in wild-type germ lines is consistent with previously described HIM-5 localization patterns (MENEELY *et al.* 2012), and rescues *him-5* mutants (Figure 23B and data not shown). We crossed *eaIs4* into *xnd-1* and *xnd-1;mys-1* mutants and probed for *him-5* transgene expression. Although we could detect the presence of *eaIs4* in the genome by PCR (Figure 23A), we did not observe expression of *eaIs4* in *xnd-1* germ lines by either live-imaging of GFP or western blotting of whole animals (Figure 23B and C). The difference in

rescue function between *him-5* expressed from its own versus a heterologous promoter strongly argues that *xnd-1* directly regulates *him-5* transcriptionally.

Expression of *eaIs4* in *xnd-1;mys-1* mutants was similar to that of *xnd-1* (Figure 23B and C), suggesting that one possible reason for persistent Him phenotype in *xnd-1;mys-1* mutants is failure to restore *him-5* expression. Consistent with diminished expression, *eaIs4* was unable to rescue the Him phenotype of either *xnd-1* or *xnd-1;mys-1* (10.76% males in *xnd-1;eaIs4*, 11.20% males in *xnd-1;mys-1;eaIs4*). These results do not support the hypothesis that either *him-5* expression or X chromosome CO formation is subject to *mys-1*-dependent changes in chromatin architecture; however, we cannot rule out the possibility that H2AK5ac in *xnd-1;mys-1* germ lines remains above the level required to see rescue.

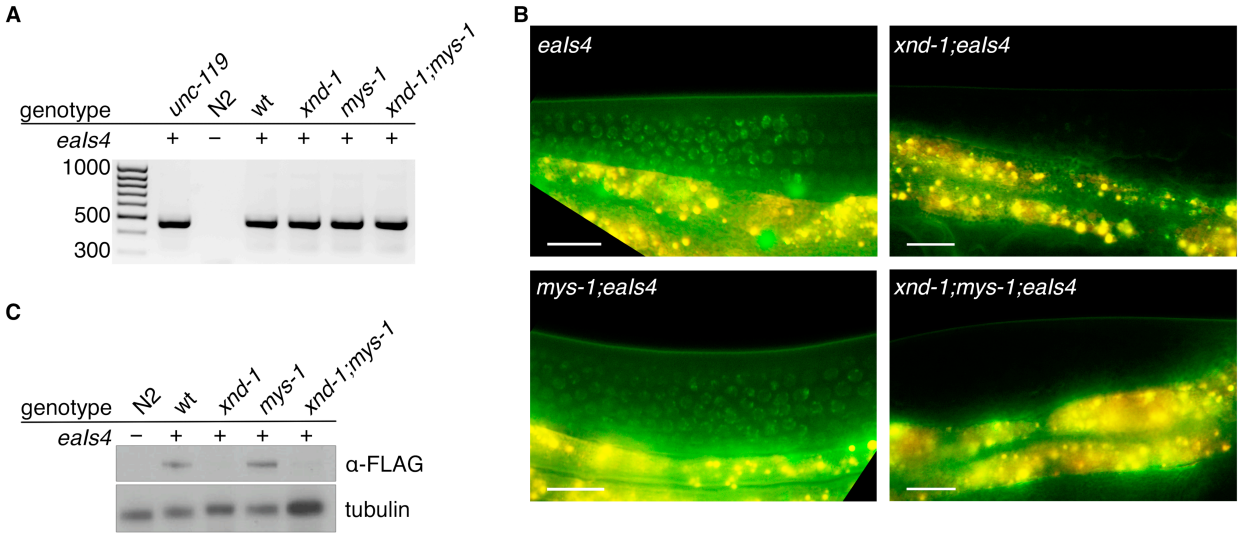

Figure 23. *him-5* expression is XND-1-dependent: A. Representative image of *eaIs4* genotyping using transgene-specific primers. Transgenic strains (indicated by +) show PCR product at ~450 bp, while N2 controls do not. *unc-119;eaIs4* is founder strain, while wt;*eaIs4* is wild-type control isolated from crossing *eaIs4* into *xnd-1;mys-1* mutants. B. Germline expression of *eaIs4* visualized by GFP fluorescence (green) in wt, *xnd-1*, *mys-1*, and *xnd-1;mys-1* transgenic hermaphrodites. In all images, the germ line is immediately above the autofluorescent intestine. The transgene does not express in either *xnd-1* or *xnd-1;mys-1* mutants. Scale bar is 10 µm. C. Expression of *eaIs4* visualized by western blot with an α-FLAG antibody. Tubulin serves as a loading control. Whole worm lysate was prepared as described in Section 3.2.8.

3.4 DISCUSSION

3.4.1 *xnd-1* is a model of genome instability

xnd-1 has described roles in assuring X chromosome DSB formation and regulating development in the *C. elegans* germ line (WAGNER *et al.* 2010; MAINPAL *et al.* 2015). Here, we show for the first time that *xnd-1* is also an important regulator of genome stability in the *C. elegans* germ line. *xnd-1* hermaphrodites exhibit reduced fecundity in early generations of homozygotes that continues to decrease over time (Figure 18), a phenotype that is characteristic of factors involved in telomere maintenance, DNA damage sensing, and chromatin modification (AHMED *et al.* 2001; HOFMANN *et al.* 2002; ANDERSEN AND HORVITZ 2007; KATZ *et al.* 2009). The low broods of *xnd-1* hermaphrodites result from a combination of decreased clutch size and increased lethality that is independent of autosomal nondisjunction (Table 9 and (WAGNER *et al.* 2010)). Consistent with a role in maintaining genome stability, *xnd-1* mutants are sensitive to IR (Figure 19), suggesting that *xnd-1* meiotic nuclei are unable to either properly respond to or repair exogenous DSBs.

3.4.2 Is *xnd-1* genome instability a repair problem or a chromatin problem?

One possibility to explain the genome instability phenotypes of *xnd-1* mutants, especially IR sensitivity, is a defect in DSB repair. In support of this, we observed evidence of chromatin abnormalities in a subset of *xnd-1* diakinesis nuclei (Figure 20). However, we observed wild-type expression of genes involved in HR repair in *xnd-1* mutants (Table 10 and Figure 20), although we cannot rule out that HR genes or proteins are misregulated another way. In contrast,

several observations suggest that *xnd-1* mutants are competent for DSB repair. First, induction of exogenous DSBs by IR restores X chromosome CO formation (WAGNER *et al.* 2010), suggesting that there is no defect in DSB repair machinery. Second, the majority of diakinesis oocytes exhibit well-condensed chromosomes (Figure 20), whereas chromosomes of DNA repair mutants can fail to form distinct bivalents. Finally, a hypomorphic allele of *mys-1* is sufficient to significantly improve *xnd-1* fitness and completely rescue *xnd-1* IR sensitivity (Table 9 and Figure 19). Collectively, these results suggest that genome instability occurs at the chromatin level in *xnd-1* mutants.

However, chromatin modification, checkpoint signaling, and DNA repair are intimately linked. In *S. cerevisiae*, H3K56 acetylation is important for chromatin reassembly following DSB repair and signals that repair is complete (CHEN *et al.* 2008). The histone chaperone Asf1 promotes acetylation of H3K56 through Rtt109; interestingly, Asf1 mutants are sensitive to DSB-inducing agents, although they are competent for DSB repair (RAMEY *et al.* 2004; LINGER AND TYLER 2005; CHEN *et al.* 2008). In *C. elegans*, the histone demethylase *spr-5* is required for efficient DSB repair, presumably by demethylation of H3K4me2 (NOTTKE *et al.* 2011). Similar to *xnd-1*, *spr-5* mutants do not show misexpression of DSB repair genes (NOTTKE *et al.* 2011). Thus, one hypothesis is that H2AK5ac is associated with checkpoint signaling. Previously, it was demonstrated that H2AK5ac is removed from chromatin in pachytene nuclei in response to IR, then replaced following repair, suggesting that H2AK5ac is associated with the DNA damage response (COUTEAU AND ZETKA 2011). In wild-type germ lines, we observe a decrease in H2AK5ac upon meiotic entry, coinciding with the onset of programmed DSB formation and HR repair. In contrast, H2AK5ac remains elevated throughout meiosis in *xnd-1* germ lines, suggesting that one reason *xnd-1* mutants display reduced fitness is impaired ability to control

the DNA damage response. In support of this, we observed that *xnd-1;atm-1* mutants exhibited similar improvements in fecundity and fitness as *xnd-1;mys-1* mutants, although we do not know if H2AK5ac is affected by loss of *atm-1*. Interestingly, our observations suggest a checkpoint signaling function for *atm-1* that is distinct from *hus-1* and *cep-1* (STERGIOU *et al.* 2007).

3.4.3 The relationship between *mys-1*, H2AK5ac, and genome stability

A missense mutation in the acetyltransferase domain of *mys-1* significantly improved *xnd-1* genome instability phenotypes. The phenotypic difference between *mys-1(n3681)*, which encodes a missense mutation with a viable outcome, and *mys-1(n4075)*, a predicted null allele which results in sterility (CEOL AND HORVITZ 2004; COUTEAU AND ZETKA 2011), suggests that *mys-1(n3681)* is a hypomorphic allele. However, we cannot determine from our studies how much MYS-1 function is retained by the *n3681* allele, or the full effect of that function. The previous observation that *mys-1(RNAi)* reduced both germline H2AK5ac and restored X chromosome CO formation in *xnd-1* mutants suggested that *mys-1* may exert its function through H2AK5ac (WAGNER *et al.* 2010).

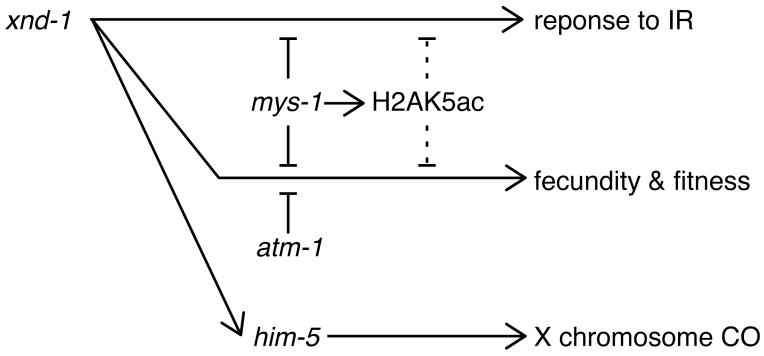

Figure 24. Model of genetic mediators of *xnd-1* phenotypes: In addition to defects in X chromosome CO formation (Wagner et al. 2010), *xnd-1* mutants exhibit genome instability phenotypes, including reduced fecundity and fitness, and IR sensitivity. A partial loss-of-function allele of *mys-1* improves *xnd-1* survival following IR, as well as fecundity and fitness, suggesting that *mys-1* negatively mediates these phenotypes in *xnd-1* mutants. H2AK5 appears to be an acetylation target of MYS-1, but a direct relationship between H2AK5ac and *xnd-1* phenotypes is unclear (dashed line). Loss of *atm-1* improves *xnd-1* fecundity and fitness, but does not affect survival following IR until high doses, where it appears to be generally required. Our data suggests that *mys-1* and *atm-1* function in parallel pathways. The relationship between *xnd-1*, *mys-1*, and *atm-1* is unknown. The reduced X chromosome CO formation in *xnd-1* mutants is due to down-regulation of *him-5*, which *xnd-1* regulates transcriptionally. Our data also implicates a role for *hus-1* and *cep-1* in CO formation independent of apoptosis (not shown).

The improved fecundity, fitness, and survival following IR in *xnd-1;mys-1* mutants coincided with a variable reduction in H2AK5ac in meiotic nuclei. The more pronounced reduction of H2AK5ac in pachytene nuclei of *mys-1(n3681)* germ lines (Figure 21) suggests that the *n3681* allele disrupts MYS-1 acetyltransferase activity, and that H2AK5 is an acetylation target during pachytene in contrast with previous results (COUTEAU AND ZETKA 2011). It is possible that *mys-1* is up-regulated in *xnd-1* mutants compared to wild-type such that even a hypomorphic allele still elicits increased germline H2AK5ac relative to wild type. Another possibility is that multiple HATs acetylate H2AK5 in *xnd-1* germ lines. It has been reported that *cra-1*, which promotes global histone acetylation by antagonizing acetyl-CoA hydrolase ACER-1, is required for accumulation of H2AK5ac; interestingly, CRA-1 expression is increased in *xnd-1* germ lines (LUI AND COLAIACOVO 2013; GAO *et al.* 2015). Finally, it is possible that there are threshold levels of H2AK5ac reduction necessary to restore X chromosome CO formation that were achieved in *xnd-1;mys-1(RNAi)* mutants, but not *xnd-1;mys-1(n3681)* mutants. Alternatively, *mys-1* may contribute to *xnd-1* phenotypes through a mechanism apart from H2AK5 acetylation. An analysis of genetic interaction networks identified *mys-1* as a "hub" gene, defined as a gene whose loss enhanced the phenotypic consequences of mutations in unrelated genes and functional pathways (LEHNER *et al.* 2006). Further studies are needed to elucidate the mechanism by which *mys-1* contributes to *xnd-1* phenotypes.

3.4.4 *him-5* is responsible for X chromosome CO formation in *xnd-1* germ lines

In wild-type germ lines, the X chromosome receives fewer DSBs than autosomes (1 DSB on X vs. ~8 DSBs on autosomes) (GAO *et al.* 2015). The X chromosome is usually silenced through repressive post-translational histone modifications (KELLY AND FIRE 1998; KELLY *et al.* 2002),

which may account for fewer programmed DSBs on the X relative to autosomes. Irradiation results in a more uniform ratio of DSBs on the X relative to the autosomes, indicating that chromatin architecture influences accessibility of the X chromosome to the DSB machinery. Indeed, RNAi against *mes-2*, which promotes H3K27 methylation in conjunction with *mes-3* and *mes-6* (BENDER *et al.* 2004), suppressed the Him phenotype of *xnd-1* (WAGNER *et al.* 2010). Despite evidence linking increased global histone acetylation to increased X chromosome DSB formation, *xnd-1* mutants still receive dramatically fewer DSBs on the X chromosome, even though germline H2AK5ac is elevated (GAO *et al.* 2015). It is possible that the increase of H2AK5ac alone is not sufficient to promote X chromosome DSB formation, or that H2AK5ac specifically hinders X chromosome DSB formation. Alternatively, additional factor(s) are required. Our results suggest that *him-5* is the additional factor needed to ensure DSB formation on the X chromosome (Figure 22). We found that *him-5* is down-regulated in *xnd-1* mutants (Figure 22A), which explains why HIM-5 is undetectable in *xnd-1* germ lines (MENEELY *et al.* 2012). Furthermore, ectopic expression of *him-5* under *pie-1* regulatory elements is sufficient to restore X chromosome CO formation (Figure 22B and Table 11), indicating that XND-1 regulates *him-5* transcriptionally.

Knowing that ectopic expression of *him-5* was sufficient to restore DSB formation on the X chromosome gave us the opportunity to test whether changes in chromatin architecture affected *him-5* expression in *xnd-1* germ lines. We found that expression of a *Phim-5::him-5::gf*p transgene (*eaIs4*) was undetectable in *xnd-1* germ lines, and was not restored by the presence of *mys-1(n3681)* (Figure 23). These results corroborate the observation that *xnd-1;mys-1* had similar male frequency to *xnd-1* (Table 9), and suggests that failure to express *him-5* may be the reason for that. Thus, the *him-5* transgenes could be useful tools to assess the relationship

between chromatin architecture and DSB formation. Of course, it is possible that *him-5* is just one of many components necessary for DSB formation.

Collectively, these results provide *xnd-1* as a model in which to study the link between chromatin factors, gene expression, and genome stability.

3.5 ACKNOWLEDGEMENTS

We thank Cynthia Wagner and Zebulin Kessler for their assistance in the construction and bombardment of the *eaIs15* transgene. Some strains were provided by the Caenorhabditis Genetics Center, which is funded by NIH Office of Research Infrastructure Programs (P40 OD010440). The anti-E7 antibody developed by Drs. M. McCutcheon and S. Carroll and deposited by Michael Klymkowsky was obtained from the Developmental Studies Hybridoma Bank, created by the NICHD of the NIH and maintained at The University of Iowa, Department of Biology, Iowa City, IA 52242. Sequencing of transgenic constructs and the *ced-3(n717)* allele was performed in the Genomics Research Core at the University of Pittsburgh.

A modified version of this paper is in preparation for submission at *Genetics*:

X chromosome crossover formation and genome stability in *Caenorhabditis elegans* are independently regulated by *xnd-1*

McClendon TB, Rana M, Amrit FR, Fukushige T, Krause M, Ghazi A, Yanowitz JL.

4.0 GENERAL DISCUSSION

The goal of this research was to characterize factors that promote genome stability in the *C. elegans* germ line. Here, we have explored two factors that maintain genome stability in the *C. elegans* hermaphrodite germ line through distinct mechanisms: *sws-1* and *xnd-1*.

4.1 DISCOVERY OF A *C. ELEGANS* SHU COMPLEX

A putative Shu2 ortholog was identified in *C. elegans* based on the conservation of the SWIM domain (GODIN *et al.* 2015). We have confirmed that *C. elegans sws-1* is functionally analogous to *S. cerevisiae* Shu2 and functions in germline HR with the RAD-51 paralogs *rfs-1* and *rip-1*, together forming a worm Shu complex (Chapter 2). This work has recently been accepted at *Genetics*.

Study of the Shu complex in metazoans has been limited due to embryonic lethality of mouse models and difficulty obtaining purified protein for biochemical studies (DEANS *et al.* 2000; THACKER 2005; KUZNETSOV *et al.* 2009; SUWAKI *et al.* 2011). Deficiencies of Shu complex components are viable in both yeast and worms, suggesting that the Shu complex may have evolved to have a more essential role in HR in higher organisms. Fortunately, *C. elegans* provides a non-lethal model in which to study Shu complex function in metazoans. The sections below discuss unanswered questions and propose future experiments.

4.1.1 Shu complex function in relation to RAD-51 filament formation and strand invasion

In *C. elegans*, there is conflicting evidence as to how the Shu complex promotes RAD-51-mediated HR and where the Shu complex functions relative to strand invasion. *In vitro* experiments suggest that the RAD-51 paralogs RFS-1 and RIP-1 are not needed for RAD-51 filament formation, but are critical for strand invasion (TAYLOR *et al.* 2015). In contrast, genetic assays suggest that both *helq-1* and *rfs-1* function post-strand invasion based on reduced brood, increased lethality, and persistent RAD-51 foci when combined with a mutant allele of the anti-recombinase *rtel-1*, which disassembles D-loops but has no detectable effect on RAD-51-ssDNA filaments (BARBER *et al.* 2008; WARD *et al.* 2010). In both cases, RAD-51 forms nucleoprotein filaments on ssDNA in the absence of either *rfs-1* or *rip-1*.

Interestingly, our results suggest that *sws-1* is needed for wild-type resolution of RAD-51 foci during meiotic HR, but needed to stabilize RAD-51 in mitosis following CPT exposure. It is possible that RAD-51 foci persist during pachytene in *sws-1* germ lines because RFS-1/RIP-1 complex-dependent structural remodeling of the RAD-51-ssDNA filament in order to invade the homologous template is hindered (TAYLOR *et al.* 2015). Alternatively, RAD-51 foci could persist due to delayed removal of RAD-51 post-strand invasion. There are two experiments that could distinguish between these possibilities. The first experiment involves determining recombination frequencies between marker genes in *rtel-1;sws-1* mutants. If *sws-1* functions upstream of RAD-51-mediated strand invasion, it may be expected to suppress the hyperrecombination phenotype of *rtel-1* mutants (YOUDS *et al.* 2010). The second experiment focuses on quantification of MSH-5 foci in pachytene nuclei. MSH-5 foci (indicative of MutS) appear in mid-pachytene in excess of eventual COs (YOKOO *et al.* 2012), suggesting that MutS may bind to most recombination intermediates. If *sws-1* functions in a pre-strand invasion step of HR, fewer MSH-5 foci would

be expected in mid-pachytene nuclei relative to wild type due to decreased formation of strand exchange intermediates.

A second possibility to address the discrepancy between requirements for RAD-51 foci formation is that *sws-1* performs different functions at different HR substrates. *rfs-1* and *rip-1* are required for RAD-51 focus formation following treatment with interstrand crosslinking agents and UV-C, but not IR and HU (WARD *et al.* 2007; TAYLOR *et al.* 2015). Despite being competent for RAD-51 focus formation following IR, *rfs-1* and *rip-1* exhibit sensitivity to IR compared to wild-type worms, though not to the same extent as that of crosslinking agents (WARD *et al.* 2007; TAYLOR *et al.* 2015). These results suggest that *rfs-1* and *rip-1* may have either a distinct or less-essential function in repair of IR-induced DSBs. Although RAD-51 focus formation in response to genotoxic stress has not been as thoroughly examined in *sws-1* germ lines, our current knowledge of *sws-1* suggests that it functions in an analogous manner to *rfs-1* and *rip-1*.

4.1.2 Identification of novel RAD-51 paralogs and interacting partners

All identified *C. elegans* Shu complex members exhibit synthetic lethality with *helq-1* (Figure 7, Chapter 2 and (WARD *et al.* 2010; TAYLOR *et al.* 2015)). This easily visible phenotype – unhatched eggs on a plate – provides the opportunity to potentially identify more RAD-51 paralogs and/or RAD-51 paralog interacting partners using genome-wide RNAi (TIMMONS AND FIRE 1998; KAMATH *et al.* 2001) and yeast-two-hybrid.

4.1.3 Visualization of SWS-1

In *S. cerevisiae*, the Shu complex functions in both mitosis and meiosis (SHOR *et al.* 2005; GODIN *et al.* 2013; SASANUMA *et al.* 2013). Although *sws-1* clearly has a role in germline HR, we were unable to determine whether *sws-1* functions primarily during mitosis, meiosis, or both. Consistent with what is observed in *S. cerevisiae* (GODIN *et al.* 2013), our results strongly implicate a role for *sws-1* in promoting HR at replication forks: first, *sws-1* enhances the deletion frequency of *dog-1* mutants, which is proposed to function in unwinding secondary DNA structures during DNA replication (CHEUNG *et al.* 2002; YOUDS *et al.* 2006); second, *sws-1* mutants showed greatest sensitivity to CPT, which creates DSBs by trapping topoisomerase I at replication forks. However, we cannot determine at this time if *sws-1* functions at replication forks during mitotic S phase or meiotic S phase. Development of either an antibody against SWS-1 or generation of an SWS-1::GFP fusion protein will help us understand what SWS-1 is doing by being able to visualize its expression in the germ line.

4.1.4 Structure/function analysis of the RAD-51 paralogs and their interacting partners

The ultimate goal of studying the Shu complex is to discover why mutations in the human RAD51 paralogs are associated with cancer predisposition. The discovery of a Shu complex in *C. elegans* allows researchers to study complete loss-of-function mutations in the RAD-51 paralogs (and their interacting partners) in a non-lethal model. Using Y2H, we were able to show that a cancer-associated mutation in human SWS1 conferred reduced interaction between *C. elegans* SWS-1 and RIP-1 (Figure 14, Chapter 2 and (GODIN *et al.* 2015)). This mutation can be introduced into native *C. elegans sws-1* by the CRISPR/Cas9 system, where we can assess the

mechanistic consequences using the readouts of germline genome instability (Figure 3, Chapter 1). Thus, *C. elegans* provides a translational research model to better understand the mechanisms by which the Shu complex promotes genome stability.

4.2 XND-1 PROVIDES INSIGHTS INTO GLOBAL MECHANISMS OF GENOME MAINTENANCE

xnd-1 was identified in a screen for meiotic recombination regulatory proteins (WAGNER *et al.* 2010). *xnd-1* mutants exhibited a *h*igh *i*ncidence of *m*ales (Him) phenotype and lethality suggestive of defects in meiotic CO formation. Interestingly, only the X chromosome failed to receive a CO, indicating that autosomal aneuploidy could not explain the poor survival of *xnd-1* mutants (WAGNER *et al.* 2010). Additionally, *xnd-1* exhibited a mortal germ line phenotype, which is shared by factors involved in telomere maintenance, DNA damage sensing, and chromatin modification (AHMED *et al.* 2001; HOFMANN *et al.* 2002; ANDERSEN AND HORVITZ 2007; KATZ *et al.* 2009), and suggested a broader role for *xnd-1* in maintaining genome stability. We therefore aimed to more thoroughly describe genome instability in *xnd-1* hermaphrodites, uncover what factors led to these phenotypes, and describe their function. *xnd-1* mutants are sensitive to IR, supporting a role in survival following exogenous DSB induction. We found that a putative partial loss-of-function allele of the histone acetyltransferase *mys-1* completely rescues *xnd-1* IR sensitivity and partially rescues the reduced fecundity and fitness, but not Him phenotype, of *xnd-1* mutants. Our efforts to uncover the mechanism by which *mys-1* mediated these phenotypes initially implicated *atm-1* based on similarities (excluding IR sensitivity)

between *xnd-1;mys-1* and *xnd-1;atm-1* mutants. However, our characterizations of *xnd-1;atm-1;mys-1* triple mutants suggests that *mys-1* and *atm-1* function in independent pathways. We also hypothesized that *mys-1*-dependent increases in H2AK5ac triggered *xnd-1* phenotypes. While we see a reduction in H2AK5ac in *xnd-1;mys-1* meiotic nuclei by immunofluorescence, further analysis is needed to confirm this result.

In contrast to *mys-1*, ectopic expression of *him-5* was sufficient to rescue the Him phenotype of *xnd-1* mutants, but had no effect on other *xnd-1* phenotypes. The ability to express *him-5* in *xnd-1* germ lines – where it is down-regulated – by placing it under *pie-1* regulatory elements suggests that XND-1 regulates *him-5* transcriptionally, consistent with the presence of putative DNA-binding elements in XND-1 protein sequence.

Despite our and other's recent gains in describing the outcomes of *xnd-1* deficiency (WAGNER *et al.* 2010; MENEELY *et al.* 2012; GAO *et al.* 2015; MAINPAL *et al.* 2015), we have all fallen short in answering "How?" Thus, this research "is still a potential battleground where dead hypotheses litter the field or rest uneasily in shallow graves, ready to emerge and haunt any conscientious scientist who tries to consolidate a victory for any particular thesis" (TAYLOR 1974). The sections below elaborate on some of these lingering ghosts.

4.2.1 Is H2AK5 acetylation the link between *mys-1* and genome instability?

The observation that knockdown of *mys-1* leads to a decrease in H2AK5ac strongly suggests that H2AK5 is an acetylation target of MYS-1 (Chapter 3 and (WAGNER *et al.* 2010)). However, the data are inconclusive as to whether H2AK5ac is the causative agent of *xnd-1* genome instability, or if a separate function of *mys-1* is to blame. If H2AK5ac is sufficient to confer genome instability phenotypes, then modulating this particular mark may induce genome instability in an

otherwise wild-type animal. To test this, we designed a series of operon transgenes containing H2A (encoded by *his-30*) driven by the *pie-1* promoter and *tbb-2* 3' UTR for constitutive expression throughout the germ line (Appendix and (MERRITT *et al.* 2008; CHRISTOPHER MERRITT 2010)). These transgenes were constructed from gene units encoding wild-type H2A, or missense mutants of H2A in which K5 is mutated to either mimic acetylation (K5Q) or to be unacetylatable (K5R). Thus, by combining different versions of H2A ($H2A^{WT}$, $H2A^{K5Q}$, $H2A^{K5R}$) into a transgene, it may be possible to titrate H2AK5ac into the germ line.

Histone modifications can influence chromatin structure to affect accessibility of the DNA, but they can also serve as a platform for signaling by recruiting effector molecules that ultimately dictate the functional outcome of a modification (YUN *et al.* 2011). Thus, we may be able to determine the functional significance of increased H2KA5ac by identifying its effector molecule, or reader. Acetylated lysine residues can be recognized by both bromo domains and the tandem PHD domain (DHALLUIN *et al.* 1999; WINSTON AND ALLIS 1999; OWEN *et al.* 2000; ZENG *et al.* 2010). One way to approach this is RNAi. If *mys-1* mediates genome stability through H2AK5ac, then knockdown of the reader in an *xnd-1* mutant may be expected to phenocopy *xnd-1;mys-1*. A query of bromo domain proteins in *C. elegans* revealed 19 candidate target genes (LETUNIC *et al.* 2015). However, given the variation in severity of *xnd-1* phenotypes and ambiguity as to whether or not H2AK5ac causes those phenotypes, genome-wide RNAi to identify suppressors of *xnd-1* phenotypes is not the optimal approach. Alternatively, a proteomics approach could be applied in which an immobilized histone peptide bearing acetylated lysine is used as bait to retrieve its reader from nuclear extracts; the binding proteins can then be identified by mass spectrometry (HUANG *et al.* 2010; YUN *et al.* 2011).

4.2.2 How does *mys-1* mediate *xnd-1* phenotypes?

TIP60 sometimes functions as a subunit in the evolutionarily conserved NuA4 complex. The NuA4 complex is composed of at least 16 subunits and is implicated in chromatin remodeling through its HAT activity, and regulating non-histone proteins through acetylation. These functions of the NuA4 complex translate to roles in regulating aspects of DNA repair/genome instability, transcription, chromatin structure, and stem cell maintenance (YAMADA 2012). In *C. elegans*, some subunits of the NuA4 complex – *ttr-1*, *mys-1*, and *epc-1* – are involved in vulval cell-fate determination. Importantly, the vulval development defect was not enhanced in double mutant combinations, suggesting that *ttr-1*, *mys-1*, and *epc-1* function together in this role (CEOL AND HORVITZ 2004). Therefore, we may be able to determine if *mys-1* mediates *xnd-1* phenotypes as part of the NuA4 complex by examining if loss of other complex members phenocopy *xnd-1;mys-1* mutants. It is interesting to speculate that *mys-1* may influence different *xnd-1* phenotypes by forming distinct subcomplexes with different NuA4 subunits, as has been suggested for the human NuA4 complex (YAMADA 2012). Indeed, this may account for the pleotropic nature of *mys-1(n3681)* in regards to *xnd-1* phenotypes.

The localization pattern of MYS-1 is currently unpublished. Development of either an antibody against MYS-1 or generation of an MYS-1::GFP fusion protein may provide insight into MYS-1 function by being able to visualize its expression in the germ line. In particular, visualization of MYS-1 may resolve whether *mys-1* is up-regulated in *xnd-1* mutant germ lines.

4.2.3 Hypotheses of XND-1 function

We have implicated *xnd-1* in CO regulation, germ line development, and genome stability ((WAGNER *et al.* 2010; MAINPAL *et al.* 2015) and Chapter 3). Although we have identified genes that enhance, partially rescue, or fully rescue select *xnd-1* phenotypes, we have yet to identify how XND-1 functions to promote these phenotypes in the first place. The current hypotheses are entertained below.

4.2.3.1 *xnd-1* is an HR factor One hypothesis is that XND-1 promotes HR repair. This is most readily supported by the poor survival of *xnd-1* mutants following treatment with IR, which induces DSBs that are substrates for HR. XND-1 localizes to chromatin from the distal end of the germ line through mid- to late-pachytene, covering the time in which meiotic DSBs are made and repaired (as well as spontaneous endogenous mitotic DNA damage) (WAGNER *et al.* 2010). Determining if XND-1 localization changes following IR could help to elucidate how XND-1 is involved in responding to DSBs. Additionally, we sometimes observe spontaneous mutations in the *xnd-1* population that are suggestive of mutagenic DNA repair. If *xnd-1* promotes HR, we may expect to see increased deletions in the *vab-1* poly G/C tract in a *dog-1;xnd-1* double mutant, as we and others have shown that HR factors are important for maintaining genome stability in poly G/C tracts when *dog-1* is absent (Figure 10, Chapter 2, (YOUDS *et al.* 2006; WARD *et al.* 2007)). Our analysis with *sws-1*, however, showed that HR factors can have a preferred substrate. Therefore, it could be informative to examine the requirement of *xnd-1* in responding to other types of genotoxic stress.

CO formation is tightly regulated in wild-type worms such that the majority of COs occur on the chromosome arms (BARNES *et al.* 1995; MENEELY *et al.* 2002). In *xnd-1* mutants, CO

distribution shifts so that there is elevated recombination in the center of both chromosome I and the X (WAGNER *et al.* 2010). Intriguingly, the dHJ resolvase *slx-1* also exhibits a shift of CO distribution to the center of the chromosomes (SAITO *et al.* 2012) raising the possibility that the shift in CO distribution observed in *xnd-1* mutants could be due to a role in HR. However, it is possible that the altered CO distribution observed in *xnd-1* mutants is the result of *him-5* down-regulation, as *him-5* mutants also exhibit this phenotype (MENEELY *et al.* 2012), and can be tested by examining CO distribution in our *xnd-1;eaIs15* transgenic strain.

The observation that IR restores X chromosome CO formation in *xnd-1* mutants suggests that *xnd-1* mutants are competent for HR once a DSB is made on the X (WAGNER *et al.* 2010) and would therefore argue against *xnd-1* being a bona fide HR factor. However, we did not observe any obvious HR defects in *sws-1* mutants (except for genotoxin sensitivity) until we removed *helq-1*, which revealed that *sws-1* and *helq-1* have redundant roles in HR repair (Chapter 2). Therefore, it remains possible that *xnd-1* may function redundantly in HR with an as-yet-unidentified factor.

4.2.3.2 *xnd-1* regulates gene expression *xnd-1* has been implicated in the positive and negative regulation of *him-5* and *cra-1*, respectively (MENEELY *et al.* 2012; GAO *et al.* 2015), suggesting that *xnd-1* may function in regulating gene expression. One way that XND-1 might do this is through transcriptional regulation of specific genes; in support of this, we have detected XND-1 binding to the *him-5* promoter by ChIP-seq (Yanowitz, personal communication). Further analysis is in progress. The protein sequence of XND-1 contains two domains that resemble AT-hooks, a DNA-binding motif associated with regulation of transcription and chromatin structure (REEVES 2001). To determine if the AT-hooks are required for XND-1 function, we generated a novel allele of *xnd-1*, *ea13*, in which the conserved R-G-R residues of the suspected stronger

AT-hook are mutated to alanine (BEWLEY *et al.* 1998; TURLURE *et al.* 2006)(McClendon, unpublished). Preliminary immunofluorescence data suggests that the AT-hooks might not be required for XND-1 DNA-binding activity, although further confirmatory studies are required. The observation that XND-1 associates with chromatin in *ea13* mutants does not preclude the possibility that both AT-hooks must be compromised to eliminate DNA-binding, but favors alternatives that XND-1 has an as-yet-undiscovered DNA binding domain, or that XND-1 associates with chromatin through interaction with another DNA-binding protein. To address the first possibility, we can mutate the R-G-R residues of both AT-hooks using CRISPR/Cas9. To address the second possibility, we could collaborate with bioinformaticians to more thoroughly analyze XND-1 protein sequence and identify putative domains, then generate deletion mutants using CRISPR/Cas9 to ascertain their effect on *xnd-1* phenotypes. To address the third possibility, we can immunoprecipitate XND-1 from worm extracts to identify and characterize interacting partners.

Rather than a direct role as a transcription factor, XND-1 may regulate gene expression through changes in chromatin structure. This hypothesis is especially attractive because it may explain the variability in severity of *xnd-1* phenotypes (KELLY 2014), and the seemingly unrelated nature of *xnd-1* phenotypes. Although we have evidence that H2AK5ac is increased in *xnd-1* germ lines (WAGNER *et al.* 2010; GAO *et al.* 2015), it is possible that other histone modifications are altered as well. We can use ChIP-seq to determine changes in chromatin structure across the genome in *xnd-1* germ lines compared to wild type. Alternatively, we can purify histones from *xnd-1* germ lines and identify PTMs by mass spectrometry to view the full spectrum of modified histones in an unbiased manner. Ideally, both approaches should be used to

determine what histone PTMs are changed in *xnd-1* germ lines, and where these marks are enriched in the genome.

4.2.4 Concluding thoughts: structure determines function

Defects in chromosome segregation during meiosis lead to aneuploid gametes. In humans, an uncommonly high number of fertilized eggs (10-30%) are aneuploid, which can result in either miscarriage or children born with physical and developmental abnormalities (HASSOLD AND HUNT 2001). Therefore, understanding how factors regulate meiotic genome stability is critical to further our knowledge of human reproduction and ultimately develop intervention strategies for the clinic. Although we have identified *xnd-1* as an important factor in *C. elegans* reproduction, the translational aspect of this research has been hindered by not being able to identify putative orthologs in other species based on conserved protein sequence. However, the roles of *xnd-1* in regulating meiotic recombination, germ cell development, and genome stability strongly suggest that *xnd-1* orthologs exist. Therefore, determining the protein structure of XND-1 is a critical next step that will provide insight as to its functional significance, facilitate identification of orthologs, and further the reach of this work.

APPENDIX

THE H2A OPERON

PURPOSE AND OVERVIEW

To test if increased acetylation of H2AK5 is sufficient to confer genome instability phenotypes in *C. elegans* germ lines, I constructed elements for an operon transgene in which a whole gene unit (*Ppie-1::gfp::H2A::tbb-2* 3' UTR, Figure 25) is connected to one or more repeat units (*operon linker::gfp::H2A::tbb-2* 3' UTR, Figure 25) in MosSCI vector pCFJ350 for single-copy insertion in the ttTi5605 locus on chromosome II (FROKJAER-JENSEN *et al.* 2008; FROKJAER-JENSEN *et al.* 2012). The *pie-1* promoter and *tbb-2* 3' UTR were chosen for constitutive expression throughout the germ line (MERRITT *et al.* 2008; CHRISTOPHER MERRITT 2010). I also created mutant versions of both whole and repeat units in which DNA encoding H2A K5 was mutated to acetylmimic glutamine (K5Q) or unacetylatable arginine (K5R) using site-directed mutagenesis. Once inserted into the germ line, the operon is transcribed into a polycistronic primary transcript, and then processed into monocistronic mRNAs. Thus, we can build MosSCI transgenes with different combinations of $H2A^{WT}$, $H2A^{K5Q}$, and $H2A^{K5R}$ to titrate H2AK5ac into the germ line.

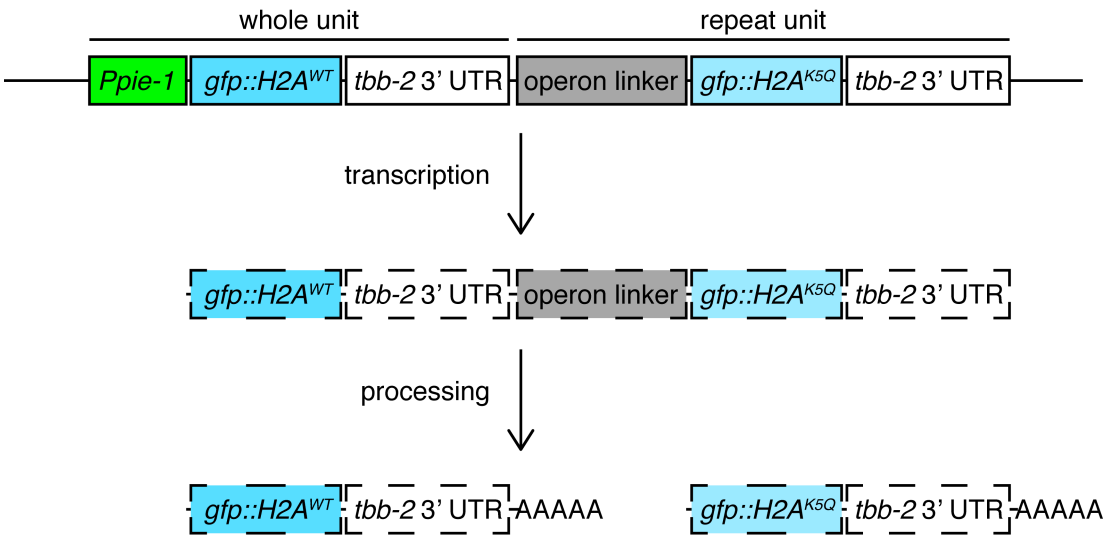

Figure 25. Overview of the H2A operon: Schematic showing the design of the operon transgene. Whole and repeat units constructed as described in Materials and Methods. The operon linker is the intercistronic region from the *gpd-2/gpd-3* operon, which has no promoter activity (HUANG *et al.* 2001); H2A is encoded by *his-30*, which has been detected in the *C. elegans* germ line by northern blot (KEALL *et al.* 2007). The operon is transcribed into a polycistronic primary transcript, and then processed into monocistronic mRNAs. Figure and experimental design adapted from (MERRITT *et al.* 2008).

MATERIALS AND METHODS

Prior to assembly in the MosSCI vector pCFJ350, H2A whole and repeat units were built into pBluescript II SK+ to facilitate site-directed mutagenesis. pBluescript II SK+ was digested with HindIII and PstI (NEB) according to manufacturer's instructions. All PCR primers are listed in Table 12, and all PCRs were performed using PrimeSTAR Max DNA polymerase (Takara R045) according to manufacturer's instructions. N2 genomic DNA was used to amplify the *pie-1* promoter (TBM-616 and TBM-609), *tbb-2* 3' UTR (TBM-614 and TBM-615), and *his-30* (H2A, TBM-612 and TBM-613). pCM1.35 and pCM1.157 (MERRITT *et al.* 2008) were used to amplify

gfp (TBM-610 and TBM-611) and the *gpd-2/gpd-3* intercistronic region (operon linker, TBM-622 and TBM-611), respectively. PCR products were purified (NucleoSpin Gel And PCR Clean-up kit, Macherey-Nagel) and assembled into pBluescript SK+ using Gibson Assembly® Master Mix (NEB E2611) according to manufacturer's instructions to form the H2A whole unit (*Ppie-1::gfp::his-30::tbb-2* 3'UTR) and the H2A repeat unit (*operon linker::gfp::his-30::tbb-2* 3'UTR). The assembled products were transformed into *E. coli* and grown overnight at 37˚C. The next day, samples from single colonies were boiled in deionized H_2O and pre-screened for correct assembly by PCR. Colonies that appeared to have integrated all elements were miniprepped and sequenced to verify error-free amplification and assembly. Error-free plasmids were saved as wild-type versions of H2A whole (pTB1) and repeat (pTB2) units, and diluted to be used as template DNA for site-directed mutagenesis. Site-directed mutagenesis to mutate H2A K5 to either glutamine (Q, TBM-618 and TBM-619) or arginine (R, TBM-620 and TBM-621) was performed with PrimeSTAR Max DNA polymerase as before. Following PCR, the product was treated with DpnI (NEB) according to manufacturer's instructions and transformed into *E. coli*. Colonies were miniprepped and sequenced to verify introduction of the target mutation. Clones containing the target mutations were saved and given the following designations: $H2A^{K5Q}$ whole unit, pTB3; $H2A^{K5R}$ whole unit, pTB4; $H2A^{K5Q}$ repeat unit, pTB5; $H2A^{K5R}$ repeat unit, pTB6.

Prior to constructing the H2A operon, MosSCI vector pCFJ350 was digested with BglII and XhoI (NEB) according to manufacturer's instructions. All H2A whole units were amplified using primers TBM-623 and TBM-624, and all H2A repeat units were amplified using primers TBM-625 and TBM-626. PCRs were performed with PrimeSTAR Max DNA polymerase, purified, and assembled into pCFJ350 as described above. The $H2A^{WT}$ operon (pTB7) was made

by assembling the whole and repeat units from pTB1 and pTB2; the $H2A^{K5Q}$ operon (pTB8) was made by assembling the whole and repeat units from pTB3 and pTB5; and the $H2A^{K5R}$ operon (pTB9) was made by assembling the whole and repeat units from pTB4 and pTB6. The assembled products were transformed into *E. coli*, pre-screened, and sequenced as described above. The end products are three plasmids each containing two copies of H2A that can be stably integrated into the *C. elegans* germ line by MosSCI.

Table 12. Primers used for construction of the H2A operon.

Primer	Sequence (5'→3')
TBM-609	CTTTACTCATCTGGAAAAGAAAATTTGATTTTTAATTG
TBM-610	TCTTTTCCAGATGAGTAAAGGAGAAGAACTTTTC
TBM-611	CACGTCCAGAACTAGTTCTAGAGCGGCC
TBM-612	TAGAACTAGTTCTGGACGTGGAAAGGGA
TBM-613	TGCATTTATCTTATTCCTTATCTCCTCCAGTCTTC
TBM-614	TAAGGAATAAGATAAATGCAAAATCCTTTCAAG
TBM-615	AGATATCCTGCAGGAATTCCTCGAGTGAGACTTTTTT CTTGGCG
TBM-616	CGAGGTCGACGGTATCGATAAGCTTACCTTTAAATAA AATCGAGAAAAAATG
TBM-617	AGTGGATCCCCCGGGCTGCAGTGAGACTTTTTTCTTG GCG
TBM-618	AGTTCTGGACGTGGACAGGGAGGCAAAGCCA
TBM-619	TGGCTTTGCCTCCCTGTCCACGTCCAGAACT
TBM-620	AGTTCTGGACGTGGACGTGGAGGCAAAGCCAAG
TBM-621	CTTGGCTTTGCCTCCACGTCCACGTCCAGAACT
TBM-622	CGAGGTCGACGGTATCGATAAGCTTAATAAAGGTTG TATATTTATTCATCTTATTGAATC
TBM-623	ATACGACTCACTAGTGGGCAGATCTACCTTTAAATAA AATCGAGAAAAAATG
TBM-624	AACCTTTATTTGAGACTTTTTTCTTGGCG

Table 12 (continued)

TBM-625	AAAAGTCTCAAATAAAGGTTGTATATTTATTCATCTT ATTG
TBM-626	AGATATCCTGCAGGAATTCCTCGAGTGAGACTTTTT TCTTGGCG

BIBLIOGRAPHY

Agostinho, A., B. Meier, R. Sonneville, M. Jagut, A. Woglar *et al.*, 2013 Combinatorial regulation of meiotic holliday junction resolution in C. elegans by HIM-6 (BLM) helicase, SLX-4, and the SLX-1, MUS-81 and XPF-1 nucleases. PLoS Genet 9**:** e1003591.

Ahmed, S., A. Alpi, M. O. Hengartner and A. Gartner, 2001 C. elegans RAD-5/CLK-2 defines a new DNA damage checkpoint protein. Curr Biol 11**:** 1934-1944.

Ahmed, S., and J. Hodgkin, 2000 MRT-2 checkpoint protein is required for germline immortality and telomere replication in C. elegans. Nature 403**:** 159-164.

Alpi, A., P. Pasierbek, A. Gartner and J. Loidl, 2003 Genetic and cytological characterization of the recombination protein RAD-51 in Caenorhabditis elegans. Chromosoma 112**:** 6-16.

Andersen, E. C., and H. R. Horvitz, 2007 Two C. elegans histone methyltransferases repress lin-3 EGF transcription to inhibit vulval development. Development 134**:** 2991-2999.

Arribere, J. A., R. T. Bell, B. X. Fu, K. L. Artiles, P. S. Hartman *et al.*, 2014 Efficient Marker-Free Recovery of Custom Genetic Modifications with CRISPR/Cas9 in Caenorhabditis elegans. Genetics.

Baillet, A., and B. Mandon-Pepin, 2012 Mammalian ovary differentiation - a focus on female meiosis. Mol Cell Endocrinol 356**:** 13-23.

Bailly, A. P., A. Freeman, J. Hall, A. C. Declais, A. Alpi *et al.*, 2010 The Caenorhabditis elegans homolog of Gen1/Yen1 resolvases links DNA damage signaling to DNA double-strand break repair. PLoS Genet 6**:** e1001025.

Bakkenist, C. J., and M. B. Kastan, 2003 DNA damage activates ATM through intermolecular autophosphorylation and dimer dissociation. Nature 421**:** 499-506.

Ball, L. G., K. Zhang, J. A. Cobb, C. Boone and W. Xiao, 2009 The yeast Shu complex couples error-free post-replication repair to homologous recombination. Mol Microbiol 73**:** 89-102.

Barber, L. J., J. L. Youds, J. D. Ward, M. J. McIlwraith, N. J. O'Neil *et al.*, 2008 RTEL1 maintains genomic stability by suppressing homologous recombination. Cell 135**:** 261-271.

Barnes, T. M., Y. Kohara, A. Coulson and S. Hekimi, 1995 Meiotic recombination, noncoding DNA and genomic organization in Caenorhabditis elegans. Genetics 141**:** 159-179.

Bender, L. B., R. Cao, Y. Zhang and S. Strome, 2004 The MES-2/MES-3/MES-6 complex and regulation of histone H3 methylation in C. elegans. Curr Biol 14**:** 1639-1643.

Bennardo, N., A. Cheng, N. Huang and J. M. Stark, 2008 Alternative-NHEJ is a mechanistically distinct pathway of mammalian chromosome break repair. PLoS Genet 4**:** e1000110.

Bessler, J. B., E. C. Andersen and A. M. Villeneuve, 2010 Differential localization and independent acquisition of the H3K9me2 and H3K9me3 chromatin modifications in the Caenorhabditis elegans adult germ line. PLoS Genet 6**:** e1000830.

Bewley, C. A., A. M. Gronenborn and G. M. Clore, 1998 Minor groove-binding architectural proteins: structure, function, and DNA recognition. Annu Rev Biophys Biomol Struct 27**:** 105-131.

Bhalla, N., D. J. Wynne, V. Jantsch and A. F. Dernburg, 2008 ZHP-3 acts at crossovers to couple meiotic recombination with synaptonemal complex disassembly and bivalent formation in C. elegans. PLoS Genet 4**:** e1000235.

Bi, X., 2015 Mechanism of DNA damage tolerance. World J Biol Chem 6**:** 48-56.

Borde, V., N. Robine, W. Lin, S. Bonfils, V. Geli *et al.*, 2009 Histone H3 lysine 4 trimethylation marks meiotic recombination initiation sites. EMBO J 28**:** 99-111.

Brenner, S., 1974 The genetics of Caenorhabditis elegans. Genetics 77**:** 71-94.

Brick, K., F. Smagulova, P. Khil, R. D. Camerini-Otero and G. V. Petukhova, 2012 Genetic recombination is directed away from functional genomic elements in mice. Nature 485**:** 642-645.

Buard, J., P. Barthes, C. Grey and B. de Massy, 2009 Distinct histone modifications define initiation and repair of meiotic recombination in the mouse. EMBO J 28**:** 2616-2624.

Burma, S., B. P. Chen, M. Murphy, A. Kurimasa and D. J. Chen, 2001 ATM phosphorylates histone H2AX in response to DNA double-strand breaks. J Biol Chem 276**:** 42462-42467.

Ceol, C. J., and H. R. Horvitz, 2004 A new class of C. elegans synMuv genes implicates a Tip60/NuA4-like HAT complex as a negative regulator of Ras signaling. Dev Cell 6**:** 563-576.

Chen, C. C., J. J. Carson, J. Feser, B. Tamburini, S. Zabaronick *et al.*, 2008 Acetylated lysine 56 on histone H3 drives chromatin assembly after repair and signals for the completion of repair. Cell 134**:** 231-243.

Chen, C. C., and J. Tyler, 2008 Chromatin reassembly signals the end of DNA repair. Cell Cycle 7**:** 3792-3797.

Cheung, I., M. Schertzer, A. Rose and P. M. Lansdorp, 2002 Disruption of dog-1 in Caenorhabditis elegans triggers deletions upstream of guanine-rich DNA. Nat Genet 31**:** 405-409.

Chin, G. M., and A. M. Villeneuve, 2001 C. elegans mre-11 is required for meiotic recombination and DNA repair but is dispensable for the meiotic G(2) DNA damage checkpoint. Genes Dev 15**:** 522-534.

Christopher Merritt, C. M. G., Dominique Rasoloson, and Geraldine Seydoux, 2010 Transgenic solutions for the germline in *WormBook*, edited by O. H. a. S. Mango.

Clancy, S., 2008 DNA damage & repair: mechanisms for maintaining DNA integrity. Nature Education 1**:** 103.

Colaiacovo, M. P., A. J. MacQueen, E. Martinez-Perez, K. McDonald, A. Adamo *et al.*, 2003 Synaptonemal complex assembly in C. elegans is dispensable for loading strand-exchange proteins but critical for proper completion of recombination. Dev Cell 5**:** 463-474.

Cole, F., S. Keeney and M. Jasin, 2010 Evolutionary conservation of meiotic DSB proteins: more than just Spo11. Genes Dev 24**:** 1201-1207.

Conradt, B., and H. R. Horvitz, 1998 The C. elegans protein EGL-1 is required for programmed cell death and interacts with the Bcl-2-like protein CED-9. Cell 93**:** 519-529.

Consortium, C. e. S., 1998 Genome sequence of the nematode C. elegans: a platform for investigating biology. Science 282**:** 2012-2018.

Corsi, A. K., B. Wightman and M. Chalfie, 2015 A Transparent Window into Biology: A Primer on Caenorhabditis elegans. Genetics 200**:** 387-407.

Cortes, D. B., K. L. McNally, P. E. Mains and F. J. McNally, 2015 The asymmetry of female meiosis reduces the frequency of inheritance of unpaired chromosomes. Elife 4**:** e06056.

Couteau, F., and M. Zetka, 2011 DNA damage during meiosis induces chromatin remodeling and synaptonemal complex disassembly. Dev Cell 20**:** 353-363.

Craig, A. L., S. C. Moser, A. P. Bailly and A. Gartner, 2012 Methods for studying the DNA damage response in the Caenorhabdatis elegans germ line. Methods Cell Biol 107**:** 321-352.

Crick, F., 1974 The double helix: a personal view. Nature 248**:** 766-769.

Crittenden, S. L., C. R. Eckmann, L. Wang, D. S. Bernstein, M. Wickens *et al.*, 2003 Regulation of the mitosis/meiosis decision in the Caenorhabditis elegans germline. Philos Trans R Soc Lond B Biol Sci 358**:** 1359-1362.

Culetto, E., and D. B. Sattelle, 2000 A role for Caenorhabditis elegans in understanding the function and interactions of human disease genes. Hum Mol Genet 9**:** 869-877.

de Massy, B., V. Rocco and A. Nicolas, 1995 The nucleotide mapping of DNA double-strand breaks at the CYS3 initiation site of meiotic recombination in Saccharomyces cerevisiae. EMBO J 14**:** 4589-4598.

Deans, B., C. S. Griffin, M. Maconochie and J. Thacker, 2000 Xrcc2 is required for genetic stability, embryonic neurogenesis and viability in mice. EMBO J 19**:** 6675-6685.

Deem, A. K., X. Li and J. K. Tyler, 2012 Epigenetic regulation of genomic integrity. Chromosoma 121**:** 131-151.

Dellaire, G., R. Kepkay and D. P. Bazett-Jones, 2009 High resolution imaging of changes in the structure and spatial organization of chromatin, gamma-H2A.X and the MRN complex within etoposide-induced DNA repair foci. Cell Cycle 8**:** 3750-3769.

Dernburg, A. F., K. McDonald, G. Moulder, R. Barstead, M. Dresser *et al.*, 1998 Meiotic recombination in C. elegans initiates by a conserved mechanism and is dispensable for homologous chromosome synapsis. Cell 94**:** 387-398.

Derry, W. B., A. P. Putzke and J. H. Rothman, 2001 Caenorhabditis elegans p53: role in apoptosis, meiosis, and stress resistance. Science 294**:** 591-595.

Dhalluin, C., J. E. Carlson, L. Zeng, C. He, A. K. Aggarwal *et al.*, 1999 Structure and ligand of a histone acetyltransferase bromodomain. Nature 399**:** 491-496.

Dickinson, D. J., J. D. Ward, D. J. Reiner and B. Goldstein, 2013 Engineering the Caenorhabditis elegans genome using Cas9-triggered homologous recombination. Nat Methods 10**:** 1028-1034.

Dietlein, F., L. Thelen and H. C. Reinhardt, 2014 Cancer-specific defects in DNA repair pathways as targets for personalized therapeutic approaches. Trends Genet 30**:** 326-339.

Doerflinger, M., J. A. Glab and H. Puthalakath, 2015 BH3-only proteins: a 20-year stock-take. FEBS J 282**:** 1006-1016.

Friedberg, E. C., 2003 DNA damage and repair. Nature 421**:** 436-440.

Frokjaer-Jensen, C., M. W. Davis, M. Ailion and E. M. Jorgensen, 2012 Improved Mos1-mediated transgenesis in C. elegans. Nat Methods 9**:** 117-118.

Frokjaer-Jensen, C., M. W. Davis, C. E. Hopkins, B. J. Newman, J. M. Thummel *et al.*, 2008 Single-copy insertion of transgenes in Caenorhabditis elegans. Nat Genet 40**:** 1375-1383.

Fukushige, T., and M. Krause, 2012 Myogenic conversion and transcriptional profiling of embryonic blastomeres in Caenorhabditis elegans. Methods 56**:** 50-54.

Gaines, W. A., S. K. Godin, F. F. Kabbinavar, T. Rao, A. P. VanDemark *et al.*, 2015 Promotion of presynaptic filament assembly by the ensemble of S. cerevisiae Rad51 paralogues with Rad52. Nat Commun 6**:** 7834.

Gao, J., H. M. Kim, A. E. Elia, S. J. Elledge and M. P. Colaiacovo, 2015 NatB domain-containing CRA-1 antagonizes hydrolase ACER-1 linking acetyl-CoA metabolism to the initiation of recombination during C. elegans meiosis. PLoS Genet 11**:** e1005029.

Garcia-Muse, T., and S. J. Boulton, 2005 Distinct modes of ATR activation after replication stress and DNA double-strand breaks in Caenorhabditis elegans. EMBO J 24**:** 4345-4355.

Garcia, V., S. E. Phelps, S. Gray and M. J. Neale, 2011 Bidirectional resection of DNA double-strand breaks by Mre11 and Exo1. Nature 479**:** 241-244.

Gartner, A., P. R. Boag and T. K. Blackwell, 2008 Germline survival and apoptosis. WormBook**:** 1-20.

Gartner, A., S. Milstein, S. Ahmed, J. Hodgkin and M. O. Hengartner, 2000 A conserved checkpoint pathway mediates DNA damage--induced apoptosis and cell cycle arrest in C. elegans. Mol Cell 5**:** 435-443.

Godin, S., A. Wier, F. Kabbinavar, D. S. Bratton-Palmer, H. Ghodke *et al.*, 2013 The Shu complex interacts with Rad51 through the Rad51 paralogues Rad55-Rad57 to mediate error-free recombination. Nucleic Acids Res 41**:** 4525-4534.

Godin, S. K., C. Meslin, F. Kabbinavar, D. S. Bratton-Palmer, C. Hornack *et al.*, 2015 Evolutionary and functional analysis of the invariant SWIM domain in the conserved Shu2/SWS1 protein family from Saccharomyces cerevisiae to Homo sapiens. Genetics 199**:** 1023-1033.

Goodyer, W., S. Kaitna, F. Couteau, J. D. Ward, S. J. Boulton *et al.*, 2008 HTP-3 links DSB formation with homolog pairing and crossing over during C. elegans meiosis. Dev Cell 14**:** 263-274.

Gubelmann, C., A. Gattiker, A. Massouras, K. Hens, F. David *et al.*, 2011 GETPrime: a gene- or transcript-specific primer database for quantitative real-time PCR. Database (Oxford) 2011**:** bar040.

Gumienny, T. L., E. Lambie, E. Hartwieg, H. R. Horvitz and M. O. Hengartner, 1999 Genetic control of programmed cell death in the Caenorhabditis elegans hermaphrodite germline. Development 126**:** 1011-1022.

Gunes, S., M. Al-Sadaan and A. Agarwal, 2015 Spermatogenesis, DNA damage and DNA repair mechanisms in male infertility. Reprod Biomed Online 31**:** 309-319.

Harris, J., M. Lowden, I. Clejan, M. Tzoneva, J. H. Thomas *et al.*, 2006 Mutator phenotype of Caenorhabditis elegans DNA damage checkpoint mutants. Genetics 174**:** 601-616.

Hassold, T., and P. Hunt, 2001 To err (meiotically) is human: the genesis of human aneuploidy. Nat Rev Genet 2**:** 280-291.

Hayashi, M., G. M. Chin and A. M. Villeneuve, 2007 C. elegans germ cells switch between distinct modes of double-strand break repair during meiotic prophase progression. PLoS Genet 3**:** e191.

Heyer, W. D., 2015 Regulation of recombination and genomic maintenance. Cold Spring Harb Perspect Biol 7**:** a016501.

Hillers, K. J., and A. M. Villeneuve, 2003 Chromosome-wide control of meiotic crossing over in C. elegans. Curr Biol 13**:** 1641-1647.

Hirsh, D., D. Oppenheim and M. Klass, 1976 Development of the reproductive system of Caenorhabditis elegans. Dev Biol 49**:** 200-219.

Hodgkin, J., 1987 Primary sex determination in the nematode C. elegans. Development 101 Suppl**:** 5-16.

Hodgkin, J., H. R. Horvitz and S. Brenner, 1979 Nondisjunction Mutants of the Nematode CAENORHABDITIS ELEGANS. Genetics 91**:** 67-94.

Hofmann, E. R., S. Milstein, S. J. Boulton, M. Ye, J. J. Hofmann *et al.*, 2002 Caenorhabditis elegans HUS-1 is a DNA damage checkpoint protein required for genome stability and EGL-1-mediated apoptosis. Curr Biol 12**:** 1908-1918.

Hong, S., and K. P. Kim, 2013 Shu1 promotes homolog bias of meiotic recombination in Saccharomyces cerevisiae. Mol Cells 36**:** 446-454.

Hong, S., Y. Sung, M. Yu, M. Lee, N. Kleckner *et al.*, 2013 The logic and mechanism of homologous recombination partner choice. Mol Cell 51**:** 440-453.

Hoogewijs, D., K. Houthoofd, F. Matthijssens, J. Vandesompele and J. R. Vanfleteren, 2008 Selection and validation of a set of reliable reference genes for quantitative sod gene expression analysis in C. elegans. BMC Mol Biol 9**:** 9.

Huang, R., M. A. Holbert, M. K. Tarrant, S. Curtet, D. R. Colquhoun *et al.*, 2010 Site-specific introduction of an acetyl-lysine mimic into peptides and proteins by cysteine alkylation. J Am Chem Soc 132**:** 9986-9987.

Huang, T., S. Kuersten, A. M. Deshpande, J. Spieth, M. MacMorris *et al.*, 2001 Intercistronic region required for polycistronic pre-mRNA processing in Caenorhabditis elegans. Mol Cell Biol 21**:** 1111-1120.

James, P., J. Halladay and E. A. Craig, 1996 Genomic libraries and a host strain designed for highly efficient two-hybrid selection in yeast. Genetics 144**:** 1425-1436.

Jantsch, V., P. Pasierbek, M. M. Mueller, D. Schweizer, M. Jantsch *et al.*, 2004 Targeted gene knockout reveals a role in meiotic recombination for ZHP-3, a Zip3-related protein in Caenorhabditis elegans. Mol Cell Biol 24**:** 7998-8006.

Jaramillo-Lambert, A., M. Ellefson, A. M. Villeneuve and J. Engebrecht, 2007 Differential timing of S phases, X chromosome replication, and meiotic prophase in the C. elegans germ line. Dev Biol 308**:** 206-221.

Jasin, M., and R. Rothstein, 2013 Repair of strand breaks by homologous recombination. Cold Spring Harb Perspect Biol 5**:** a012740.

Jenuwein, T., and C. D. Allis, 2001 Translating the histone code. Science 293**:** 1074-1080.

Jones, M. R., J. C. Huang, S. Y. Chua, D. L. Baillie and A. M. Rose, 2012 The atm-1 gene is required for genome stability in Caenorhabditis elegans. Mol Genet Genomics 287**:** 325-335.

Kaidi, A., and S. P. Jackson, 2013 KAT5 tyrosine phosphorylation couples chromatin sensing to ATM signalling. Nature 498**:** 70-74.

Kaletta, T., and M. O. Hengartner, 2006 Finding function in novel targets: C. elegans as a model organism. Nat Rev Drug Discov 5**:** 387-398.

Kamath, R. S., M. Martinez-Campos, P. Zipperlen, A. G. Fraser and J. Ahringer, 2001 Effectiveness of specific RNA-mediated interference through ingested double-stranded RNA in Caenorhabditis elegans. Genome Biol 2**:** RESEARCH0002.

Kapuscinski, J., 1995 DAPI: a DNA-specific fluorescent probe. Biotech Histochem 70**:** 220-233.

Karpenshif, Y., and K. A. Bernstein, 2012 From yeast to mammals: recent advances in genetic control of homologous recombination. DNA Repair (Amst) 11**:** 781-788.

Katz, D. J., T. M. Edwards, V. Reinke and W. G. Kelly, 2009 A C. elegans LSD1 demethylase contributes to germline immortality by reprogramming epigenetic memory. Cell 137**:** 308-320.

Kaur, T., and M. V. Rockman, 2014 Crossover heterogeneity in the absence of hotspots in Caenorhabditis elegans. Genetics 196**:** 137-148.

Keall, R., S. Whitelaw, J. Pettitt and B. Muller, 2007 Histone gene expression and histone mRNA 3' end structure in Caenorhabditis elegans. BMC Mol Biol 8**:** 51.

Keeney, S., C. N. Giroux and N. Kleckner, 1997 Meiosis-specific DNA double-strand breaks are catalyzed by Spo11, a member of a widely conserved protein family. Cell 88**:** 375-384.

Keeney, S., and N. Kleckner, 1995 Covalent protein-DNA complexes at the 5' strand termini of meiosis-specific double-strand breaks in yeast. Proc Natl Acad Sci U S A 92**:** 11274-11278.

Kelly, K. O., A. F. Dernburg, G. M. Stanfield and A. M. Villeneuve, 2000 Caenorhabditis elegans msh-5 is required for both normal and radiation-induced meiotic crossing over but not for completion of meiosis. Genetics 156**:** 617-630.

Kelly, W. G., 2014 Transgenerational epigenetics in the germline cycle of Caenorhabditis elegans. Epigenetics Chromatin 7**:** 6.

Kelly, W. G., and A. Fire, 1998 Chromatin silencing and the maintenance of a functional germline in Caenorhabditis elegans. Development 125**:** 2451-2456.

Kelly, W. G., C. E. Schaner, A. F. Dernburg, M. H. Lee, S. K. Kim *et al.*, 2002 X-chromosome silencing in the germline of C. elegans. Development 129**:** 479-492.

Kessler, Z., and J. Yanowitz, 2014 Methodological considerations for mutagen exposure in C. elegans. Methods 68**:** 441-449.

Kimble, J., and P. Simpson, 1997 The LIN-12/Notch signaling pathway and its regulation. Annu Rev Cell Dev Biol 13**:** 333-361.

Kimble, J. E., and J. G. White, 1981 On the control of germ cell development in Caenorhabditis elegans. Dev Biol 81**:** 208-219.

Kimura, A., and M. Horikoshi, 1998 Tip60 acetylates six lysines of a specific class in core histones in vitro. Genes Cells 3**:** 789-800.

Kornberg, R. D., 1974 Chromatin structure: a repeating unit of histones and DNA. Science 184**:** 868-871.

Kouzarides, T., 2007 Chromatin modifications and their function. Cell 128**:** 693-705.

Krejci, L., V. Altmannova, M. Spirek and X. Zhao, 2012 Homologous recombination and its regulation. Nucleic Acids Res 40**:** 5795-5818.

Krokan, H. E., and M. Bjoras, 2013 Base excision repair. Cold Spring Harb Perspect Biol 5**:** a012583.

Kruhlak, M. J., A. Celeste, G. Dellaire, O. Fernandez-Capetillo, W. G. Muller *et al.*, 2006 Changes in chromatin structure and mobility in living cells at sites of DNA double-strand breaks. J Cell Biol 172**:** 823-834.

Kutscher, L. M., and S. Shaham, 2014 Forward and reverse mutagenesis in C. elegans. WormBook**:** 1-26.

Kuznetsov, S. G., D. C. Haines, B. K. Martin and S. K. Sharan, 2009 Loss of Rad51c leads to embryonic lethality and modulation of Trp53-dependent tumorigenesis in mice. Cancer Res 69**:** 863-872.

Lans, H., and W. Vermeulen, 2015 Tissue specific response to DNA damage: C. elegans as role model. DNA Repair (Amst) 32**:** 141-148.

Lant, B., and W. B. Derry, 2014 Fluorescent visualization of germline apoptosis in living Caenorhabditis elegans. Cold Spring Harb Protoc 2014**:** 420-427.

Lehner, B., C. Crombie, J. Tischler, A. Fortunato and A. G. Fraser, 2006 Systematic mapping of genetic interactions in Caenorhabditis elegans identifies common modifiers of diverse signaling pathways. Nat Genet 38**:** 896-903.

Lemmens, B. B., N. M. Johnson and M. Tijsterman, 2013 COM-1 promotes homologous recombination during Caenorhabditis elegans meiosis by antagonizing Ku-mediated non-homologous end joining. PLoS Genet 9**:** e1003276.

Lemmens, B. B., and M. Tijsterman, 2011 DNA double-strand break repair in Caenorhabditis elegans. Chromosoma 120**:** 1-21.

Letunic, I., T. Doerks and P. Bork, 2015 SMART: recent updates, new developments and status in 2015. Nucleic Acids Res 43**:** D257-260.

Li, G. M., 2008 Mechanisms and functions of DNA mismatch repair. Cell Res 18**:** 85-98.

Lieber, M. R., 2010 The mechanism of double-strand DNA break repair by the nonhomologous DNA end-joining pathway. Annu Rev Biochem 79**:** 181-211.

Lindahl, T., and D. E. Barnes, 2000 Repair of endogenous DNA damage. Cold Spring Harb Symp Quant Biol 65**:** 127-133.

Linger, J., and J. K. Tyler, 2005 The yeast histone chaperone chromatin assembly factor 1 protects against double-strand DNA-damaging agents. Genetics 171**:** 1513-1522.

Liu, J., T. C. Wu and M. Lichten, 1995 The location and structure of double-strand DNA breaks induced during yeast meiosis: evidence for a covalently linked DNA-protein intermediate. EMBO J 14**:** 4599-4608.

Liu, T., L. Wan, Y. Wu, J. Chen and J. Huang, 2011 hSWS1.SWSAP1 is an evolutionarily conserved complex required for efficient homologous recombination repair. J Biol Chem 286**:** 41758-41766.

Livak, K. J., and T. D. Schmittgen, 2001 Analysis of relative gene expression data using real-time quantitative PCR and the 2(-Delta Delta C(T)) Method. Methods 25**:** 402-408.

Luger, K., A. W. Mader, R. K. Richmond, D. F. Sargent and T. J. Richmond, 1997 Crystal structure of the nucleosome core particle at 2.8 A resolution. Nature 389**:** 251-260.

Lui, D. Y., and M. P. Colaiacovo, 2013 Meiotic development in Caenorhabditis elegans. Adv Exp Med Biol 757**:** 133-170.

Luijsterburg, M. S., and H. van Attikum, 2011 Chromatin and the DNA damage response: the cancer connection. Mol Oncol 5**:** 349-367.

MacQueen, A. J., M. P. Colaiacovo, K. McDonald and A. M. Villeneuve, 2002 Synapsis-dependent and -independent mechanisms stabilize homolog pairing during meiotic prophase in C. elegans. Genes Dev 16**:** 2428-2442.

MacQueen, A. J., C. M. Phillips, N. Bhalla, P. Weiser, A. M. Villeneuve *et al.*, 2005 Chromosome sites play dual roles to establish homologous synapsis during meiosis in C. elegans. Cell 123**:** 1037-1050.

MacQueen, A. J., and A. M. Villeneuve, 2001 Nuclear reorganization and homologous chromosome pairing during meiotic prophase require C. elegans chk-2. Genes Dev 15**:** 1674-1687.

Mainpal, R., J. Nance and J. L. Yanowitz, 2015 A germ cell determinant reveals parallel pathways for germ line development in Caenorhabditis elegans. Development 142**:** 3571-3582.

Makarova, K. S., L. Aravind and E. V. Koonin, 2002 SWIM, a novel Zn-chelating domain present in bacteria, archaea and eukaryotes. Trends Biochem Sci 27**:** 384-386.

Mankouri, H. W., H. P. Ngo and I. D. Hickson, 2007 Shu proteins promote the formation of homologous recombination intermediates that are processed by Sgs1-Rmi1-Top3. Mol Biol Cell 18**:** 4062-4073.

Marin, V. A., and T. C. Evans, 2003 Translational repression of a C. elegans Notch mRNA by the STAR/KH domain protein GLD-1. Development 130**:** 2623-2632.

Martin, J. S., N. Winkelmann, M. I. Petalcorin, M. J. McIlwraith and S. J. Boulton, 2005 RAD-51-dependent and -independent roles of a Caenorhabditis elegans BRCA2-related protein during DNA double-strand break repair. Mol Cell Biol 25**:** 3127-3139.

Martin, V., C. Chahwan, H. Gao, V. Blais, J. Wohlschlegel *et al.*, 2006 Sws1 is a conserved regulator of homologous recombination in eukaryotic cells. EMBO J 25**:** 2564-2574.

Martinez-Perez, E., and M. P. Colaiacovo, 2009 Distribution of meiotic recombination events: talking to your neighbors. Curr Opin Genet Dev 19**:** 105-112.

Mazin, A. V., O. M. Mazina, D. V. Bugreev and M. J. Rossi, 2010 Rad54, the motor of homologous recombination. DNA Repair (Amst) 9**:** 286-302.

Meneely, P. M., A. F. Farago and T. M. Kauffman, 2002 Crossover distribution and high interference for both the X chromosome and an autosome during oogenesis and spermatogenesis in Caenorhabditis elegans. Genetics 162**:** 1169-1177.

Meneely, P. M., O. L. McGovern, F. I. Heinis and J. L. Yanowitz, 2012 Crossover distribution and frequency are regulated by him-5 in Caenorhabditis elegans. Genetics 190**:** 1251-1266.

Merritt, C., D. Rasoloson, D. Ko and G. Seydoux, 2008 3' UTRs are the primary regulators of gene expression in the C. elegans germline. Curr Biol 18**:** 1476-1482.

Mets, D. G., and B. J. Meyer, 2009 Condensins regulate meiotic DNA break distribution, thus crossover frequency, by controlling chromosome structure. Cell 139**:** 73-86.

Miller, K. A., D. M. Yoshikawa, I. R. McConnell, R. Clark, D. Schild *et al.*, 2002 RAD51C interacts with RAD51B and is central to a larger protein complex in vivo exclusive of RAD51. J Biol Chem 277**:** 8406-8411.

Mukherjee, S., A. D. Ridgeway and D. J. Lamb, 2010 DNA mismatch repair and infertility. Curr Opin Urol 20**:** 525-532.

Muzzini, D. M., P. Plevani, S. J. Boulton, G. Cassata and F. Marini, 2008 Caenorhabditis elegans POLQ-1 and HEL-308 function in two distinct DNA interstrand cross-link repair pathways. DNA Repair (Amst) 7**:** 941-950.

Nabeshima, K., A. M. Villeneuve and M. P. Colaiacovo, 2005 Crossing over is coupled to late meiotic prophase bivalent differentiation through asymmetric disassembly of the SC. J Cell Biol 168**:** 683-689.

Negrini, S., V. G. Gorgoulis and T. D. Halazonetis, 2010 Genomic instability--an evolving hallmark of cancer. Nat Rev Mol Cell Biol 11**:** 220-228.

Nottke, A. C., S. E. Beese-Sims, L. F. Pantalena, V. Reinke, Y. Shi *et al.*, 2011 SPR-5 is a histone H3K4 demethylase with a role in meiotic double-strand break repair. Proc Natl Acad Sci U S A 108**:** 12805-12810.

O'Driscoll, M., 2012 Diseases associated with defective responses to DNA damage. Cold Spring Harb Perspect Biol 4.

O'Neil, N. J., J. S. Martin, J. L. Youds, J. D. Ward, M. I. Petalcorin *et al.*, 2013 Joint molecule resolution requires the redundant activities of MUS-81 and XPF-1 during Caenorhabditis elegans meiosis. PLoS Genet 9**:** e1003582.

Oktay, K., V. Turan, S. Titus, R. Stobezki and L. Liu, 2015 BRCA Mutations, DNA Repair Deficiency, and Ovarian Aging. Biol Reprod 93**:** 67.

Owen, D. J., P. Ornaghi, J. C. Yang, N. Lowe, P. R. Evans *et al.*, 2000 The structural basis for the recognition of acetylated histone H4 by the bromodomain of histone acetyltransferase gcn5p. EMBO J 19**:** 6141-6149.

Paix, A., Y. Wang, H. E. Smith, C. Y. Lee, D. Calidas *et al.*, 2014 Scalable and versatile genome editing using linear DNAs with microhomology to Cas9 Sites in Caenorhabditis elegans. Genetics 198**:** 1347-1356.

Pasierbek, P., M. Jantsch, M. Melcher, A. Schleiffer, D. Schweizer *et al.*, 2001 A Caenorhabditis elegans cohesion protein with functions in meiotic chromosome pairing and disjunction. Genes Dev 15**:** 1349-1360.

Petalcorin, M. I., V. E. Galkin, X. Yu, E. H. Egelman and S. J. Boulton, 2007 Stabilization of RAD-51-DNA filaments via an interaction domain in Caenorhabditis elegans BRCA2. Proc Natl Acad Sci U S A 104**:** 8299-8304.

Praitis, V., E. Casey, D. Collar and J. Austin, 2001 Creation of low-copy integrated transgenic lines in Caenorhabditis elegans. Genetics 157**:** 1217-1226.

Prakash, R., Y. Zhang, W. Feng and M. Jasin, 2015 Homologous recombination and human health: the roles of BRCA1, BRCA2, and associated proteins. Cold Spring Harb Perspect Biol 7**:** a016600.

Ramey, C. J., S. Howar, M. Adkins, J. Linger, J. Spicer *et al.*, 2004 Activation of the DNA damage checkpoint in yeast lacking the histone chaperone anti-silencing function 1. Mol Cell Biol 24**:** 10313-10327.

Reddy, K. C., and A. M. Villeneuve, 2004 C. elegans HIM-17 links chromatin modification and competence for initiation of meiotic recombination. Cell 118**:** 439-452.

Reeves, R., 2001 Molecular biology of HMGA proteins: hubs of nuclear function. Gene 277**:** 63-81.

Rinaldo, C., P. Bazzicalupo, S. Ederle, M. Hilliard and A. La Volpe, 2002 Roles for Caenorhabditis elegans rad-51 in meiosis and in resistance to ionizing radiation during development. Genetics 160**:** 471-479.

Rog, O., and A. F. Dernburg, 2015 Direct Visualization Reveals Kinetics of Meiotic Chromosome Synapsis. Cell Rep.

Rogakou, E. P., C. Boon, C. Redon and W. M. Bonner, 1999 Megabase chromatin domains involved in DNA double-strand breaks in vivo. J Cell Biol 146**:** 905-916.

Rosu, S., K. A. Zawadzki, E. L. Stamper, D. E. Libuda, A. L. Reese *et al.*, 2013 The C. elegans DSB-2 protein reveals a regulatory network that controls competence for meiotic DSB formation and promotes crossover assurance. PLoS Genet 9**:** e1003674.

Saito, T. T., D. Y. Lui, H. M. Kim, K. Meyer and M. P. Colaiacovo, 2013 Interplay between structure-specific endonucleases for crossover control during Caenorhabditis elegans meiosis. PLoS Genet 9**:** e1003586.

Saito, T. T., F. Mohideen, K. Meyer, J. W. Harper and M. P. Colaiacovo, 2012 SLX-1 is required for maintaining genomic integrity and promoting meiotic noncrossovers in the Caenorhabditis elegans germline. PLoS Genet 8**:** e1002888.

Saito, T. T., J. L. Youds, S. J. Boulton and M. P. Colaiacovo, 2009 Caenorhabditis elegans HIM-18/SLX-4 interacts with SLX-1 and XPF-1 and maintains genomic integrity in the germline by processing recombination intermediates. PLoS Genet 5**:** e1000735.

Sasanuma, H., M. S. Tawaramoto, J. P. Lao, H. Hosaka, E. Sanda *et al.*, 2013 A new protein complex promoting the assembly of Rad51 filaments. Nat Commun 4**:** 1676.

Sato, A., B. Isaac, C. M. Phillips, R. Rillo, P. M. Carlton *et al.*, 2009 Cytoskeletal forces span the nuclear envelope to coordinate meiotic chromosome pairing and synapsis. Cell 139**:** 907-919.

Scharer, O. D., 2013 Nucleotide excision repair in eukaryotes. Cold Spring Harb Perspect Biol 5**:** a012609.

Schmittgen, T. D., and K. J. Livak, 2008 Analyzing real-time PCR data by the comparative C(T) method. Nat Protoc 3**:** 1101-1108.

Schumacher, B., M. Hanazawa, M. H. Lee, S. Nayak, K. Volkmann *et al.*, 2005 Translational repression of C. elegans p53 by GLD-1 regulates DNA damage-induced apoptosis. Cell 120**:** 357-368.

Schumacher, B., K. Hofmann, S. Boulton and A. Gartner, 2001 The C. elegans homolog of the p53 tumor suppressor is required for DNA damage-induced apoptosis. Curr Biol 11**:** 1722-1727.

Schvarzstein, M., D. Pattabiraman, D. E. Libuda, A. Ramadugu, A. Tam *et al.*, 2014 DNA helicase HIM-6/BLM both promotes MutSgamma-dependent crossovers and antagonizes MutSgamma-independent interhomolog associations during caenorhabditis elegans meiosis. Genetics 198**:** 193-207.

Sedelnikova, O. A., E. P. Rogakou, I. G. Panyutin and W. M. Bonner, 2002 Quantitative detection of (125)IdU-induced DNA double-strand breaks with gamma-H2AX antibody. Radiat Res 158**:** 486-492.

Shaye, D. D., and I. Greenwald, 2011 OrthoList: a compendium of C. elegans genes with human orthologs. PLoS One 6**:** e20085.

She, Z., Z. Q. Gao, Y. Liu, W. J. Wang, G. F. Liu *et al.*, 2012 Structural and SAXS analysis of the budding yeast SHU-complex proteins. FEBS Lett 586**:** 2306-2312.

Shor, E., J. Weinstein and R. Rothstein, 2005 A genetic screen for top3 suppressors in Saccharomyces cerevisiae identifies SHU1, SHU2, PSY3 and CSM2: four genes involved in error-free DNA repair. Genetics 169**:** 1275-1289.

Smagulova, F., I. V. Gregoretti, K. Brick, P. Khil, R. D. Camerini-Otero *et al.*, 2011 Genome-wide analysis reveals novel molecular features of mouse recombination hotspots. Nature 472**:** 375-378.

Smolikov, S., A. Eizinger, A. Hurlburt, E. Rogers, A. M. Villeneuve *et al.*, 2007a Synapsis-defective mutants reveal a correlation between chromosome conformation and the mode of double-strand break repair during Caenorhabditis elegans meiosis. Genetics 176**:** 2027-2033.

Smolikov, S., A. Eizinger, K. Schild-Prufert, A. Hurlburt, K. McDonald *et al.*, 2007b SYP-3 restricts synaptonemal complex assembly to bridge paired chromosome axes during meiosis in Caenorhabditis elegans. Genetics 176**:** 2015-2025.

Smolikov, S., K. Schild-Prufert and M. P. Colaiacovo, 2009 A yeast two-hybrid screen for SYP-3 interactors identifies SYP-4, a component required for synaptonemal complex assembly and chiasma formation in Caenorhabditis elegans meiosis. PLoS Genet 5**:** e1000669.

Snowden, T., S. Acharya, C. Butz, M. Berardini and R. Fishel, 2004 hMSH4-hMSH5 recognizes Holliday Junctions and forms a meiosis-specific sliding clamp that embraces homologous chromosomes. Mol Cell 15**:** 437-451.

Squatrito, M., C. Gorrini and B. Amati, 2006 Tip60 in DNA damage response and growth control: many tricks in one HAT. Trends Cell Biol 16**:** 433-442.

Stamper, E. L., S. E. Rodenbusch, S. Rosu, J. Ahringer, A. M. Villeneuve *et al.*, 2013 Identification of DSB-1, a protein required for initiation of meiotic recombination in Caenorhabditis elegans, illuminates a crossover assurance checkpoint. PLoS Genet 9**:** e1003679.

Stergiou, L., K. Doukoumetzidis, A. Sendoel and M. O. Hengartner, 2007 The nucleotide excision repair pathway is required for UV-C-induced apoptosis in Caenorhabditis elegans. Cell Death Differ 14**:** 1129-1138.

Sun, Y., X. Jiang, S. Chen, N. Fernandes and B. D. Price, 2005 A role for the Tip60 histone acetyltransferase in the acetylation and activation of ATM. Proc Natl Acad Sci U S A 102**:** 13182-13187.

Sun, Y., X. Jiang, Y. Xu, M. K. Ayrapetov, L. A. Moreau *et al.*, 2009 Histone H3 methylation links DNA damage detection to activation of the tumour suppressor Tip60. Nat Cell Biol 11**:** 1376-1382.

Sung, P., and H. Klein, 2006 Mechanism of homologous recombination: mediators and helicases take on regulatory functions. Nat Rev Mol Cell Biol 7**:** 739-750.

Suwaki, N., K. Klare and M. Tarsounas, 2011 RAD51 paralogs: roles in DNA damage signalling, recombinational repair and tumorigenesis. Semin Cell Dev Biol 22**:** 898-905.

Szostak, J. W., T. L. Orr-Weaver, R. J. Rothstein and F. W. Stahl, 1983 The double-strand-break repair model for recombination. Cell 33**:** 25-35.

Takanami, T., A. Mori, H. Takahashi and A. Higashitani, 2000 Hyper-resistance of meiotic cells to radiation due to a strong expression of a single recA-like gene in Caenorhabditis elegans. Nucleic Acids Res 28**:** 4232-4236.

Tao, Y., X. Li, Y. Liu, J. Ruan, S. Qi *et al.*, 2012 Structural analysis of Shu proteins reveals a DNA binding role essential for resisting damage. J Biol Chem 287**:** 20231-20239.

Taylor, J. H., 1974 Symposium No. 4: Melosis. Introduction by the Chairman. Genetics 78**:** 187-191.

Taylor, M. R., M. Spirek, K. R. Chaurasiya, J. D. Ward, R. Carzaniga *et al.*, 2015 Rad51 Paralogs Remodel Pre-synaptic Rad51 Filaments to Stimulate Homologous Recombination. Cell 162**:** 271-286.

Thacker, J., 2005 The RAD51 gene family, genetic instability and cancer. Cancer Lett 219**:** 125-135.

Timmons, L., and A. Fire, 1998 Specific interference by ingested dsRNA. Nature 395**:** 854.

Turlure, F., G. Maertens, S. Rahman, P. Cherepanov and A. Engelman, 2006 A tripartite DNA-binding element, comprised of the nuclear localization signal and two AT-hook motifs, mediates the association of LEDGF/p75 with chromatin in vivo. Nucleic Acids Res 34**:** 1653-1665.

van Haaften, G., R. H. Plasterk and M. Tijsterman, 2004 Genomic instability and cancer: scanning the Caenorhabditis elegans genome for tumor suppressors. Oncogene 23**:** 8366-8375.

Vaz, F., H. Hanenberg, B. Schuster, K. Barker, C. Wiek *et al.*, 2010 Mutation of the RAD51C gene in a Fanconi anemia-like disorder. Nat Genet 42**:** 406-409.

Vermezovic, J., L. Stergiou, M. O. Hengartner and F. d'Adda di Fagagna, 2012 Differential regulation of DNA damage response activation between somatic and germline cells in Caenorhabditis elegans. Cell Death Differ 19**:** 1847-1855.

Vilenchik, M. M., and A. G. Knudson, 2003 Endogenous DNA double-strand breaks: production, fidelity of repair, and induction of cancer. Proc Natl Acad Sci U S A 100**:** 12871-12876.

Wagner, C. R., L. Kuervers, D. L. Baillie and J. L. Yanowitz, 2010 xnd-1 regulates the global recombination landscape in Caenorhabditis elegans. Nature 467**:** 839-843.

Wang, A. T., T. Kim, J. E. Wagner, B. A. Conti, F. P. Lach *et al.*, 2015 A Dominant Mutation in Human RAD51 Reveals Its Function in DNA Interstrand Crosslink Repair Independent of Homologous Recombination. Mol Cell 59**:** 478-490.

Ward, J. D., L. J. Barber, M. I. Petalcorin, J. Yanowitz and S. J. Boulton, 2007 Replication blocking lesions present a unique substrate for homologous recombination. EMBO J 26**:** 3384-3396.

Ward, J. D., D. M. Muzzini, M. I. Petalcorin, E. Martinez-Perez, J. S. Martin *et al.*, 2010 Overlapping mechanisms promote postsynaptic RAD-51 filament disassembly during meiotic double-strand break repair. Mol Cell 37**:** 259-272.

Waters, K., A. Z. Yang and V. Reinke, 2010 Genome-wide analysis of germ cell proliferation in C.elegans identifies VRK-1 as a key regulator of CEP-1/p53. Dev Biol 344**:** 1011-1025.

Watt, P. M., E. J. Louis, R. H. Borts and I. D. Hickson, 1995 Sgs1: a eukaryotic homolog of E. coli RecQ that interacts with topoisomerase II in vivo and is required for faithful chromosome segregation. Cell 81**:** 253-260.

Winston, F., and C. D. Allis, 1999 The bromodomain: a chromatin-targeting module? Nat Struct Biol 6**:** 601-604.

Wu, H., N. Mathioudakis, B. Diagouraga, A. Dong, L. Dombrovski *et al.*, 2013 Molecular basis for the regulation of the H3K4 methyltransferase activity of PRDM9. Cell Rep 5**:** 13-20.

Yamada, H. Y., 2012 Human Tip60 (NuA4) Complex and Cancer, pp. 217-240 in *Colorectal Cancer Biology - From Genes to Tumor*, edited by R. Ettarh. InTech.

Yanowitz, J. L., 2008 Genome integrity is regulated by the Caenorhabditis elegans Rad51D homolog rfs-1. Genetics 179**:** 249-262.

Yin, Y., and S. Smolikove, 2013 Impaired resection of meiotic double-strand breaks channels repair to nonhomologous end joining in Caenorhabditis elegans. Mol Cell Biol 33**:** 2732-2747.

Yokoo, R., K. A. Zawadzki, K. Nabeshima, M. Drake, S. Arur *et al.*, 2012 COSA-1 reveals robust homeostasis and separable licensing and reinforcement steps governing meiotic crossovers. Cell 149**:** 75-87.

Youds, J. L., D. G. Mets, M. J. McIlwraith, J. S. Martin, J. D. Ward *et al.*, 2010 RTEL-1 enforces meiotic crossover interference and homeostasis. Science 327**:** 1254-1258.

Youds, J. L., N. J. O'Neil and A. M. Rose, 2006 Homologous recombination is required for genome stability in the absence of DOG-1 in Caenorhabditis elegans. Genetics 173**:** 697-708.

Yun, M., J. Wu, J. L. Workman and B. Li, 2011 Readers of histone modifications. Cell Res 21**:** 564-578.

Zalevsky, J., A. J. MacQueen, J. B. Duffy, K. J. Kemphues and A. M. Villeneuve, 1999 Crossing over during Caenorhabditis elegans meiosis requires a conserved MutS-based pathway that is partially dispensable in budding yeast. Genetics 153**:** 1271-1283.

Zeng, L., Q. Zhang, S. Li, A. N. Plotnikov, M. J. Walsh *et al.*, 2010 Mechanism and regulation of acetylated histone binding by the tandem PHD finger of DPF3b. Nature 466**:** 258-262.

Zetka, M. C., I. Kawasaki, S. Strome and F. Muller, 1999 Synapsis and chiasma formation in Caenorhabditis elegans require HIM-3, a meiotic chromosome core component that functions in chromosome segregation. Genes Dev 13**:** 2258-2270.

Zhang, H., Z. M. Xiong and K. Cao, 2014 Mechanisms controlling the smooth muscle cell death in progeria via down-regulation of poly(ADP-ribose) polymerase 1. Proc Natl Acad Sci U S A 111**:** E2261-2270.

Zickler, D., and N. Kleckner, 1998 The leptotene-zygotene transition of meiosis. Annu Rev Genet 32**:** 619-697.